TECHNISCHE UNIVERSITÄT MÜNCHEN

II. Medizinische Klinik und Poliklinik des

Klinikum rechts der Isar

JNKs are stress-dependent regulators of acinar maintenance and tumor suppressors in PDAC

Tobias Sebastian Leibfritz

Vollständiger Abdruck der von der Fakultät für Medizin der

Technischen Universität München zur Erlangung des akademischen Grades eines

Doktor der Naturwissenschaften (Dr. rer. nat.)

genehmigten Dissertation.

Vorsitzender: Univ.-Prof. Dr. R. M. Schmid

Prüfer der Dissertation:

1. apl. Prof. Dr. J. Th. Siveke

2. Univ.-Prof. Angelika Schnieke, Ph.D.

Die Dissertation wurde am 23. 04. 2015 bei der Technischen Universität München eingereicht und durch die Fakultät für Medizin am 16. 09. 2015 angenommen.

Meinen Eltern und

meinem Verlobten

Darin besteht das Wesen der Wissenschaft.

Zuerst denkt man an etwas, das wahr sein könnte. Dann sieht man nach, ob es der Fall ist und im Allgemeinen ist es nicht der Fall.

Bertrand Russel, Philosoph und Mathematiker, 1872-1970

Publications and Presentations

Parts of this thesis were presented on an international conference.

International Presentations

JNKs as new tumor suppressors in PDAC
3rd International Conference on Tumor Microenvironment and Cellular Stress
Mykonos, Greece, 21 - 26 September 2014

Table of content

1 Summary

Pancreatic ductal adenocarcinoma has a lifetime risk of about 1.6 % and is the 4th leading cause of cancer-related death in the developed world. Cellular stress such as chronic inflammation is a well-described trigger of PDAC and other types of cancer. The c-Jun N-terminal kinase (JNK)-module of the MAP kinase cascade plays a pivotal role in the detection of cellular stress and the induction of downstream response pathways. Interestingly, both tumorigenic and tumor-suppressive effects have been described for this cascade. Therefore, the effects of JNK signaling knockout were investigated in the Kras^{G12D}-model of PDAC.

Mice with pancreas-specific knockout of JNK1 and JNK2 were born with expected Mendelian ratio and had no impaired lineage specification. Adult animals did not suffer from any obvious macroscopic defects and their body weight did not differ from that of controls. Over time, however, JNK-deficient mice were not able to maintain acinar cell differentiation. While terminal differentiation markers were unchanged at eight weeks of age, transdifferentiation into duct-like structures was accelerated. Furthermore, induced acute pancreatitis revealed an inability of JNK knockout mice to regain terminal differentiation and to resolve induced pancreatic lesions within four weeks.

JNK knockout in the oncogenic Kras^{G12D} background resulted in dramatically reduced life span of only four to five weeks. The development of acinar ductal metaplasia (ADM) and pancreatic intraepithelial neoplasia (PanIN) was accompanied by a strong fibrotic reaction and terminal mice showed multifocal PDAC. Interestingly, however, proliferation and apoptosis were unchanged. Acinar cell restricted Elastase-CreER;Kras^{G12D};JNK knockout mice developed PDACs about 30 weeks after induction compared to normal pancreata in Elastase-CreER;Kras^{G12D} mice suggesting acinar cells as cells of origin for tumor development. This establishes JNK1 and JNK2 as important tumor suppressors in PDAC.

While AKT signaling remained unaffected in JNK knockout mice, ERK signaling was upregulated probably due to the existing precursor lesions. γH2AX a histone variant involved in the DNA damage response, however, was not affected. Analysis of p53 in Kras^{G12D};JNK$^{\Delta/\Delta}$ mice showed nuclear localization and upregulation at 14 days of age, however, minor shifts in band size indicate differences in posttranslational modification of p53, which might impair p53's transactivational abilities. Sox9, a marker for precursor-like cells in the pancreas, was strongly upregulated in Kras^{G12D};JNK knockout mice.

Unbiased arrays of seven day old Kras^{G12D};JNK knockout mice versus controls revealed a marked enrichment in inflammatory signatures. No cooperation of Kras^{G12D};JNK knockout mice with NF-κB could be detected, but STAT3 signaling was markedly upregulated. Unexpectedly, IL6-triggered activation of STAT3 in JNK-inhibited Kras^{G12D}-positive pancreatic cancer cells did not reveal a disinhibitory effect

of JNKs on STAT3, although this had been previously reported. Knockout of STAT3 from epithelial cells in the $Kras^{G12D}$;JNK knockout mouse did not change overall survival or histology notably.

In summary, JNK signaling is important for acinar maintenance in the pancreas, inhibits quick transdifferentiation towards ADM and is required for redifferentiation of ADM after induced acute pancreatitis. Furthermore this study identifies JNK1 and JNK2 as strong tumor suppressors in PDAC.

2 Introduction

2.1 Anatomy and physiology of the pancreas

The pancreas is located in the upper abdominal cavity between duodenum (head of the pancreas), stomach and spleen (tail of the pancreas) (Figure 1). Heterotopic pancreas, pancreas tissue at other sites without vascular or anatomic continuity with the pancreas is rare [1]. The pancreas consists of two functionally different compartments: the endocrine and exocrine pancreas. The endocrine tissue is organized as insular cell aggregations, the islets of Langerhans, which are dispersed throughout the organ [2]. These islets consist of five different cell types: α-cells secreting glucagon, β-cells secreting insulin, δ-cells producing somatostatin, ε-cells producing ghrelin and the pancreatic polypeptide secreting PP-cells. All these hormones regulate blood glucose homeostasis and nutrient metabolism [3]. The exocrine compartment constitutes roughly 90 % of the pancreatic tissue mass and consists of grape-like structures of acinar cells, which connect to the ductal system through centroacinar cells. Ductal cells secrete bicarbonate rich mucus that flushes the hydrolytic digestive proenzymes produced by the acini into the duodenum. In the duodenum pancreatic proenzymes, such as trypsinogen, are activated via regulated partial proteolysis to break down food into its monomeric components [4].

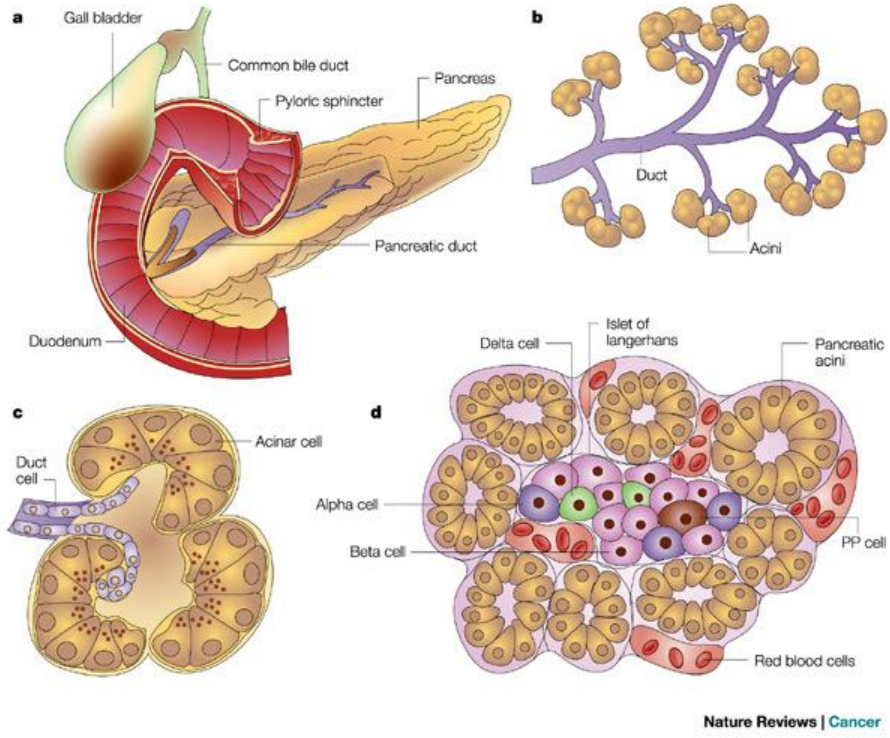

Figure 1 Macroscopic and microscopic anatomy of the pancreas
(A) Macroscopic anatomy of the pancreas and its surrounding structures (B) Simplified scheme of pancreatic acini (berry-shaped terminations of exocrine glands) connected to the pancreatic duct system (C) Secretory acinar cells clustered in berries that connect to the ductal system (D) Schematic of an islet of Langerhans with its different endocrine cells surrounded by acinar berries [5]. Reprinted by permission from Macmillan Publishers Ltd: Nature Reviews Cancer 2002 Dec;2(12):897-909, copyright 2002.

2.2 Development of the pancreas

Pancreatic development is an orchestrated program of proliferation, branching and differentiation [6]. In mice it begins between embryonic day (E)8.5 and E9.5 [7]. A patch of progenitor cells in the ventral foregut segregates into extrahepatic bile duct system and Pdx1 positive progenitors of the ventral pancreatic bud [8-10]. This process depends on the transcription factors Sox17 and Hes1. Both ventral and dorsal pancreatic evaginations fuse around E11.5 after gut rotation and develop into a pseudostratified epithelium that resolves into a complex branched epithelium populated with distinct multipotent progenitor cells (MPCs) [11]. These cells only exist transiently until about E14 and express Ptf1a, Pdx1, c-myc and Cpa1 [12]. Importantly, Pdx1 and Ptf1a are the earliest detectable known pancreas specific transcription factors. Both are used for pancreas-specific activation or inactivation of genes in the Cre/LoxP or the Flip/Frt systems (see 2.5.1). Further important transcription factors for progenitor cell expansion and suppression of premature endocrine cell development are Rbpj and the PTF-J complex (Ptf1a, Rbpj and any commonly expressed bHLH transcription factor) executing Notch-dependent functions, Hnf1b and Sox9 [13-16]. Between E12.5 and E14 MPCs segregate into bipotent precursors of islet and ductal cells as well as cells with acinar commitment [17]. These two compartments now mutually exclusively express Hnf1b/Hnf6 and Cpa1. By E14 a branched structure of rapidly proliferating pre-acinar cells at the tips that are connected by epithelial trunks has formed. At this point, an intricate gene regulatory network (GRN) of transcription factors such as Ptf1a, Pdx1, Hes1, Nkx6.1, Prox1, Nr5a2, Gata4, Gata6, Sox9, Ngn3 and others transform the established precursor populations into terminally differentiated acinar, ductal and endocrine cells with their specific functions in enzyme, mucin or hormone production respectively [18].

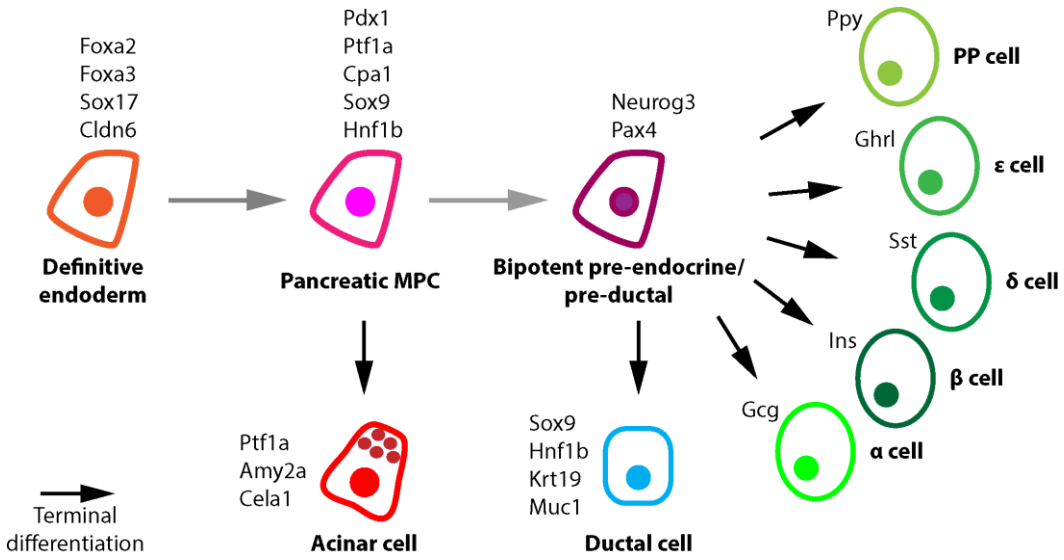

Figure 2 Lineage specification during pancreatic embryonic development
Simplified consecutive lineage specification of definitive endoderm via multipotent precursor cells (MPC) to form terminally differentiated pancreatic cell lineages. A selection of the most important transcription factors expressed at each stage is shown. Own picture adapted from Magnuson *et al*. [19]

2.3 Acute and chronic pancreatitis

Acute pancreatitis is an inflammatory process associated with a mild to life-threatening partial self-digestion of the pancreas [20]. Common causes for acute pancreatitis are gallstones obstructing the pancreatic main duct and alcohol abuse. Symptoms include severe pain in the upper abdomen, nausea, obstipation, vomiting and fever. A mouse model in which cerulein, a cholecystokinin analogue is injected intraperitoneally has been established to study this disease. Cerulein then triggers the activation of pancreatic enzyme secretion [21]. The underlying detailed molecular mechanism of the downstream effects of cerulein is poorly understood but involves dysregulated calcium signaling in the acinar cell [22]. The pancreas shows extraordinary cellular plasticity and regenerates to normal histological architecture within days after severe acute pancreatitis. This regeneration is driven by the exocrine compartment that undergoes proliferation and redifferentiation after a transient dedifferentiation. This process of acinar dedifferentiation is executed through acinar ductal metaplasia during which acinar cells aquire duct-like morphological and molecular features (ADM, see below). During ADM, embryonal markers such as Ptf1a , Pdx1, ß-catenin and Notch are reactivated [23, 24]. ß-catenin is a key player, which is upregulated during regeneration and is blocked by mutant Kirsten rat sarcoma (Kras) signaling leading to ADM [25]. In addition it has been shown that knockout of Notch results in impaired regeneration also leading to prolonged ß-catenin activation [26]. Interestingly, the nuclear receptor Nr5a2 maintains acinar differentiation and is required for efficient acinar regeneration [27]. Upon pancreas specific deletion in the $Kras^{G12D}$ background (see 2.5.2), mice succumb to severe ADM and pancreatic intraepithelial neoplasia (PanIN) development around 3 weeks after birth. Similarly, Numb, an acinar differentiation marker, is down regulated during acute pancreatitis. Upon pancreas-specific deletion acinar regeneration is severely inhibited [28]. The regenerative process was linked to focal adhesion kinase signaling thereby identifying integrin binding as an important mechanism. In an attempt to identify master regulators of differentiation Reichert *et al*. performed microarrays across pancreatic development, pancreatitis and PanINs. From this screen, Prrx1b emerged. This homeobox protein is expressed during acute pancreatitis and was found to bind and regulate the Sox9 promoter [29]. Sox9 itself is yet another master regulator of ADM (see 2.6.4.4). Taken together these studies reveal that cellular stress and perturbations leading to dedifferentiation and ADM increase the susceptibility to oncogenic stimuli and are likely a central initial step for malignant transformation.

Chronic pancreatitis is a prolonged inflammatory process involving progressive destruction of pancreas parenchyma and replacement by fibrous tissue, eventually leading to malnutrition and diabetes [30]. Patients usually present with persistent abdominal pain and steatorrhea. Besides hereditary factors such as defects in the CFTR (cystic fibrosis) gene, alcohol abuse and smoking are main risk factors of chronic pancreatitis. Chronic pancreatitis itself is a known risk factor for pancreatic cancer [31]. This has been demonstrated in an experiment activating the $Kras^{G12Vgeo}$

oncogene in 60 day old mice. While embryonal activation of $Kras^{G12Vgeo}$ results in progressive development of pancreatic precursor lesions and PDAC in later life, activation of $Kras^{G12Vgeo}$ in mature differentiated cell did not even lead to precursor lesion formation. Only upon low-dose cerulein treatment mimicking chronic pancreatitis PanIN and PDAC developed [32]. This was extended by the finding that even activation of $Kras^{G12V}$ in combination with deletion of either $p16^{INK4A}$/$p19^{ARF}$ or p53, well known tumor suppressors, on day 60 post partum did not result in detectable lesions 12 months later. Furthermore, it was shown that cerulein treatment did not only initiate ADM and PanIN formation but also inhibited oncogene-induced senescence (OIS), likely mediated by the ensuing inflammatory response [33]. Together these reports demonstrate that stress, like persistent inflammation is more important for tumor development in the pancreas than knockout of tumor suppressors in the absence of trigger-events.

2.4 Pancreatic cancer

2.4.1 Basic clinicopathological data

In 2014, an estimated 82 300 people die from pancreatic cancer in the European Union with both sexes being affected equally [34]. In Germany, the median age at diagnosis is 71 years in males and 76 years in females with a life time risk of developing pancreatic cancer of 1,6 % [35]. Of all patients, only 5-10 % have a family history of pancreatic cancer [36, 37]. Environmental risk factors include tobacco smoke (2.5 to 3.6 times compared to non-smokers [38]), excessive intake of alcohol, obesity, diabetes, chronic pancreatitis and blood group [39]. Pancreatic cancers can be divided according to the two main functions of the pancreas into neuroendocrine and exocrine malignancies.

2.4.2 Neuroendocrine Malignancies

Neuroendocrine malignancies are rare and account for about 1-4 % [40, 41] of all pancreatic cancers. They are divided based on the cell of origin into insulinomas, glucagonomas, somatostatinomas, gastrinomas and VIPomas. The main symptoms are determined by the respective hormone produced in excess and released into the blood stream or secondary effects due to the tumor mass. Progression free survival ranges from 218 months in stage I to 24 months in stage IV [42]. Notably, however, 90 % of neuroendocrine tumors are nonproductive islet tumors of the pancreas causing symptoms due to mass effects or metastasis [43]. Several neuroendocrine malignancies are associated with inherited syndromes such as multiple endocrine metaplasia (MEN) -1 or von Hippel-Lindau syndrome (vHL) [44].

2.4.3 Exocrine Malignancies

2.4.3.1 Rare exocrine malignancies

An array of rare exocrine malignancies exist that are further subclassified according to WHO standards [45]. For instance, one rarely encountered tumor is acinar cell carcinoma which is responsible for 1-2 % of all pancreatic cancers [46]. It is cell-rich,

rarely displays a fibrotic reaction, stains positive for digestive enzymes and genetic alterations in the ß-catenin pathway are frequently detected. Possibly the rarest pancreatic tumor entity is pancreatoblastoma, which is associated with Beckwith-Wiedeman syndrome. Only 33 cases have been reported so far [47, 48].

2.4.3.2 Pancreatic ductal adenocarcinoma (PDAC)

PDAC constitutes more than 90 % of exocrine pancreatic cancers and develops in 60-70 % of cases in the pancreas head, in about 10-15 % in the tail and roughly 5-10 % involve the whole pancreas [49]. Although it is only the tenth most common cancer in the Western world PDAC is the fourth leading cause of cancer-related death. Five-year survival has changed significantly over the last 40 years rising from 2,5 % (1975-1977) to 7,2 % (2004-2010) in the developed world [50], likely due to increased awareness and earlier detection because of better imaging technologies. The five-year survival is at approximately 7 % but may be even less due to wrong diagnosis in long-term survivors as demonstrated by Carpelan-Holström *et al*. [51] and five-year survival accordingly would be <1 %.

Pancreatic cancer still has the lowest survival rates of all cancers despite huge efforts in preclinical and therapeutic research. This is due to a number of reasons: First, patients present rather late in the clinic due to unspecific, non-acute symptoms, such as dull pain in the upper abdomen [52]. Second, correct diagnosis of PDAC is often delayed since differential diagnosis itself is challenging. As a result, diagnosis frequently occurs only at late stages when the tumor has already metastasized [53, 54]. At the time of diagnosis only 10 % of patients present with localized and therefore resectable disease resulting in a 5-year relative survival of 25 %. More than 80 % of patients, however, are diagnosed with either regional (involving adjacent lymph nodes) or distant, meaning metastatic, disease leading to a 5-year survival of only 10 % and 2 % respectively [50, 55]. Third, once diagnosed, PDAC shows an intriguing resistance to chemotherapy and irradiation. Standard of care treatment for decades was gemcitabine, a nucleotide analogue that offered the patient an additional median survival benefit of 5 weeks and reduced side effects compared to 5-Fluoruracil (5-FU) [56]. Gemcitabine is sometimes combined with the EGFR inhibitor erlotinib, which further improves survival by merely 2 weeks compared to gemcitabine alone [57, 58]. Unfortunately, only a small number of patients respond to this combination therapy while toxicity is significantly increases. In 2011, a novel combination of several chemotherapeutics (FOLFIRINOX) resulted in increased overall survival in a subset of PDAC patients, which is now considered standard of care for metastatic disease in fit patients [59, 60]. Current translational preclinical and low phase clinical trials target various signaling pathways and for example include inhibitors of IGF-1, MEK or VEGF [61]. These new approaches will hopefully improved survival further.

The cell of origin in PDAC was initially suspected to be the ductal cell since PDAC is characterized by a ductal morphology [62]. This hypothesis has been challenged by findings that ductal cells are quite resistant to genetic and chemical perturbations

and do not easily transform into PDACs [63-65]. Moreover, the tumors that develop from ductal cells in genetically engineered mouse models (GEMMs) do not resemble the human tumor morphology. Over the past years, a body of data has been assembled, mainly through *in vivo* mouse models using cell lineage tracing in combination with endogenous $Kras^{G12D}$ activation that shifts the idea towards acinar cells being the cell of origin in PDAC [66]. This is supported by the observation that mice with genetic alterations targeting the acinar compartment develop PDACs that very closely resemble the human disease [67] and recapitulate many human features such as acinar ductal metaplasia, PanIN development, abundant stroma, inflammatory reactions and metastasis under immunocompetent conditions. These murine tumors are essentially indistinguishable from human tumors concerning virtually all of the pathologically established markers (personal communication Irene Esposito 2013). Acinar cells are now considered to undergo ductal reprogramming leading to various types of precursor lesion and eventually PDAC [31]. Many genetically engineered mouse models of PDAC therefore employ acinar-specific promoters to drive Cre-recombinase expression (see 2.5.2).

Pancreatic ductal adenocarcinoma is evolving from various precursor lesions, which may have different cells of origin. These lesions comprise pancreatic intraepithelial neoplasia (PanIN), intraductal papillary mucinous neoplasm (IPMN) and mucinous cystic neoplasm (MCN). Whether acinar ductal metaplasia (ADM) and atypical flat lesions (AFL) are also precursors of PDAC is still under debate (see below).

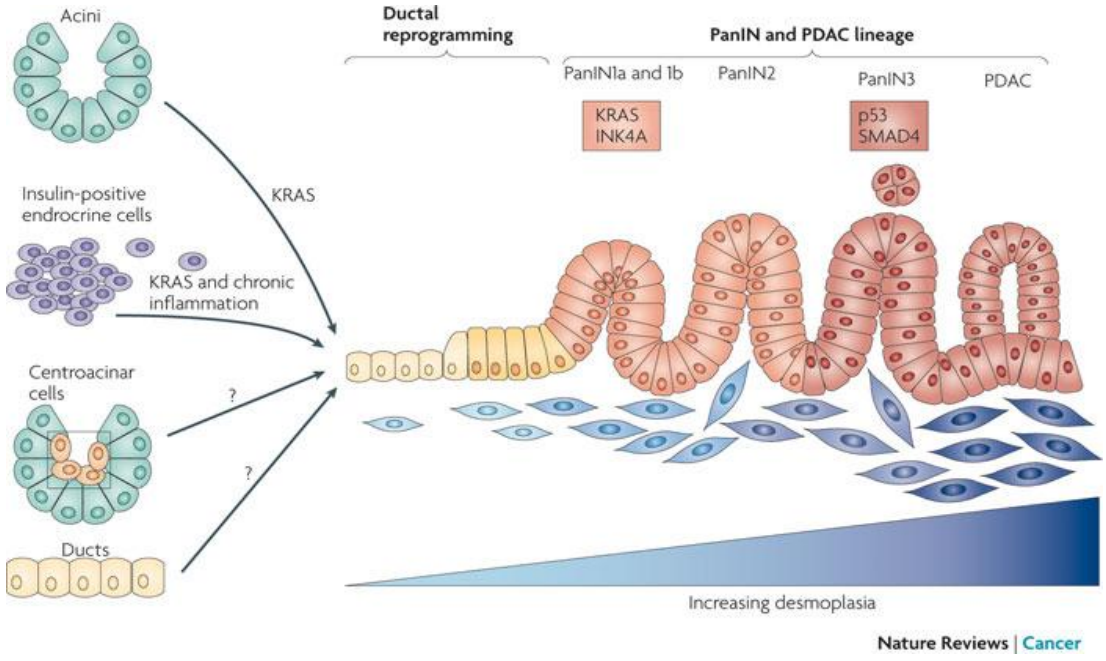

Figure 3 Cell of origin in PDAC and PanIN progression model
Although the cell of origin in PDAC could still be ductal several recent studies hint towards acinar cells or even endocrine cells as cell of origin. It has been suggested that ductal reprogramming under the influence of oncogenic $Kras^{G12D}$ leads to a progressive sequence of pancreatic intraepithelial neoplasia (PanIN) towards PDAC [68]. Reprinted by permission from Macmillan Publishers Ltd: Nature Reviews Cancer 2010 Oct;10(10):683-95, copyright 2010.

PanINs are the by far predominant and best-studied precursor lesions. According to the grade of dysplasia seen they are further subdivided into low-grade PanIN1a and

PanIN1b, intermediate-grade PanIN2 and high-grade PanIN3, while newer classification systems differentiate low-grade and high-grade PanINs. PanIN1 are flat epithelial lesions with tall columnar cells, basolateral nuclei and abundant supranuclear mucin and sometimes papillary, micropapillary or basally pseudostratified architecture. PanIN2 are characterized by nuclear atypia such as loss of polarity, nuclear crowding, enlarged nuclei or hyperchromatism but fall short of nuclear atypia seen in PanIN3 such as loss of polarity, prominent nucleoli or even dystrophic goblet cells. In addition PanIN3 often show “budding” of small clusters of epithelial cells into the duct lumen and luminal necrosis. As PanIN3 do not breach the basal lamina, they are already considered to be carcinoma-in-situ [69, 70] (Figure 3). This histological progression is paralleled by a characteristic genetic progression. Low-grade and intermediate-grade lesions harbor mutations in Kirsten rat sarcoma viral oncogene homolog (Kras) and EGFR [71, 72]. Intermediate dysplastic PanINs moreover acquire inactivating mutations of the tumor suppressor *CDKN2A* (p16) [73] while high-grade lesions often have additional mutations in *TP53* (p53) and *DPC4* (SMAD4) [74].

IPMN, in contrast, are macroscopic lesions usually with a diameter of more than one centimeter in humans [70]. They arise slightly more common in males (~ 60 % of cases) and more often in the head of the pancreas than in the body. Diagnosis occurs usually between 60-70 years of age. Depending on the mucins produced IPMNs can be subdivided into several classes [75]. In addition to the genes that are mutated in PanINs, GNAS and RNF43 are mutated in a major fraction of IPMNs [76, 77].

MCN are mostly unifocal and arise in the body or the tail of the pancreas. They are predominant in females (90 %) and usually diagnosed at the age of 40-50 years [78]. Roughly a quarter of cysts removed from the pancreas are MCN (23 %) [79]. Unlike IPMN they do not significantly involve the ductal system and have by definition a distinctive “ovarian-type” stroma, which expresses estrogen and progesterone receptors [80]. In contrast to IPMN no GNAS mutations were found in MCN [81].

ADM designates a process of cellular plasticity in acinar cells. Upon stress signals such as inflammation acinar cells dedifferentiate and revert to a progenitor-like state with ductal morphology. Stimuli eliciting ADM include for instance cerulein treatment, aberrant Notch signaling [82] and stimulation of the EGFR pathway with TGFα [83]. ADM allows cells to proliferate and thus to repair the damaged tissue and finally re-establish normal acinar differentiation and tissue architecture. On a molecular basis ADM is further characterized through transient upregulation of Wnt/β-catenin [25], NFATc1/ SOX9 [84] and GATA6 [85] signaling. ADM is increasingly believed to be an alternative route to PDAC (for instance via AFL) as opposed to PDAC occurring through the PanIN sequence [86].

So-called atypical flat lesions (AFL) have recently been proposed to be an alternative route to PDAC that might be as important as PanINs [87]. AFL appear in areas of ADM that present as tubular structures with cuboidal cells surrounded by a

characteristic morphological structure of onion shaped loose but highly cellular stroma with whorls of spindle cells [88]. Cytological atypia ranges from enlarged nuclei with prominent nucleoli over a high nuclear to cytoplasm ratio to the presence of mitoses.

Similar to the progression model for colorectal carcinoma [89] a progression model of PDAC [90] has been proposed. This is supported by the findings that some precursors are spatially closely associated with the occurrence of PDAC [91]. Furthermore, there is a positive correlation between the number of lesions present in the pancreas and the detection of PDAC [92] and third that some clinical studies suggested a temporal correlation of patients with proven precursors and the later development of PDAC [93]. Notably, precursor lesions were also found to harbor the same mutation patterns as the particular PDAC in the respective patient [94]. However, it is still under investigation if PDAC arises through a sequence of precursor lesions or if only one or several particular precursor lesions can give rise to PDAC. Furthermore it will be of importance to clarify if PDAC develops from a pool of ill-defined stem cells that still has to be conclusively demonstrated to exist in the pancreas or if terminal differentiated cells revert to a progenitor or progenitor-like state (see 2.2) and are then susceptible to transformation. Thus, precursor lesions are probably the crucial stage to be detected in order to “cure” PDAC even before it arises [74, 95].

PDAC morphology varies from well-differentiated glandular-type ductal patterns to undifferentiated uniform cell masses, which is reflected by the tumor grade. Higher grades, in other words less differentiated tumors are more aggressive and associated with a poorer prognosis [96]. The degree of differentiation might be influenced by the amount of desmoplasia, a strong fibrotic reaction predominant in PDAC. This abundant deposit of extracellular matrix is mainly produced by activated pancreatic stellate cells but probably also by fibroblasts and infiltrating inflammatory cells and consists mainly of fibronectin and laminins. PDACs thus exhibit increased stiffness and elevated hydrostatic pressure. The latter in combination with an already compromised vasculature [97] is a probable cause for the inefficient intratumoral drug delivery seen in PDAC [98]. In contrast, recent reports demonstrated more undifferentiated and aggressive pancreatic cancer when targeting the stromal compartment implying a protective role against PDAC development [99, 100].

Importantly, already in 1988, the genetic driver of PDAC was suggested to be mutations in the Kras gene at codon 12 present in virtually all samples tested [101]. Since then it became evident that Kras mutations are one of the earliest events in PDAC formation being already present in low grade PanINs. Human PDACs display a variety of Kras mutations with an overwhelming majority of $Kras^{G12D}$ [102]. The tumorigenic potential of these different mutations was recently tested in zebrafish resulting in codon 12 mutations to be the most effective [103]. Today $Kras^{G12D}$ (less frequently $Kras^{G12V}$) is the acknowledged driver mutation employed by most of the

mouse models to generate PDAC [104]. Several other mutations have so far been identified to play a role in PDAC progression and metastasis. The ones with the highest frequency of mutations being p53 and SMAD4. The identification of mutations triggered after activation of Kras mutants will hopefully reveal novel drug targets to advance patient therapy.

Efforts have been made to further sub-categorize PDAC. Three different PDAC subtypes have recently been unveiled through unsupervised clustering algorithms of PDAC array data [105]. It is tempting to speculate that different precursor lesions can give rise to PDAC and particular precursors evolve into distinct subtypes of PDAC. PDACs have also been subtyped according to the specific mutation-repair mechanism affected and the different types of chromosomal instability associated. It will be interesting to see the extent of overlap between subtypes found through different methodology. Also, as sequencing has become exponentially cheaper over the last two decades, this technology is very promising for personalized medicine approaches in the future, tailoring the therapy needed according to the mutational status of the respective patient's PDAC entity [105, 106].

2.5 Mouse models of pancreatic ductal adenocarcinoma

2.5.1 Cre-LoxP-Recombination Technology

In order to improve treatment of pancreatic ductal adenocarcinoma two approaches can be followed. First, detection and resection of precursor lesions or very small tumors that cannot yet be visualized with standard imaging techniques and have not yet metastasized [107]. Unfortunately, this approach is not feasible with the current available imaging technology. Furthermore, the onset of metastasis and the resulting window for curative intervention are still controversial [108, 109]. The second approach is to understand the fundamental basic biology of PDAC with its intricate network of signaling pathways leading to all the features making PDAC so disastrous. For both approaches, model systems are needed that closely reflect the human disease. Historically, pancreatic cancer cell line cultures [110], subcutaneous or orthotopic injection of pancreatic cancer cell lines [111-114], treatment of Syrian hamsters with chemical carcinogens [115] and transgenic animals not targeting the endogenous locus of Kras [63, 116, 117] have yielded a body of findings in PDAC research that could not be translated into beneficial outcomes in mouse or human disease. In most cases, tumor histology did not even resemble human PDAC. Furthermore, the lack of pancreas-specific activation of proto-oncogenes limited the interpretation of results due to widespread tumor formation throughout the body. These whole-body deletions also frequently lead to an embryonically lethal phenotype preventing the analysis of the respective gene function in tumorigenesis. For these reasons, Cre/LoxP technology was eventually employed to drive tumor formation in mouse models. The gene coding for Cre recombinase is absent in mammalian genomes but may be introduced by homologous recombination. This enables the replacement of the coding region of a gene of interest with the Cre coding sequence and results in Cre expression regulated by the respective

promoter. Homotetrameric Cre-recombinase then recognizes LoxP sites, specific 34 bp DNA recognition sequences for recombination [19]. Depending on LoxP sequence orientation Cre recombinase either excises the interjacent part (tandemly oriented) or flips its orientation. This enables inactivation of genes or part of genes if flanked by LoxP sites or activation of genes if a LoxP-flanked stop codon is introduced before the transcription start site of the gene of interest (see Figure 4). To allow temporal in addition to spatial control of recombination Cre recombinase can be fused to estrogen receptor (ER) variants [118, 119]. Injection or oral administration of tamoxifen at particular time points unmasks a nuclear localization signal within the ER variant dragging the fusion protein into the nucleus, where Cre will recombine available LoxP sites [120].

Similar results can be obtained with the Flp/Frt recombinase technology [121] or the recently discovered site-specific recombination system Dre/Rox [122]. The combination of Cre and Flp systems allows the alteration of different genes in a spatially and temporarily controlled manner. Thus, as described by Schönhuber *et al.*, development of PDAC can be initiated in a Cre/LoxP-independent manner and allows to modulate other genes at later stages in tumor development recapitulating human events more closely. Inactivation of genes in already existing tumors also validates their role in tumor maintenance and progression and may be informative for potential beneficial therapeutic approaches.

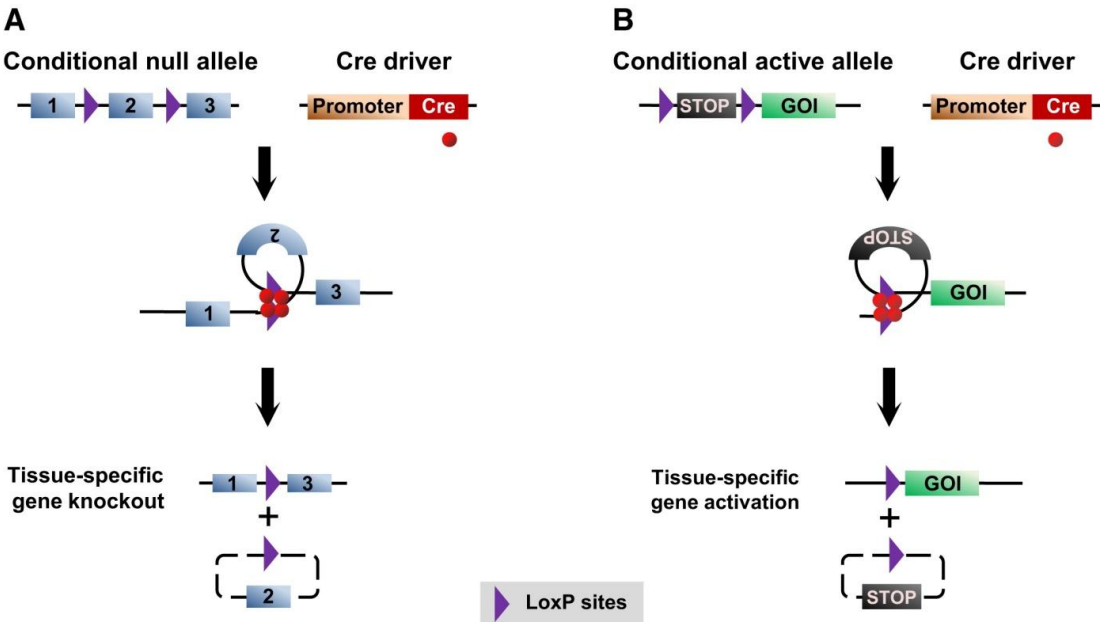

Figure 4 Mechanism of the Cre-LoxP recombination technology
(A) To generate null alleles, exon 2 is flanked by LoxP sites. Cell lineage specific promoters drive the expression of Cre recombinase in selected tissues. Cre recombinase then cuts and rejoins DNA at the LoxP sites thereby excising exon 2 from the genome (B) To activate a gene of interest (GOI) with Cre recombinase, it is first silenced with a LoxP flanked STOP codon. Recombination excludes the STOP codon from the genome and transcription can proceed to drive tissue-specific expression of the GOI. Reprinted from Cell Metabolism, 2013 Jul 2;18(1):9-20, M.A. Magnuson, A. B. Osipovich, Pancreas-Specific Cre Driver Lines and Considerations for Their Prudent Use, ©2013, with permission from Elsevier.

2.5.2 Pancreas-specific Cre driver lines and Kras^{G12D}

In 2003, Hingorani *et al*. targeted the endogenous Kirsten rat sarcoma (Kras) gene in the pancreas and generated a mouse model that for the first time closely resembled human PDAC. Glycine 12 of Kras was replaced by aspartic acid (G12D) and a LoxP-stop-LoxP (LSL) cassette was inserted between promoter and coding region [67]. Expression of pancreas-specific Cre recombinase excises the stop cassette from the LSL-Kras^{G12D} construct and now allows transcription of oncogenic Kras. Other variants of mutated Kras constructs exist [123]. Expression of Cre recombinase from the pancreas-specific Ptf1a or Pdx1 promoter during development (see 2.2) for activation of Kras^{G12D} results in mice, of which 50 % will have developed PDAC at one year of age. These tumors very closely resemble human PDACs, including pancreatic intraepithelial neoplasia, acinar ductal metaplasia, abundant stroma, inflammatory reactions and metastasis under immunocompetent conditions and are indistinguishable from human tumors regarding most of the pathologically established markers (personal communication Irene Esposito). Nevertheless, several issues must be taken into account. These include activation of mutated Kras in other organ systems expressing Ptf1a, for instance in retina and cerebellum [124, 125] or Pdx1, for example in skin [126]. As a result, extra-pancreatic tumors may also develop in these models. Additionally, Cre is already expressed during murine embryonic development, likely not a typical scenario in human tumorigenesis and thus in contrast to human PDAC that is believed to develop from sporadic mutations acquired by “adult” cells. In mice, precursor lesions can already be detected a few weeks after birth. They then progressively inactivate or acquire mutations in numerous other genes (see 2.4.3.2), mostly well-known tumor suppressor genes such as p16 or p53 (see 2.6.2.1), to give rise to full blown tumors in the context of activated Kras^{G12D}. As a result, mice – similar to men - develop tumors at an advanced age.

Thus, these genetically engineered mouse models (GEMMs) allow to assess the distinctive impact of particular genes/proteins on PDAC initiation and progression and to disentangle some of the signaling networks fostering PDAC [127]. At the same time, they allow us to assess the dangers and the clinical potential of a particular pathway for future translational approaches.

2.6 Molecular signaling pathways in PDAC

Several pathways active in healthy pancreatic tissue and their changes in precursor lesions and PDAC have been scrutinized and there is virtually no pathway that has not been implicated in PDAC development. Whereas alterations in low-grade PanINs include for instance Kras and EGFR, mutations in p16/p19 are found in intermediate-grade PanINs and loss of p53 is a feature of high-grade dysplastic lesions and PDAC. The pathways affected regulate growth and survival, inflammation, morphogenesis and embryonic development.

2.6.1 Protooncogenes

2.6.1.1 Kras

The mostly affected and most important pathway in PDAC is probably the mitogen activated protein kinase (MAPK) cascade, especially the Ras-Raf-MEK-ERK module integrating extracellular growth cues. With Kras being mutated or epigenetically misregulated in already >92 % of PanIN1 and nearly 100 % in PanIN3 or PDAC [102], this protein is the unequivocal driver of PDAC. Physiologically, Kras is active in a guanosine triphosphate (GTP) bound state. With the help of GTPase-activating proteins (GAPs), it hydrolyses GTP to GDP thereby inactivating itself. GDP is released from Kras with the help of guanine nucleotide exchange factors (GEFs) enabling Kras to be activated again by binding GTP. Active Kras exerts a plethora of functions centered on growth, differentiation and survival [128]. In PDAC, the most commonly found mutations affect codon 12 of Kras, changing glycine (G) to aspartic acid (D) or valine (V). They greatly diminish the ability of Kras to hydrolyze GTP to GDP and trap it in its GTP-bound active state. This renders the cell independent of external growth stimuli and enables rapid proliferation if other constraints such as terminal differentiation are lacking [129]. The importance of Kras for PDAC is further highlighted by a report showing that sustained activation of $Kras^{G12D}$ is required for maintenance of precursor lesions and the tumor itself, a process called “oncogene addiction” [130]. The major downstream pathways of mutated Kras comprise (1) the phosphorylation cascade of MAP3Ks (such as Raf) phosphorylating MAP2Ks (for instance MEK) phosphorylating MAP1Ks (for example ERK), which then integrate and process proliferation signals [131], (2) the PI3K/PDK1/AKT survival pathway [132] and (3) the RalGEF pathway required for metaplastic transdifferentiation [133, 134].

2.6.1.2 Rac1

Rac1 is a representative of the second major MAPK module relaying morphogenic signals in the cell. This member of the Rho family of GTPases is important for the transdifferentiation process of ADM. Knockout of Rac1 inhibited the formation of ADM in cerulein-induced acute pancreatitis and resulted in reduced formation of ADM, PanIN and PDAC in the $Kras^{G12D}$ background. In the rare cases where PDAC developed mice showed a markedly prolonged survival [135]. Although constitutively active Rac1 does not induce pancreatic carcinogenesis in the absence of oncogenic Kras [132] array-comparative genomic hybridization revealed RIOK3, a Rac1 interacting protein and PAK4 as players in PDAC motility and invasion [136]. Moreover, cooperation of mutant p53 and oncogenic Kras activated RhoA in spatially confined areas of the cell to drive invasion in 3D culture [137]. Thus although Rac1 is not an autonomous driver of PDAC, it likely plays an important role in PDAC development and metastasis.

2.6.2 Tumor suppressors

2.6.2.1 p53 and p21

p53 prevents the formation of a huge variety of human cancers [138]. In agreement with a key role in tumor suppression alterations in p53 activity are also detected in high-grade PanINs and 84 % of PDACs. Inactivating mutations of p53 make up for roughly 75 % while another 9 % have deleted the p53 gene partially or completely [139]. Besides inactivating mutations and deletions of the p53 gene hypermethylation of the p53 promoter region can lead to a loss of p53. One essential function of p53 in delaying tumors is the homotetrameric transactivation of its targets, the most important probably being p21. This protein inhibits the progression through the G1/S cell cycle checkpoint by inhibiting cyclin-dependent kinases (CDK), such as CDK2, CDK1 and CDK4/6 complexes. p21 is further known to be an important player in the cellular senescence pathway, inhibiting extensive cellular proliferation of terminally differentiated cells [140]. Whether p21 acts as a tumor suppressor in PDAC is still under investigation [141, 142]. Under physiological conditions, p53 is regulated by posttranslational modifications [143]. For example, JNK phosphorylates p53 thereby marking it for ubiquitination and subsequent proteasomal degradation [144]. Many p53 mutations impair this proteasomal degradation. Accumulated mutated p53, however, is unable to transactivate its target genes but still acts as a scaffold protein, thereby resulting in a dominant negative phenotype [145]. Stress signals inhibit JNK-mediated phosphorylation of p53 between residues 97 to 155 and results in phosphorylation of the N-terminus instead, which disrupts binding of Mdm2 to p53. In the absence of Mdm2, p53 accumulates, translocates into the nucleus and binds promoter target sequences [146].

Knockout or mutation of p53 usually greatly accelerates PDAC tumor formation. The lifespan of $Kras^{G12D}$ mice with homozygous deletion of p53 is dramatically shortened to roughly 150 days due to big desmoplastic tumors that metastasize to liver (63 %), lung (44 %), diaphragm (37 %), adrenals (22 %) and less frequently to other sites [147]. Notably, deletion of p53 in mice overcomes p21-induced senescence and growth arrest [145]. In a recent study, it was reported that p53 mutant mice show a greater tendency to metastasize in contrast to p53 null mice, although this issue is still a matter of debate. Further investigation into the invasive capabilities of p53-deficient versus p53-mutant tumors revealed a pool of cells in p53 mutant mice with increased RhoA activity, which were absent in the p53-deficient mice [137]. Mutated p53 ($p53^{R172H}$) does not only increase invasiveness but also chromosomal instability. Heterozygous mutant p53 generated a selection pressure against the remaining p53 wild type allele and was associated with aberrant chromosomal rearrangements and nonreciprocal translocations [147].

2.6.2.2 p16 and p19

Using alternate reading frames, both $p16^{INK4A}$ (p16) and $p19^{ARF}$ (p19) are derived from the same gene, the Ink4A/Arf locus. Inactivation of p16/p19 is already found in intermediate grade PanINs and in up to 98% of PDAC [148-150]. p19 inhibits Mdm2-

mediated degradation of p53 leading to increased p53 levels. However, p53-independent functions of p19 have also been described. p16 inhibits the phosphorylation of the retinoblastoma (Rb) protein. Accordingly, cyclin-dependent kinase 4 (CDK4) and CDK6 cannot dissociate from their D-type cyclins anymore, restraining cells in G1 phase. Continued activation of p16 suppresses tumor formation by oncogene-induced senescence (OIS) [151]. Specific targeting of p16 in $CKp53^{LoxP/LoxP}$ background resulted in significantly reduced tumor latency suggesting cooperative roles for p16 and p53. Interestingly, the majority of tumors arising in $CKp53^{LoxP/LoxP}$ or $CKp16^{LoxP/LoxP}$ mice were ductal adenocarcinomas while p16 deficiency in combination with loss of p53 led to tumors with anaplastic features [152]. Notably, it has recently also been shown that deficiency of p16 is sufficient for $Kras^{G12D}$-induced transformation of human pancreatic epithelial cell lines [153].

2.6.3 Inflammatory pathways

2.6.3.1 Signal transducer and activator of transcription (STAT)

Of all STATs in the pancreas STAT3 has probably been characterized most extensively. Although this transcription factor is involved in cellular self-renewal, cancer cell survival and inflammation, it is dispensable for pancreatic development and homeostasis. Upon phosphorylation at tyrosine 705, STAT3 homo- or heterodimerizes (via its Src homology-2 (SH-2) domains) with other STAT proteins and translocates into the nucleus where it induces expression of its target genes. Activation canonically follows IL6 mediated activation of the glycoprotein (gp) 130 receptor, which in turn activates Janus-activated kinases (JAK) proteins that phosphorylate STAT3. Other triggers for STAT3 signaling include leukemia inhibiting factor (LIF), oncostatin M and IL11 [154]. As part of a negative feedback loop, SOCS3, an inhibitor of STAT3 signaling is also induced upon STAT3 activation [155]. Constitutive activation of STAT3 has been reported in 30 to 100 % of human tumors [156] and STAT3 has been shown to play a central role in the development of ADM [157] in Pdx1 overexpressing mice. Inactivation of STAT3 not only inhibits the formation of early precursor lesions but also attenuates the progression to invasive PDAC [158]. Interestingly, cancer cells themselves produce only low levels of IL6. The predominant sources are infiltrating inflammatory cells, especially macrophages, that secrete a soluble IL6 receptor to promote IL6 trans-signaling. Deletion of STAT3 from the pancreas however, did not prevent the initiation of precursor lesions, but blocked their progression, while deletion of Socs3 from the pancreas accelerated PDAC development [159]. This establishes a strong link between myeloid cells mediating inflammation and PDAC development.

2.6.3.2 Nuclear factor kappa B (NF-κB)

The transcription factor nuclear factor kappa B (NF-κB) is a key regulator of inflammation and proliferation. Constitutive NF-κB activation in chronic pancreatitis is risk factor for PDAC. Pancreatic cancer cells themselves acquire growth advantages probably through auto- and paracrine loops of expressed death ligands, which trigger NF-κB signaling. Notably, constitutive NF-κB signaling has also been

implicated in chemoresistance of PDAC. Important upstream players of NF-κB are interleukin (IL)1α, IL1ß and IL8, which have been shown to foster PDAC. Nevertheless, the relative contribution of NF-κB signaling to PDAC development is still controversial and there have been reports denying a profound involvement of this transcription factor in PDAC development [32].

2.6.4 Growth and Developmental pathways

2.6.4.1 PI3K/AKT

The PI3K/AKT survival pathway recently received a lot of attention due to its prognostic value in PDAC [160] and its already established drugability [161]. While AKT1 is overexpressed in 20-70 % of human PDAC and AKT2 is overexpressed in 10-20 % of cases, PTEN, a negative regulator of AKT signaling, is lost in about 60 % of PDAC [162-165]. The involvement of the PI3K-PDK1-AKT signaling axis in PDAC development has been demonstrated by mice expressing p110α^{H1047R}, a dominant active subunit of the PI3 kinase [132]. The inhibitory PI3K phosphatase PTEN was further demonstrated to slow down Kras-induced PDAC progression [166]. Mechanistically, it has been suggested that PI3K signaling induces a 'weak' senescence program bypassing 'strong' Kras-induced senescence [167].

2.6.4.2 SMAD4

SMAD4 is a downstream transcription factor of transforming growth factor ß (TGFß), bone morphogenetic protein (BMP) and activin signaling. It is mutated in about 50 % of human PDACs [168]. Conditional inactivation of SMAD4 did not affect embryonic development or maintenance of pancreatic architecture but induced either an IPMN or a MCN phenotype in the Pdx1$^{Cre/+}$;Kras^{G12D} background. While Bardeesy *et al*. detected a phenotype with cystic lesion similar to IPMN in the human context [169], Izeradjene *et al*. observed an MCN phenotype [170]. Besides these effects, SMAD4 has also been implicated in the upregulation of epithelial-mesenchymal transition (EMT) signaling as assessed by slug, vimentin or E-Cadherin markers [169, 171]. Furthermore, also overexpression of TGFα in the Kras^{G12D} background results in cystic lesions resembling IPMN [172]. This pancreatobiliary type was associated with increased STAT3 and EGFR signaling. Representative for aberrant receptor tyrosine kinase signaling, the latter has been shown to be crucial for PDAC initiation [173].

2.6.4.3 Notch pathway

Notch signaling is essential for pancreatic development and different Notch isoforms either promote or block progression to PDAC. During embryonic development, low to intermediate levels of Notch signaling induce the expression of Sox9 which in turn triggers the expression of Ngn3. Later on, endocrine differentiation by Ngn3 downregulates Sox9 in a negative feedback loop. In contrast to that, high Notch signaling levels induce the expression of the Notch target gene Hes1 which represses Ngn3, thereby maintaining Sox9 expression resulting in ductal differentiation [174]. Knockout of Notch1 or chemical inhibition of Notch signaling was

shown to impair pancreatic regeneration [26]. Furthermore, overexpression of Notch in adult pancreatic acinar cells has been shown to induce transdifferentiation to ductal intraepithelial neoplasia [175], which is in line with a report suggesting that knockout of Notch2 but not Notch1 stops progression of PanINs and inhibits development of PDAC [176]. In another study Notch1 was found to function as a tumor suppressor and knockout of Notch1 increased tumor incidence and progression [177].

2.6.4.4 Sox9

SRY-related HMG box factor 9 (Sox9) is a transcription factor involved in the embryonal process of generation of bipolar cells able to adopt endocrine or ductal fates [174]. In physiologic pancreatic architecture, Sox9 is expressed in ducts and centroacinar cells that connect the ductal system to the terminal acinar berries [13]. In duct ligation-induced pancreatitis, Sox9 is required for strong acinar-ductal reprogramming [178]. Importantly, virtually all precursor lesions in the pancreas from ADM over MCN, IPMN to PanIN and PDAC aberrantly express Sox9. Though not absolutely required for the formation of ADM, Sox9 was shown to be necessary for acinar reprogramming into PanIN. Sox9 destabilized the acinar state and promoted the expression of ductal markers [179]. All in all, Sox9 seems to cooperate with mutated Kras to increase acinar plasticity and thus initiate ADM and PanIN development and potentially progression to PDAC.

With oncogenic $Kras^{G12D}$ relaying growth stimuli and Rac1 relaying morphogenic clues, two of the major MAP kinase cascade modules have already been assessed in PDAC. At the start of this PhD project the role of the cellular stress response integrated by p38 and JNK kinases, the third major module in MAP kinase cascade had not been investigated yet.

2.7 c-Jun N-terminal kinase (JNK) signaling pathway

2.7.1 JNK signaling pathway

c-Jun N-terminal kinase (JNK) is also called stress activated protein kinase (SAPK). Together with their genetic relatives the p38 kinases, they form a module in the mitogen activated protein kinase (MAPK) cascade responsible for relaying, amplifying and integrating stress signals [180]. So far, JNK signaling has been shown to predominantly regulate cellular differentiation, cell growth, survival and apoptosis [181]. Three distinct isoforms of JNKs have been described: JNK1 (MAPK8), JNK2 (MAPK9) and JNK3 (MAPK10). While JNK1 and JNK2 are ubiquitously expressed JNK3 is mainly found in brain, testis and heart [182]. Furthermore, JNKs are alternatively spliced into α- and ß-isoforms. These isoforms consist of 384 or 427 amino acids and run at roughly 46 and 55 kDa, respectively in the SDS-PAGE [183]. JNKs belong to the Ser/Thr class of protein kinases and are further regulated by JNK-interacting proteins (JIPs), which serve as signaling scaffolds [184]. The functional redundancy of JNK1 and JNK2 isoforms is still under debate and seems to depend on the specific cellular context.

The cell detects not only extracellular stress such as osmotic disturbances or cytokines signaling but also intracellular stress such as UV-induced DNA damage. The stress signal is then relayed from MAP3Ks to MAP2Ks and eventually to the JNK proteins, which are MAPKs. While a diverse range of MAP3Ks (e.g. TAK1, MEKK1-4 or MLK2,3) has been identified, only two kinases (MKK4/7) are known to phosphorylate JNK directly (see Figure 5). MKK4 and MKK7 phosphorylate the conserved TXY tripeptide motif in the activation loop, also called T-loop, of JNKs. This activation can both take place in the cytoplasm and the nucleus of the cell. Notably, MKK4 has also been reported to crossactivate p38 kinases, which constitute the second major stress relaying and integrating pathway of the cell [185]. Once activated, JNKs use an ATP-dependent mechanism to phosphorylate various target proteins such as its name-giver and major target c-Jun. Upon phosphorylation of serine 63 and serine 73 c-Jun can heterodimerize with Fos proteins to form the transcription factor AP-1 [186]. Other downstream targets include p53, γH2AX, Bax, Bak, Bcl2, Bcl-XL and 14-3-3 proteins [180]. JNK signaling is turned off by specific and unspecific phosphatases such as MAPK phosphatases (MKPs) [187, 188] or E3-ubiquitin ligases such as SPOP [189]. JNK signaling further depends on the temporal pattern of activation. Transient activation of JNK proteins promotes cell survival while prolonged JNK activation triggers apoptosis [190]. This difference has been suggested to stem from differential phosphorylation kinetics of Bcl-2 depending on the particular partner Bcl-2 is bound to [191].

Compound knockout of JNK1 and JNK2, however, results in an embryonic lethal phenotype with neural tube closure and brain defects during midgestation [192]. Furthermore, epithelial development in the epidermis, intestine and lung is impaired with markedly reduced EGF receptor function [192]. Thus, initial experiments on JNK signaling were performed in mouse embryonic fibroblasts (MEFs) of JNK knockout mice or conducted in the presence of JNK inhibitors. Several inhibitors of JNK proteins have been discovered so far, varying considerably in inhibitory concentration 50 % (IC_{50}) and specificity. One of the more common JNK inhibitors is SP600125 [193] with a low IC_{50} of ~0,1 µM but considerable inhibition of other kinases [194]. A more specific inhibitor was recently invented named JNK-IN-8 with an IC50 of 4.7, 18.7 and 0.98 nM for JNK1, JNK2 and JNK3 respectively. Specificity was demonstrated by the KINOMEscan methodology and radioactive-based enzymatic assays of the National Centre for Protein Kinase Profiling in Dundee.

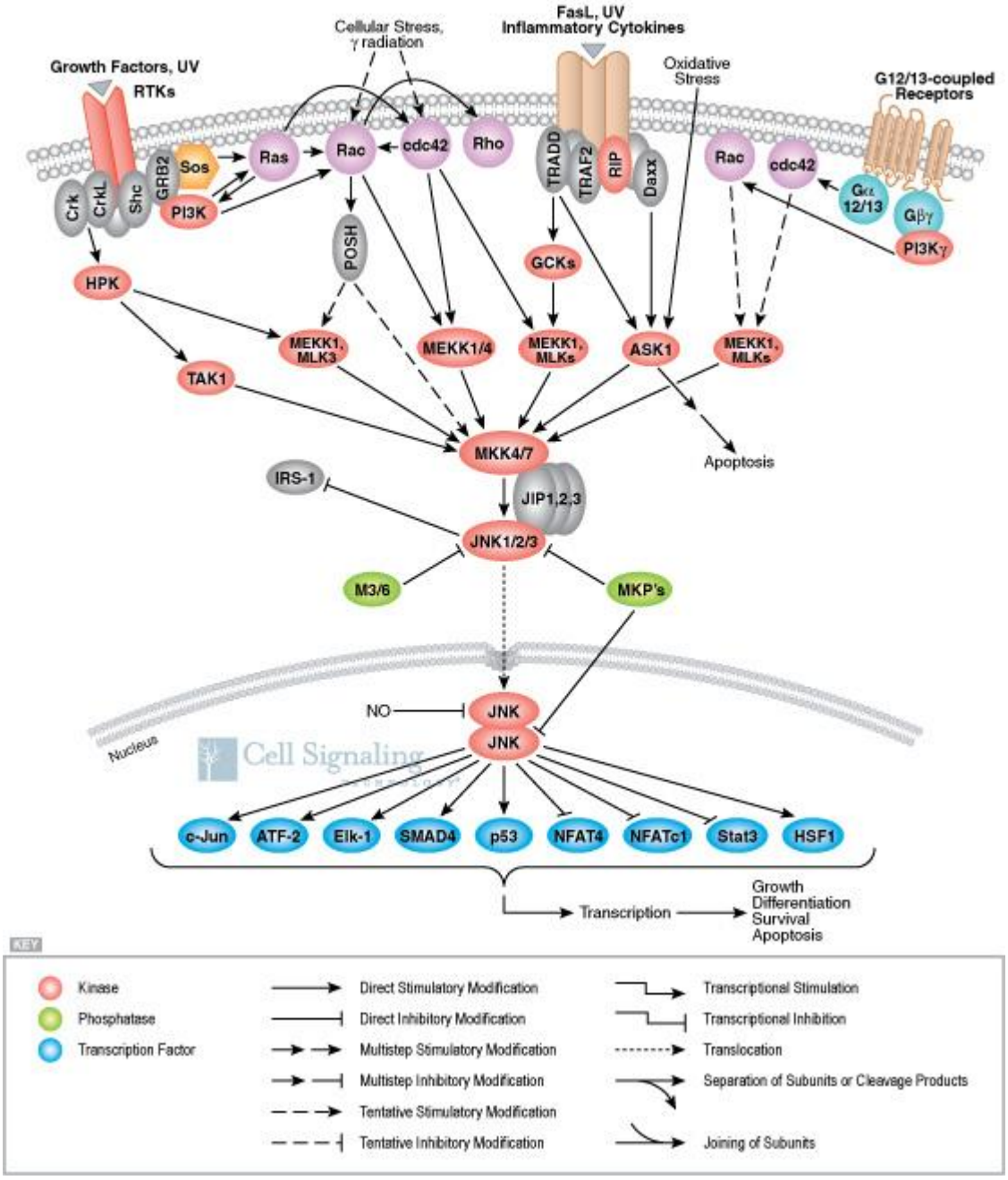

Figure 5 Signaling network of c-Jun N-terminal kinases
Different forms of stress such as aberrant receptor tyrosine kinase (RTK) signaling, UV light or others converge on MKK4 and MKK7 the JNK upstream kinases. These phosphorylate JNKs, which themselves phosphorylate their targets, mainly transcription factors such as c-Jun, p53 and NFATc1. Illustration reproduced courtesy of Cell Signaling Technology, Inc. (www.cellsignal.com).

2.7.2 JNK signaling in non-cancerous disease

JNKs have been implicated in the extension of life span. It was shown that JNK influences aging of eukaryotic cells in Drosophila and C. elegans through FOXO phosphorylation [195, 196]. JNK signaling as a major cell signaling pathway is involved in many diseases. In the immune system JNKs have been implicated in controlling T-Helper cell balance [197] and disruption of JNK2 attenuated autoimmune diabetes [198]. Furthermore, JNKs have been implicated in encephalomyelitis, another autoimmune disease, where they regulate the expression of IL10 [199]. Also JNKs

play a role in rheumatoid arthritis, where they regulate the expression of metalloproteinases and TNFα [200]. In atherosclerosis JNK2 but not JNK1 has been shown to attenuate foam cell formation of macrophages and reduced plaque formation [201]. Further to type1 diabetes, knockout of JNK1 or JIP1 led to resistance against obesity and insulin resistance after high-fat diet [202]. Recently, a JNK dependent regulation of ER stress in an XBP1 knockout mouse was shown to cause spontaneous enteritis with increased susceptibility to colitis and inflammatory bowel disease [203]. JNK signaling, furthermore, has also been implicated in a variety of nervous system disorders, such as the function of GABAergic motoneurons, Purkinje cell misalignment during embryonal development, reduced apoptosis after induced ischemic stroke, Parkinson's disease, Alzheimer's disease, Pick's disease, and other cortical neurodegenerative diseases [204, 205].

2.7.3 JNK signaling in cancer

The importance of JNK signaling in tumor development was first noticed by the transforming capabilities of c-Jun in cooperation with Ha-Ras [206]. This is further substantiated by the finding that c-Jun mutated at Ser-63 and Ser-73, the JNK target site, is unable to rescue transformation-defective c-Jun-null fibroblasts [207]. However, while primary rat embryonic fibroblasts could be transformed with high c-Jun activity, chicken embryonic fibroblasts showed an inverse correlation between transformation and c-Jun activity [208]. Other groups furthermore reported increased tumorigenic potential of JNK-deficient MEFs compared to wild type cells [209]. This already pointed to the context specific role of JNK signaling that since then has been emerging through various other studies with conditional knockout mice.

JNK2-deficient mice and mice harboring specific MKK4 deletion in keratinocytes showed resistance to chemical-induced carcinogenesis protocols [210, 211]. Quite to the opposite JNK1-deficient mice showed an increased susceptibility to papillomas [212]. On the other hand, JNK1-deficient mice have decreased incidence of gastric cancer under N-methyl-N-nitrosurea treatment [213] and mice with a deficiency in JNK1 or a compound deficiency in JNK1 and JNK2 are less susceptible to diethylnitrosamine-phenobarbital (DEN)-induced hepatocellular carcinomas (HCC) compared to wild type littermates [214]. Similar results were obtained by inhibiting JNK signaling with D-JNKI1 in DEN-induced HCC settings [215]. This tumor promoting effect has been suggested to arise from JNKs ability to upregulate c-Myc and cyclin D1 expression.

Interestingly other groups reported JNKs as tumor suppressors. For instance, mice with MKK4-deficiency developed lung tumors earlier in the $Kras^{G12D}$ background than their littermates [216]. Also, loss of JNK1 or JNK2 enhanced mammary tumor development in polyoma middle T antigen transgenic mice [217]. Similarly, large prostate tumors arise in conditional JNK1/JNK2-deficient prostate epithelium in phosphatase and tensin homolog (Pten)-deficient mice [218]. This effect could stem from increased p53 protein stability upon phosphorylation by JNK that might contribute to oncogene-induced senescence (OIS) and cell cycle arrest.

Furthermore, disruption of JNK1 in pre-B-cells inhibited transformation *in vitro and in vivo* [219]. In addition, cancer genome sequencing has revealed clusters of mutations in multiple genes of the JNK pathway, especially MKK4 in various tumors such as pancreas, lung, breast, colon and prostate making JNKs a putative target for cancer therapy [220]. As JNK signaling seems to be cell type and isoform specific and with its dual role in different cancers care must be taken in the decision to target JNKs.

2.7.4 JNK signaling in pancreatitis and PDAC

Regarding the pancreas, conflicting data has been published so far in the setting of acute pancreatitis. Two reports are in favor of a protective effect of JNK on pancreatitis. Treatment with SP600125 attenuated JNK and ERK signaling and protected mice from cerulein-induced histological damage [221]. Also melittin, a compound from bee venom, has been shown to inhibit cerulein-induced pancreatitis via inhibition of the JNK pathway [222]. In contrast, betacellulin, a ligand of the epidermal growth factor receptor was shown to activate JNK signaling and attenuated severity of induced acute pancreatitis [223].

Interestingly, the importance of JNK signaling in PDAC development has been stressed by sleeping beauty mutagenesis and other deep sequencing screens revealing several gene alterations in the JNK signaling pathway in PDAC. The gene affected the most in all screens was MKK4, one of the JNK upstream kinases [224, 225].

In *in vivo* pancreatic cancer JNK has been involved in IL1ß mediated inhibition of integrin signaling leading to increased migratory potential of pancreatic cancer cells [226]. Okada *et al*. recently suggested that systemic inhibition of JNK depletes cancer stem cells and cancer stem-like cells from pancreatic tumors, although not inhibiting tumor bulk growth and implicated JNK as a target for cancer therapy [227]. This has been tested by treatment of mice with SP600125 or siRNA against JNKs and resulted in reduced growth of pancreatic cancer cell lines and decreased growth of murine pancreatic cancer and prolonged survival in $Ptf1a^{Cre/+};Kras^{G12D};Tgfbr2^{LoxP/LoxP}$ mice [228]. Importantly, knockout of MKK4 and MKK7 in inducible $Pdx1^{CreER/+};Kras^{G12D}$ mice sensitized pancreatic epithelial cells to $Kras^{G12D}$-induced mPanIN formation and strongly accelerated development of malignant lesions [229]. This report also stressed the requirement of MKK4 and MKK7 for acinar regeneration in the setting of induced-acute pancreatitis and suggested that STAT3 signaling might be involved in the initiation and progression to PDAC.

3 Aims of this thesis

Main aim of this thesis was the assessment of the contribution of JNK proteins on the initiation and progression of PDAC and the analysis of the underlying signaling networks of a potential phenotype in genetically engineered mouse models (GEMM). To this end a conditional knock-out model for JNKs in the background of the well-established Ptf1a$^{Cre/+}$;Kras^{G12D} PDAC model was employed. In addition, the impact of STA3 signaling on the course of compound JNK-deficiency in pancreas-specific Kras^{G12D} mice was investigated. This data will hopefully result in a better understanding of PDAC biology and therefore enable us to enhance early discovery of relevant precursor lesions and assessment of putative therapeutic targets.

4 Material and Methods

4.1 Material

4.1.1 Devices

iDia	IME-DC	Hof, Germany
Stripettor Plus	Corning	Tewksbury, USA
Hera Cell 240 Incubator	ThermoScientific	Waltham, USA
ASP300S	Leica Biosystems	Nussloch, Germany
eg1150h	Leica Biosystems	Nussloch, Germany
MicromHM355S	ThermoScientific	Waltham, USA
Microm HM560 (Cryotome)	ThermoScientific	Waltham, USA
ImagerA1	Zeiss	Oberkochen, Germany
Axiovert200M	Zeiss	Oberkochen, Germany
GFL Typ1003	GFL	Burgwedel, Germany
T100 ThermalCycler	BioRad	Hercules, USA
Maxwell	Promega	Madison, USA
Nanodrop 2000	Peqlab	Erlangen, Germany
LightCycler480	Roche	Manheim, Germany
SilentCrusherM	Heidolph	Schwabach, Germany
Centrifuge 5415D	Eppendorf	Hamburg, Germany
Centrifuge 5810R	Eppendorf	Hamburg, Germany
Centrifuge 5415R	Eppendorf	Hamburg, Germany
MC6400	Hartenstein	Würzburg, Germany
Consent E844	Sigma Aldrich	Munich, Germany
GelCaster System	BioRad	Hercules, USA
GelDoc	BioRad	Hercules, USA
MW7809	Severin	Sundern, Germany
Sonoplus UW2070	Bandelin	Berlin, Germany
KS38R425	Siemens	Munich, Germany
GS34V420	Siemens	Munich, Germany
Hera Freeze	ThermoScientific	Waltham, USA
Thermomixer Compact	Eppendorf	Hamburg, Germany
XL-120	Taylor Wharton	Mildstedt, Germany
Ice machine	Ziegra	Isernhagen, Germany
Multiskan FC	ThermoScientific	Waltham, USA
ResearchPlus	Eppendorf	Hamburg, Germany
Glas bottles	Schott	Mainz, Germany
MiniPROTEAN	BioRad	Hercules, USA
Powerpac Basic	BioRad	Hercules, USA
Hyperprocessor	GE	Freiburg, Germany
V150	Systec	Wettenberg, Germany
MacMini	Apple	Cork, Ireland
440-43N	Kern	Balingen, Germany

TP214	DenverInstrument	Bohemia, USA
Duomax1030	Heidolph	Schwabach, Germany
MR3001	Heidolph	Schwabach, Germany
Reax top	Heidolph	Schwabach, Germany
Surgical scissors	FST	Heidelberg, Germany
TR118	OregonScientific	Buckinghamshire, UK
CL-1000 (UV crosslinking device)	UVP	Upland, CA, USA

4.1.2 Software

LightCycler 480 Release 1.5.0 SP4
Prism
GSEA software (broadinstitute.org)
Adobe Illustrator
Adobe Photoshop
Microsoft Office
UCSC cancer genome browser
Aperio Imagescope

4.1.3 Consumables, chemicals and diagnostics

Accucheck Sensor Comfort Pro	Roche	Mannheim, Germany
Petri dish 6 cm (628161)	GreinerBioOne	Frickenhausen, Germany
Petri dish 10 cm (351029)	VWR	Darmstadt, Germany
6-well plate (353224)	VWR	Darmstadt, Germany
96-well plate, flat bottom (353072)	VWR	Darmstadt, Germany
15/50 ml plastic tubes	GreinerBioOne	Frickenhausen, Germany
8-well culture slide (354118)	Corning	Amsterdam, Netherlands
Stericup Express Plus	Merck	Darmstadt, Germany
TEMED	Carl Roth	Karlsruhe, Germany
APS	CarlRoth	Karlsruhe, Germany
peqGold DNA ladder	Peqlab	Erlangen, Germany
Scalpell No23	Feather	Osaka, Japan
PBS powder	Merck	Darmstadt, Germany
D-PBS	LifeTechnologies	Darmstadt, Germany
DMEM	LifeTechnologies	Darmstadt, Germany
Non-essential amino acids (NEAA)	Life Technologies	Darmstadt, Germany
L-Glutamine	LifeTechnologies	Darmstadt, Germany
PenStrep	LifeTechnologies	Darmstadt, Germany
Trypsin/EDTA	LifeTechnologies	Darmstadt, Germany
Stripetten	GreinerBioOne	Frickenhausen, Germany
Histosecpastillen	Merck	Darmstadt, Germany
Embedding cassettes	BioOptica	Milano, Italy
HCl	Merck	Darmstadt, Germany
Ammonia	Merck	Darmstadt, Germany
PFA 4%	SantaCruz	Heidelberg, Germany

Ethanol 70/86/96/100%	Otto Fischar	Saarbrücken, Germany
Water	Braun	Melsungen, Germany
Roti Histol	Carl Roth	Karlsruhe, Germany
Tissue-Tek	SakuraFinetek	Staufen, Germany
Hematoxylin Gill III	Merck	Darmstadt, Germany
Eosin 2 %	Waldeck	Münster, Germany
ImmEdge	Vector	Burlingame, USA
Pertex	Medite	Burgdorf, Germany
FCS	LifeTechnologies	Darmstadt, Germany
GlacialAcid	Merck	Darmstadt, Germany
EDTA	Carl Roth	Karlsruhe, Germany
Unmasking stock solution	Vector	Burlingame, USA
Proteinase K	Roche	Mannheim, Germany
Hydrogenperoxide 30%	Merck	Darmstadt, Germany
Triton X-100	Sigma Aldrich	Munich, Germany
Tween	Carl Roth	Karlsruhe, Germany
ABC-Kit	Vector	Burlingame, USA
DAB-Kit	Vector	Burlingame, USA
Glutaraldehyde	Carl Roth	Karlsruhe, Germany
Methanol	Merck	Darmstadt, Germany
DAPI mounting medium	Vector	Burlingame, USA
Kapa2G Mouse Genotyping Kit	Peqlab	Erlangen, Germany
LE-Agarose	BiozymScientific	HessischOldendorf, Ger
Ethidiumbromide	Carl Roth	Karlsruhe, Germany
Maxwell 16LEV SimplyRNA Kit	Promega	Madison, USA
2-Mercaptoethanol	Sigma Aldrich	Munich, Germany
OrangeG	Sigma Aldrich	Munich, Germany
Oligo(dT) primer (C110A)	Promega	Madison, USA
dNTP mix	Promega	Madison, USA
Superscript II RT Kit	LifeTechnologies	Darmstadt, Germany
FirstStrandbuffer	LifeTechnologies	Darmstadt, Germany
DTT	LifeTechnologies	Darmstadt, Germany
DirectRed 80	Sigma Aldrich	Munich, Germany
RNAseOUT	LifeTechnologies	Darmstadt, Germany
SybrGreen	Roche	Mannheim, Germany
CellScraper	TPP	Trasadingen, Switzerland
CompeteMiniProteinaseInhibitor	Roche	Mannheim, Germany
PhosSTOPPhosphataseInhibitor	Roche	Mannheim, Germany
Pierce BCA Protein Assay	ThermoScietific	Rockford, USA
Inject Solo	Braun	Melsungen, Germany
Sterican	Braun	Melsungen, Germany
SafeSealTips	BiozymScientific	HessischOldendorf, Ger
Sodium dodecyl sulfate (SDS)	Carl Roth	Karlsruhe, Germany
Whatman paper	GE	Freiburg, Germany

Rotipherese Gel 30	Carl Roth	Karlsruhe, Germany
Immobilon PVDF	Merck	Darmstadt, Germany
TrisPufferan	Carl Roth	Karlsruhe, Germany
Glycine	SigmaAldrich	Munich, Germany
DMSO	SigmaAldrich	Munich, Germany
NEAA	LifeTechnologies	Darmstadt, Germany
Kleenex	KimberlyClarke	Roswell, USA
Skim milk powder	SigmaAldrich	Munich, Germany
Albumin fraction V	Carl Roth	Karlsruhe, Germany
ECL	GE	Freiburg, Germany
SuperSignal West Femto MaxSens	ThermoScientific	Waltham, USA
Hyperfilm	GE	Freiburg, Germany
Isofluran	CP Pharma	Burgdorf, Germany
NaCl	SigmaAldrich	Munich, Germany
JNK-IN-8	Merck	Darmstadt, Germany
IL6	Peprotec	Hamburg, Germany
Reaction tubes (Eppis)	Eppendorf	Hamburg, Germany
Cryotubes	Sarstedt	Nümbrecht, Germany
LightCycler480 multiwellpalte 96	Roche	Mannheim, Germany
Permanent Markers	VWR	SanFransisco, CA, USA
Primer	EurofinsGenomice	Ebersberg, Germany
SemperCare gloves	Sempermed	Clearwater, USA
McCoys 5A medium	LifeTechnologies	Darmstadt, Germany
Waymouths medium	LifeTechnologies	Darmstadt, Germany
Bovine Serum Albumin (BSA)	Carl Roth	Karlsruhe, Germany
Soy bean trypsin inhibitor (SBTI)	Sigma Adrich	Munich, Germany
Rat tail collagen (354236)	BD	SanJose, CA, USA
Collagease VIII (C2139)	Sigma Aldrich	Munich, Germany
Amphotericin B	LifeTechnologies	Darmstadt, Germany
Bovine pituitary extract	LifeTechnologies	Darmstadt, Germany
SELENIX	LifeTechnologies	Darmstadt, Germany
Pancrex	Sniff	Soest, Germany
HEPES 1M	Life Technologies	Darmstadt, Germany
UriScan SGL strip	YD Diagnostics	Seo, Korea
NucleoSpin RNA II Kit	MachereyNagel	Düren, Germany

4.1.4 Solutions and buffers

Sirius Red staining solution

0.5	g	DirectRed 80
500	ml	saturated aqueous solution of picric acid (1.3 %)

Unmasking Solutions

15	ml	VectaShield Unmasking solution (low or high pH)
1600	ml	distilled water

Phosphate buffered saline (PBS) 1x

9.55	g	PBS powder
1	l	distilled water

Non-denaturing lysis buffer (NDLB)

50	mM	Tris-HCl pH 7.4
300	mM	NaCl
5	mM	EDTA
1	% (w/v)	Triton X-100

Lämmli buffer (5x)

5	g	SDS
25	ml	Glycerin 50 %
1.8	g	Tris-HCl
25	mg	Bromphenolblau
2.5	ml	b-Mercaptoethanol

ad 50 ml distilled water, pH 6.8

PAGE stacking gel buffer

181.71	g	Tris
10	%	SDS

ad 1 l with distilled water, adjust pH to 8.8

PAGE resolving gel buffer

60	g	Tris
10	%	SDS

ad 1 l with distilled water, adjust pH to 6.8

PAGE running buffer

30	g	Tris base
144	g	Glycine
10	g	SDS

ad 1l distilled water

Transfer buffer

14.4	g	Glycine
3	g	Tris
100	ml	MeOH (optional for proteins larger than 20 kDa)

ad 1 l with distilled water

10x TBS(T)

80	g	NaCl
31.5	g	Tris-HCl

ad 1 l distilled water, pH 7.6

1	%	Tween (for TBST)

TAE 50x

242	g	Tris
37.2	g	DinatriumEDTAdihydrat
60.0	g	acetic acid (100 %)

ad 1 l with distilled water

SOL1

McCoy's medium with L-glutamin and phenol red

0.1	%	BSA
0.2	mg/ml	Soy bean trypsin inhibitor (SBTI)

SOL2

SOL1

1.2	mg/ml	Collagenase VIII

SOL3

Waymouth's medium with L-glutamin and phenol red, aginine free

0.1	%	BSA
0.2	mg/ml	SBTI
0.5	%	PenStrep
0.25	µg/ml	Amphotericin B
50	µg/ml	Bovine pituitary extract
30	%	Fetal Calf Serum (FCS)
1	%	SELENIX, Invitrogen

HSL buffer for EMSA

2	ml	HEPES 1 M
2.045	g	NaCl
100	µl	$MgCl_2$ 0.1 M
500	µl	EDTA 0.1 M
1	ml	EGTA 0.1 M
10	ml	NP40 10 %

ad 100 ml with distilled water, supplement with proteinase and phosphatase inhibitors

4.2 Methods

4.2.1 Mice

4.2.1.1 Strains

$Ptf1a^{Cre/+}$ [124], Elastase-CreER [230], $Kras^{LSL\text{-}G12D/+}$ [231], $JNK1^{LoxP/LoxP}$ [232], $JNK2^{LoxP/LoxP}$ [233] and $Stat3^{LoxP/LoxP}$ [234] strains have been described previously. Experiments were carried out in accordance with the German Federal Animal Protection Laws and approved by the Institutional Animal Care and Use Committees of the Technische Universität München. Mice were intercrossed to obtain the genotypes listed in Table 1. For genotyping, mouse tail tissue or ear mark tissue taken between three and four weeks of age was used. DNA was isolated and PCR was performed as described in 4.2.4.1 and 4.2.4.2. Littermates without Cre expression served as wild type (wt) controls. Mice were killed, either on particular time points or notable symptoms of disease when euthanization criteria were met. An overdose of isoflurane anesthesia was followed by cervical dislocation.

Table 1 Mouse genotypes and abbreviations

Genotype	Abbreviation
Ptf1a$^{wt/Cre}$	Cre
Ptf1a$^{wt/Cre}$;JNK1$^{wt/LoxP}$;JNK2$^{wt/LoxP}$	JNK1$^{+/\Delta}$;JNK2$^{+/\Delta}$
Ptf1a$^{wt/Cre}$;JNK1$^{LoxP/LoxP}$;JNK2$^{LoxP/LoxP}$	JNK1$^{\Delta/\Delta}$;JNK2$^{\Delta/\Delta}$/ JNK$^{\Delta/\Delta}$
Ptf1a$^{wt/Cre}$;Kras$^{wt/LSL-G12D}$	Kras^{G12D}
Ptf1a$^{wt/Cre}$;Kras$^{wt/LSL-G12D}$;JNK1$^{wt/LoxP}$;JNK2$^{wt/LoxP}$	Kras^{G12D};JNK$^{+/\Delta}$
Ptf1a$^{wt/Cre}$;Kras$^{wt/LSL-G12D}$;JNK1$^{LoxP/LoxP}$;JNK2$^{wt/LoxP}$	Kras^{G12D};JNK1$^{\Delta/\Delta}$;JNK2$^{+/\Delta}$
Ptf1a$^{wt/Cre}$;Kras$^{wt/LSL-G12D}$;JNK1$^{wt/LoxP}$;JNK2$^{LoxP/LoxP}$	Kras^{G12D};JNK1$^{+/\Delta}$;JNK2$^{\Delta/\Delta}$
Ptf1a$^{wt/Cre}$;Kras$^{wt/LSL-G12D}$;JNK1$^{LoxP/LoxP}$;JNK2$^{LoxP/LoxP}$	Kras^{G12D};JNK$^{\Delta/\Delta}$
Ptf1a$^{wt/Cre}$;Kras$^{wt/LSL-G12D}$;STAT3$^{wt/LoxP}$;JNK1$^{LoxP/LoxP}$;JNK2$^{LoxP/LoxP}$	Kras^{G12D};STAT3$^{+/\Delta}$;JNK$^{\Delta/\Delta}$
Ptf1a$^{wt/Cre}$;Kras$^{wt/LSL-G12D}$;STAT3$^{LoxP/LoxP}$;JNK1$^{LoxP/LoxP}$;JNK2$^{LoxP/LoxP}$	Kras^{G12D};STAT3$^{\Delta/\Delta}$;JNK$^{\Delta/\Delta}$
Elastase-CreER; Kras$^{wt/LSL-G12D}$;JNK1$^{wt/LoxP}$;JNK2$^{wt/LoxP}$	ElaCreER;Kras^{G12D};JNK$^{+/\Delta}$
Elastase-CreER; Kras$^{wt/LSL-G12D}$;JNK1$^{LoxP/LoxP}$;JNK2$^{LoxP/LoxP}$	ElaCreER;Kras^{G12D};JNK$^{\Delta/\Delta}$

4.2.1.2 Cerulein-induced acute pancreatitis

Acute pancreatitis was induced with cerulein, a cholecystokinin analogue, in 8 week old mice and age matched controls as established by Jensen *et al*. [23] with a total of eight intraperitoneal (i.p.) injections of 50 µg/kg body weight per hour. Mice were sacrificed 24 h, 72 h, 7 days or 4 weeks after the last injection and histologically analyzed (n ≥ 3 mice per group).

4.2.1.3 Blood glucose measurement

Blood glucose measurement was performed with the iDia device and AccuCkeck2000 testing stripes. Mice tail vein blood was incubated on the test stripe according to the manufacturer's instructions.

4.2.1.4 Pancreatic exocrine insufficiency test

After weaning (21 days post partum) mice were started on Pancrex chow, which contained already the enzymes necessary for digestion. Mice were fed with this chow until euthanazation criteria were met and overall survival was compared using Kaplan-Meier survival analysis.

4.2.2 Cell culture

4.2.2.1 Isolation and culture of primary murine tumor cells

Small pieces of fibrotic murine tumor were resected and placed into a sterile 10 cm tissue culture dish containing culture medium (DMEM, 10 % FCS, 1% PenStrep, 1% NEAA). Pieces were incubated for 24 - 48 h at 37 °C in 5 % CO_2 to allow cells to grow and attach to the dish. Thereafter, pieces were removed and cells were passaged with 0.25 % Trypsin/EDTA at least three times to ensure absence of fibroblast contamination before using them in further experiments.

4.2.2.2 Culture of murine pancreatic cancer cell lines

Murine pancreatic cancer cell lines were incubated in culture medium (see 4.2.2.1) at 37 °C in 5 % CO_2 and splitted with 0.25 % Trypsin/EDTA before reaching maximum confluence.

4.2.2.3 Isolation of acinar cells and 3D culture

Mice were sacrificed and pancreata washed one with ice-cold PBS. Pancreata were cut to small pieces and resuspended for digestion in 5 ml SOL2. After 10 min at 37 °C and transfer to Falcon tubes, 10 ml SOL1 was added to the mixture and centrifuged at 18 °C for 5 min at 300 rpm. Supernatant was discarded and pellet resuspended in 5 ml SOL2. After additional 10 min at 37 °C the mixture is pressed gently through a 100 µm filter and acini are washed in SOL1 and again pressed gently through the filter. One additional washing step with SOL1 was followed by centrifugation at 18 °C 5 min 300 rpm. Supernatant was discarded and pellet resuspended in SOL3 for 60 min allowing acinar berries to recover. Acinar explants were then embedded in rat tail collagen in 8-well culture slides.

4.2.2.4 JNK-IN-8 Inhibitor Assays

JNK-IN-8 was diluted in DMSO according to manufacturer's recommendations. Cell culture medium was either supplemented with JNK-IN-8 at 1 µg/ml for treatment or equal volume of DMSO for controls. JNK inhibitor was added to the culture medium at least 3 h prior to experimental procedure as suggested by Lim *et al*.

4.2.3 Histological analysis

4.2.3.1 Paraformaldehyde Fixation and Conservation

Tissue of sacrificed mice was rapidly removed and immediately incubated over night at 4 °C in 4 % paraformaldehyde/PBS (pH 7,4) for fixation. Tissue was either stored for up to 3 days in 70 % ethanol or directly dehydrated and paraffinized with increasing concentrations of ethanol followed by xylol ensued by paraffin using a Leica S300 tissue processing unit. Tissue was embedded in liquid paraffin and cooled for hardening. Formalin-fixed, paraffin-embedded (FFPE) blocks were stored at room temperature. Blocks were cooled to -20 °C for cutting on a microtome to 1,5 µm slices and transferred to a 50 °C water bath for stretching. Sections were collected on microscopy slides and allowed to dry overnight or for at least 3 h at 37 °C.

4.2.3.2 Cryo Conservation

Fresh tissue of sacrificed mice was embedded in Tissue-Tek medium and immediately flash frozen in liquid nitrogen. Cryo sections were cut at -20 °C on a Microm HM560.

4.2.3.3 Hematoxylin & Eosin staining (HE)

Hematoxylin & Eosin is a two-compound stain, the first staining acidic structures in blue, the latter staining basic structures in red. Sections were deparaffinized with 2 changes of xylol and rehydrated in distilled water after decreasing ethanol row (twice

100 %, twice 86 % and twice 70 % ethanol 3 minutes each). Slides were stained with hematoxylin for 3 minutes followed by four changes of distilled water for washing. Differentiation was performed with briefly dipping the slide into HCl-acidified water followed by blueing in ammonia water. After further washing in distilled water and one change of 70 % ethanol slides were counterstained in eosin for 1 minute. Washing was carried out in 3 changes of 100 % ethanol ensuing embedding in Pertex mounting medium.

4.2.3.4 Sirius Red staining

Picro Sirius Red stains collagen in the extracellular matrix. Paraffin sections were deparaffinized according to the HE protocol (see 4.2.3.3) and stained with 300 µl of Sirius Red Staining Solution for 1 h. Slides were washed once with 0.5 % (v/v) glacial acid and counterstained with hematoxylin for 10 seconds. After 4 changes in distilled water, slides were dehydrated in a rising row of ethanol (2x 70 %, 2x 96 %, 2x 100 % each 3 min) and two changes of xylol and were finally Pertex-embedded.

4.2.3.5 Immunohistochemistry (IHC)

Slides were deparaffinized according to the HE protocol (see 4.2.3.3). Antigen unmasking was performed either through boiling slides 15 min (microwave or pressure cooker) in citrate buffer (pH 6 or pH 11) or EDTA depending on the first antibody used (see Table 2). Alternatively partial proteinase K digestion (20µg/ml, 10mM Tris/HCL pH 8.0, 15 min, RT) was performed for unmasking. Unmasking with citrate buffer was followed by 20 min cool down, which was not necessary for EDTA. After unmasking endogenous peroxidases were inactivated by 10 min 3 % hydrogen peroxide. After one change of distilled water nuclei were permeabilized with 0.3 % Triton X-100/PBS for 3 min and washed three times for 3 min with PBS. Blocking solution was used according to the first antibody used as indicated in Table 2. First antibody was incubated over night at 4 °C in a wet chamber in blocking solution as indicated in Table 2. Next morning slides were rewarmed to room temperature and washed 3 times for 3 min with PBS. Adequate secondary antibody was applied in a 1:1000 dilution in respective blocking solution for 1 h. 30 min prior to use Avidin-Biotin-Complexes were generated using the ABC-Kit. After discarding of secondary antibody ABC solution was put on the slide for 1 h. DAB reaction followed five washing steps of 2 x 1 min and 3 x 3 min with PBS. DAB-Kit was used according to the manufacturer's instructions. DAB reaction was allowed to develop for equal amounts of time for all slides and stopped in distilled water. Slides were counterstained with hematoxylin for 3 seconds. After four changes of distilled water slides encountered rising ethanol row (2x 70%, 2x 96 %, 2x 100 %), two changes of xylol and were embedded in Pertex.

For quantification representative slides of each mouse were chosen and several pictures per slide were taken. Calculations were performed using the AxioVision 4.8 software of at least 3 mice per group.

Table 2 Primary antibodies and conditions for IHC

Antigen	Host	Dilution	Unmasking	Block	Company
Amylase	Rb	1:1000	citrate high pH	5 % GS/PBS	Sigma (A8273)
CK19 Troma III	Rat	1:500	citrate low pH	5 % RB/PBS	DSHB (m0888)
F4/80	Rat	1:250	Proteinase K	5 % RB/PBS	eBioscience (48-4801)
Insulin	Gp	1:500	citrate low pH	5 % GS/PBS	DAKO (A0564)
Ki67	Rb	1:2500	citrate low pH	5 % GS/PBS	abcam (15580)
cleaved Caspase 3	Rb	1:500	citrate low pH	5 % GS/PBS	CellSignaling (9664)
pSTAT3	Rb	1:400	EDTA	5 % GS/PBS	CellSignaling (9145)
Muc5AC	Ms	1:200	citrate low pH	5 % GS/PBS	Neomarkers (m5145-P1)
pJNK	Rb	1:250	citrate low pH	5 % GS/PBS	CellSignaling (4668)
JNK	Rb	1:250	citrate low pH	5 % GS/PBS	CellSignaling (9258)
γH2AX	Ms	1:1000	citrate low pH	5 % GS/PBS	Millipore (05-636)
p53	Rb	1:1000	citrate low pH	5 % GS/PBS	Leica (CM5p)
Sox9	Rb	1:1000	citrate low pH	5 % GS/PBS	Milipore (A35535)
ß-catenin	Rb	1:50	citrate low pH	5 % GS/PBS	CellSignaling (9562)
αSMA	Rb	1:250	citrate low pH	5 % GS/PBS	abcam (5964)

Rb=rabbit, Gp=guinea pig, Ms=mouse, GS=goat serum, RS=rabbit serum

4.2.3.6 Immunofluorescence staining

Acinar explants were washed once in ice-cold PBS and then fixed in equal amounts of 4 % PFA/ Methanol at 4 °C over night. After removal of fixing agent explants were washed three times with PBS for 3 min and blocked with 10 % BSA/PBS for at least one hour at room temperature. First antibody (CK19 1:300) in 0.1 TritionX100/PBS was incubated over night at 4 °C. Next morning slides were rewarmed to room temperature and washed 3 times for 3 min with PBS. Fluorescence-labeled secondary antibody was applied in a 1:500 dilution in blocking solution for 4 h at room temperature in the dark. Five washing steps of 2 x 1 min and 3 x 3 min with PBS were followed by adding DAPI-containing mounting medium. Analysis of explants was performed on an AxioVert200M microscope.

4.2.4 RNA/DNA Analyses

4.2.4.1 DNA isolation from mouse tissue (tail/earmark)

DNA was isolated from tail tips or earmarks using the Kapa Express Extract Kit. Tissue was immersed in 100 µl lysis Buffer containing 2 units of KAPA Express Extract Enzyme for 10 min at 700 rpm and 75 °C and afterwards heat-inactivated at 96 °C for 5 min. Samples were vortexed for at least 15 seconds and not spinned down as recommended by the manufacturer. One µl of supernatant was directly used as template in the genotyping PCR.

4.2.4.2 Genotyping PCR

Genotyping PCRs were carried out in a Primus 96 plus, MWG Biotech or a T100 Thermal Cycler, BioRad. For genotyping 9.5 µl 2x KAPA2G Fast HotStart Genotyping Mix with dye was diluted 1:1 with distilled water and mixed with 1 µl of PrimerMix (respective primers each in a concentration of 10 pmol/µl, see Table 3). Then 1 µl of DNA lysate was added. After 3 min at 95 °C 35 PCR cycles were performed at 95 °C denaturation for 20 seconds, 58 °C annealing for 20 seconds and 72 °C elongation for 35 seconds, followed by a final elongation step for 5 min. Genotyping results were visualized in a 1.5 % (w/v) agarose TAE gel containing 0.5 ng/ml ethidiumbromide.

Table 3 PCR conditions and primers for genotyping

Name	Primer name	Primer sequence	Expected band size
Cre	Cre01	5'-ACC AGC CAG CTA TCA ACT CG-3'	wt 324 bp
	Cre02	5'-TTA CAT TGG TCC AGC CACC-3'	Cre 199 bp
	Cre03	5'-CTA GGC CAC AGA ATT GAA AGA TCT-3'	
	Cre04	5'-GTA GGT GGA AAT TCT AGC ATC ATC C-3'	
ElaCre	ElaCre F	5'-GAT TTA CGG CGC TAA GGA TGA CT-3'	tg 800 bp
	ElaCre R	5'-AGG GTG CTG GAC AGA AAT GTG TA-3'	
Kras	Kras_UP1	5'-CAC CAG CTT CGG CTT CCT ATT-3'	wt 280 bp
	Kras_URP1	5'-AGC TAA TGG CTC TCA AAG GAA TGT A-3'	Kras 180 bp
	Kras_mutUP	5'-CCA TGG CTT GAG TAA GTC TGC-3'	
JNK1	JNK1_fw	5'-AGG ATT TAT GCC CTC TGC TTG TC-3'	wt 540 bp
	JNK1_rev	5'-GAA CCA CTG TTC CAA TTT CCA TCC-3'	LoxP 330 bp
JNK2	JNK2_fw	5'-GTT TTG TAA AGG GAG CCG AC-3'	wt 224 bp
	JNK2_rev	5'-CCT GAC TAC TGA GCC TGG TTT CTC-3'	LoxP 264 bp
STAT3	STAT3_A	5'-CCT GAA GAC CAA GTT CAT CTG TGT GAC-3'	wt 220 bp
	STAT3_B	5'-CAC ACA AGC CAT CAA ACT CTG GTC TCC-3'	LoxP 320 bp

4.2.4.3 RNA isolation

For RT-PCR and array experiments pancreatic tissue was immediately homogenized in RA1-buffer containing 1 % (v/v) β-mercaptoethanol and flash frozen in liquid nitrogen. Total RNA was extracted from these lysates using the Maxwell 16 LEV simplyRNA Tissue Kit according to the manufacturer's protocol. RNA concentration was evaluated on a Nanodrop 2000 spectrophotometer and quality was checked with OrangeG buffer on a 1 % (w/v) agarose TAE gel. Further quality assessment for arrays was performed elsewhere (see 4.2.4.6)

4.2.4.4 cDNA Synthesis

For cDNA synthesis 1 µg of RNA was incubated with 500 ng of Oligo(dT) primers and 1 µl 10 mM dNTP mix in a total volume of 12 µl for 5 min at 65 °C. Four µl of 5x First-strand buffer, 2 µl of 0,1 M DTT and 40 units of RNaseOUT were added and incubated at 25 °C for 2 min. Then, 200 units (1 µl) of Superscript II were added, the mix resuspended and incubated at 42 °C for 50 min. Inactivation occurred at 70 °C for 15 min.

4.2.4.5 qRT-PCR

Quantitative RT-PCR was performed on the Lightcycler480 system using the SYBR Green master mix. RT-PCRs were run 40 cycles at 95 °C for 10 seconds, 55 °C for 20 seconds and 72 °C for 10 seconds. Primers were used at 10 pM final concentration (see Table 4) and designed to be intron spanning whenever possible. To ensure primer specificity melting curve analysis was performed. CyclophilinA served as housekeeper. For calculation of C_t values $2^{\wedge -\Delta ct(housekeeper)-\Delta ct(target\ gene)}$ was used. P-values were calculated using Prism 5 software under the assumption of non-normal distribution (Mann-Whitney U test). Specificity of product was controlled by melting curve analysis.

Table 4 Primer sequences for qRT-PCR

Name	Primer name	Primer sequence	Expected band size
Amylase	Amyl_fw	5'-TGGTCAATGGTCAGCCTTTTTC-3'	208 bp
	Amyl_rev	5'-CACAGTATGTGCCAGCAGGAAG-3'	
Cpa1	Cpa1_fw	5'-TACACCCACAAAACGAATCGC-3'	150 bp
	Cpa1_rev	5'-GCCACGGTAAGTTTCTGAGCA-3'	
Mist1	Mist1_fw	5'- GCGCGTACGGCCTCG -3'	96 bp
	Mist1_rev	5'- GGGCCGGTTTTTGGTCTTCAT -3'	
Nr5a2	Nr5a2_fw	5'-CTGCTGGACTACACGGTTTGC-3'	100 bp
	Nr5a2_rev	5'-CTGCCTGCTTGCTGATTGC-3'	
Ptf1a	Ptf1a_fw	5'-ATCGAGGCACCCGTTCAC-3'	74 bp
	Ptf1a_rev	5'-GGAAAGAGAGTGCCCTGCAA-3'	
Sox9	Sox9_fw	5'-CCACGTGTGGATGTCGAAG-3'	207 bp
	Sox9_rev	5'-CTCAGCTGCTCCGTCTTGAT-3'	
Hnf1b	Hnf1b_fwd	5'-GGCCTACGACCGGCAAAAGA-3'	95 bp
	Hnf1b_rev	5'-GGGAGACCCCTCGTTGCAAA-3'	
CyclophilinA	CyphiA_fw	5'-CCAGGATTCATGTGCCAGGGT-3'	197 bp
	CyphiA_rev	5'-ATCCAGCCATTCAGTCTTGGC-3'	

4.2.4.6 GeneChip Microarray Assay

Sample processing was performed at an Affymetrix Service Provider and Core Facility, "KFB - Center of Excellence for Fluorescent Bioanalytics" (Regensburg, Germany; www.kfb-regensburg.de). Sample preparation for microarray hybridization was carried out as described in the Affymetrix GeneChip 3' IVT Express Kit User Manual (Affymetrix, Inc., Santa Clara, CA, USA). In brief, 250 ng of total RNA were reverse transcribed into double-stranded copy DNA (cDNA) followed by an *in vitro* transcription generating biotin-labeled amplified RNA (aRNA). The length of the purified aRNA products was assessed using an Agilent 2100 bioanalyzer (Agilent Technologies, Palo Alto, USA). Following fragmentation, 6 µg aRNA were hybridized to an Affymetrix Mouse Genome 430 PM 16-Array Plate. For hybridization, washing, staining and scanning an Affymetrix GeneTitan system was used.

4.2.5 Proteinbiochemistry

4.2.5.1 Isolation of protein from mouse tissue or cells

To obtain protein crude extract murine tissue was flash frozen immediately after sacrificing the mice and stored at -80 °C. These samples were homogenized on ice in 250 - 600 µl non-denaturing lysis buffer (NDLB) containing protease and phosphatase inhibitors using the SilentCrusherM. Alternatively, mouse cell lines were grown to 80 % confluency, washed once in ice-cold PBS, scratched of the culture dish in ice cold PBS on ice and centrifuged for 5 min at 1600 rpm. Supernatant was discarded and cell pellet was resuspended in 80 - 200 µl of NDLB containing protease and phosphatase inhibitors. Tissue lysates or lysates from cultured cells were afterwards sonicated for 10 seconds and incubated on ice for 5 min. Lysates were centrifuged at 4 °C and 13.2 krpm for 5 min and supernatant was stored at -20 °C prior to use.

4.2.5.2 Quantification of protein concentration

To determine absolute protein concentration of crude extracts the BCA kit was used according to the manufacturer's instructions. Standard curve was obtained with 2 µg/µl BSA in a range between 0 to 0.05 µg/µl. 200 µl of protein detection solution were mixed with 1 to 2 µl of crude extract and incubated for 30 min at 37 °C. Absorbance was measured at 580 nm with an ELISA microplate reader and compared to the standard after subtraction of blank.

4.2.5.3 SDS polyacrylamide gel electrophoresis (SDS-PAGE) and Western Blot

To separate protein lysates according to molecular weight, sodium dodecylsulfate (SDS) polyacrylamide gel electrophoresis (PAGE) was employed. 30 – 50 µg protein lysate were supplemented with 5 x Lämmli buffer and denatured at 95 °C for 5 min. Protein separation was performed in 7.5 – 12.5 % two-compound stacking/resolving gels (see Table 5) in PAGE running buffer at 100 V in BioRad Mini Protean Gel Systems. Transfer to methanol activated PVDF membrane took place at 100 V for 60 to 90 min in transfer buffer, depending on target protein size. During blotting, gel and membrane were patched between Whatman papers and sponges and blotting chamber was cooled with ice for the time of transfer. Afterwards, membranes were blocked either with 5 % (w/v) skim milk powder/TBST or 5 % bovine serum albumin (BSA)/TBST for 30 min to avoid unspecific antibody binding. Then, membranes were incubated with primary antibody at 4 °C over night in foil (see Table 6). The following day, the membrane was washed thrice with TBST for 3 min and incubated with respective HRP-coupled secondary antibody (1:10.000) (see Table 7) in the respective blocking solution for 1 h at room temperature. After five washing steps (2x 1 min, 3x 3 min) in TBST and one rinse in TBS, protein bands were visualized using ECL Western Blotting Detection Reagent or Super Signal West Femto Maximum Sensitivity Substrate and Amersham Hyperfilm.

Table 5 PAGE gel components and linear resolution range

Gel (%)	AA	H2O	buffer	TEMED	APS	Linear Range
Stacking	0.75 ml	3.0 ml	Stacking 1.3 ml	10 µl	25 µl	-
Resolving 7.5	3.9 ml	7.6 ml	Resolving 4.0 ml	25 µl	50 µl	~36-94 kDa
Resolving 10.0	5.1 ml	6.4 ml	Resolving 4.0 ml	25 µl	50 µl	~16-68 kDa
Resolving 12.5	6.5 ml	5.0 ml	Resolving 4.0 ml	25 µl	50 µl	~14-55 kDa

AA = Acrylamide; TEMED = Tetramethylethylendiamine; APS = Amoniumperoxodisulfate

Table 6 Primary antibodies and conditions for Western Blot

Antigen	Species	Dilution	Block	Company
Hsp90	Rb	1:3000	5% Milk/TBST	SantaCruz (7947)
pStat3	Rb	1:1000	5 % BSA/TBST	CellSignaling (9131)
tStat3	Ms	1:1000	5 % BSA/TBST	BD (610190)
JNK	Rb	1:200	5% Milk/TBST	CellSignaling (9258)
pJNK	Rb	1:1000	5% Milk/TBST	CellSignaling (4668)
gH2AX	Ms	1:1000	5% Milk/TBST	Milipore (05-636)
p53	Rb	1:1000	5% Milk/TBST	Leica Biosystems (CM5p)
p53 Ser15	Rb	1:1000	5% Milk/TBST	CellSignaling (12571)
pERK	Ms	1:1000	5% Milk/TBST	CellSignaling (9106)
ERK	Rb	1:1000	5% Milk/TBST	SantaCruz (93/194)
pAKT	Rb	1:1000	5% Milk/TBST	CellSignaling (2965)
AKT	Gt	1:500	5% Milk/TBST	SantaCruz (1619)
pp65	Rb	1:1000	5% Milk/TBST	CellSignaling (3033)

Rb = rabbit; Ms = mouse; Gt = goat; BSA = bovine serum albumin

Table 7 Horseradish-peroxidase (HRP)-coupled secondary antibodies

Antibody	Species	Dilution	Company
anti-rabbit	Goat	1:10.000	GE Healthcare, UK
anti-goat	Donkey	1:10.000	GE Healthcare, UK
anti-mouse	Rabbit	1:10.000	GE Healthcare, UK

4.2.5.4 EMSA

EMSAs were performed at the Charité, Berlin, by Dr. Björn Lamprecht with HSL lysed samples according to the following protocol. Pieces of frozen murine pancreatic tissue were taken up in HSL buffer and homogenized. Protein samples (1 - 10 µg) were mixed with shift cocktail (10 µl 2x shift buffer, 1µl 100 mM DTT, 1µl 10mg/ml BSA, 1µl 2µg/µl poly dIdC, 20.000 cpm hybridized labeled oligos) and incubated 10 min at room temperature. Samples were separated on a 5 % TBE polyacrylamide gel at 180 V for 30 min and then dried on whatman paper. Autoradiography was performed at -80 °C for hours to days. For more detailed instructions see Lamprecht *et al*. [235].

4.2.6 Data analysis

4.2.6.1 General Statistical Analysis

Statistical analysis was performed for at least 3 animals per group if not stated otherwise. Counting of immunohistochemically stained sections was carried out for at least 3 different optical fields of at least 3 mice per group. Normal distribution was not assumed. Samples were thus analyzed with the nonparametric Mann-Whitney U test. For calculation of significance and p-values GraphPad Prism was used.

4.2.6.2 Microarray data analysis

Summarized probe set signals were calculated by using the RMA [236] algorithm with the Affymetrix GeneChip Expression Console Software. After exporting into Microsoft Excel, average signal values, comparison fold changes and significance P values were calculated. Probe sets with a fold change above 2.0 fold and a student's t test P value lower than 0.05 were considered as significantly regulated. Furthermore, Gene Set Enrichment Analysis (GSEA) was performed, as previously described [237, 238].

5 Results

MAP kinase signaling is hyperactivated in more than 90% of PDACs and Kras, the driver of PDAC, is mutated (G12D) in almost all cases. Until recently, the effect of stress kinase signaling, especially the effect of c-Jun N-terminal kinase (JNK) signaling, another MAPK module, has not been assessed. Therefore, the role of JNKs in pancreatic development and PDAC initiation and progression was investigated.

5.1 JNK activity in human and murine tissue

5.1.1 Levels of JNK activation gradually decrease from human tumor-adjacent tissue towards PDAC

To analyze the distribution of activated (pTyr183, pThr185) JNK (pJNK) proteins in human PDAC samples, immunohistochemistry for pJNK was performed. Whereas activated JNK could be detected in epithelial tissue adjacent to human PDACs, pancreatic precursor lesions showed only slight nuclear expression of active JNKs and PDACs did not stain for active JNK signaling, except for occasional staining of blood vessels or stromal tissue. Active JNK signaling could not be detected in healthy human pancreas that served as negative control. As the majority of tumors stained with decreasing intensity from adjacent tissue towards tumor bulk, inactivation of JNK signaling may be a prerequisite for the development of PDAC.

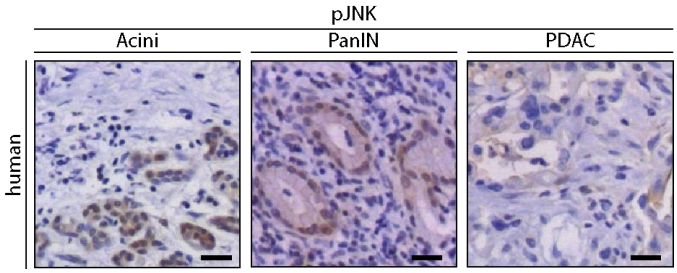

Figure 6 Expression of active JNK (pJNK) in human tissue samples
JNK signaling is activated in acinar cells adjacent to the tumor. Only low levels of pJNK are detectable in PanINs and it seems to be absent from PDAC. Only few stromal cells show pJNK staining. Scale bar: 20 µm.

5.1.2 JNK signaling seems to be inactive in murine tissue

Neither murine acinar cells of $Kras^{G12D}$ mice nor different precursor lesions display active JNK signaling. Although slight staining is visible in PDAC, it is not localized within the nuclei.

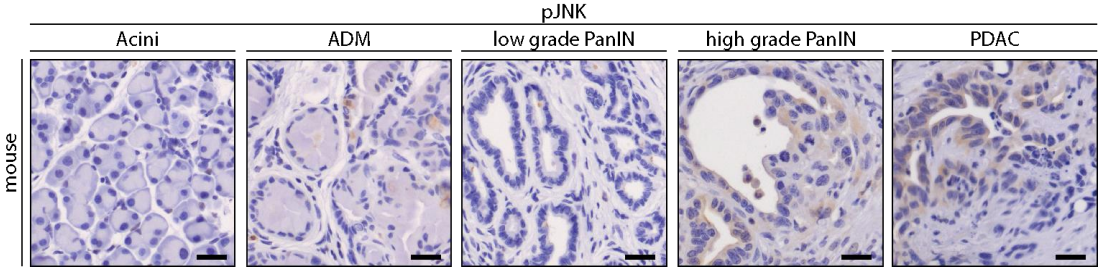

Figure 7 Expression of pJNK in murine tissue
Neither acini nor various murine precursor lesions or PDAC display pJNK expression. Scale bar: 20 µm.

5.1.3 JNK signaling is activated during early stages of acute pancreatitis

During cerulein-induced acute pancreatitis (iAP) JNK signaling is activated. While wild type mice are negative for phosphorylated active JNK directly prior to induction, pJNK can be detected in all epithelial cells of the pancreas already one hour after the first cerulein injection. This signal can only be detected in a fraction of nuclei 8 h after the last cerulein injection and diminishes at 24 and 72 h.

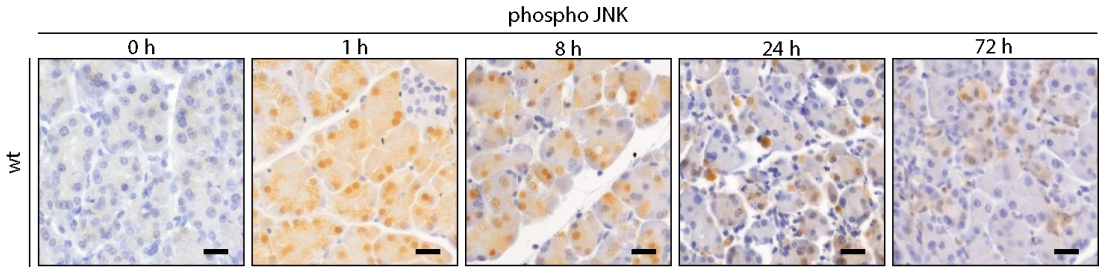

Figure 8 Active JNK signaling during the course of induced acute pancreatitis
JNK signaling is inactive in wild type unstimulated murine tissue. JNK signaling is active 1 h after iAP and then vanishes between 8 and 24 h. Scale bar: 20 µm.

5.2 Pancreatic JNK-deficiency

5.2.1 Pancreatic JNK-deficiency does not influence overall organ development or lineage specification

To test the effect of JNK signaling on pancreas development and acute pancreatitis, mice harboring LoxP-flanked (floxed) JNK1 and JNK2 alleles were crossed with mice expressing Cre recombinase under the pancreas-specific transcription factor 1 alpha (Ptf1a) promoter ($Ptf1a^{Cre/+}$). The Ptf1a gene is coding for the p48 protein, one of the earliest transcription factors determining pancreatic cell fate. The JNK3 locus was left unaffected since it is not expressed in the pancreas. The pancreas-specific JNK-deficient mice (henceforth $JNK^{\Delta/\Delta}$, compound deficient JNK or JNK knockout mice) were born according to Mendelian ratio and developed normally without obvious morphological defects.

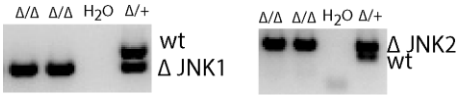

Figure 9 Genotyping results of two JNK1/JNK2 compound deficient mice versus heterozygous controls

To confirm the knockout of JNK genes, Western Blot for total JNK protein was performed on adult $JNK^{\Delta/\Delta}$ and wild type mice (Figure 10). JNK protein levels are greatly, reduced in $JNK^{\Delta/\Delta}$ mice in contrast to controls. Remaining detectable JNK was speculated to stem from stromal tissue. To confirm this and the specificity of the total JNK antibody used, tissue of wild type versus $JNK^{\Delta/\Delta}$ mice was immunostained. As expected, JNK knockout mice do not display any JNK protein in epithelial cells, while the stromal compartment remained unaffected (Figure 11). To confirm the specificity of the pJNK antibody used, wild type and JNK-deficient mice were injected with cerulein to induce acute pancreatitis and sacrificed one hour later.

While staining is clearly detectable in the nuclei of the wild type mice, JNK-deficient mice do not show staining in epithelial cells suggesting specific detection of JNK by the used antibody (Figure 12).

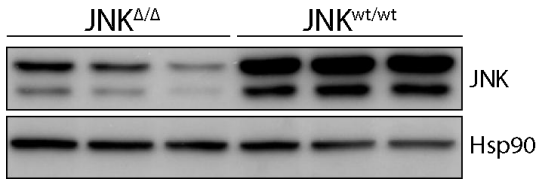

Figure 10 Total JNK in JNK knockout versus control mice
Expression of JNK is greatly diminished in different biological samples of JNK$^{\Delta/\Delta}$ mice compared to wt controls.

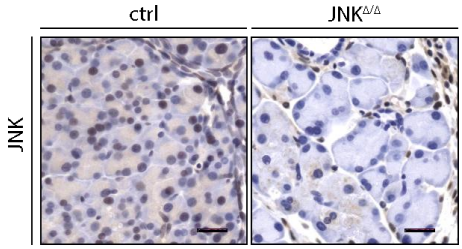

Figure 11 Immunohistochemistry of JNK in JNK$^{\Delta/\Delta}$ versus control mice
Epithelial cells in JNK knockout mice are devoid of any JNK staining while stromal cells and cells in the wt control express JNK protein. Scale bar: 20 µm.

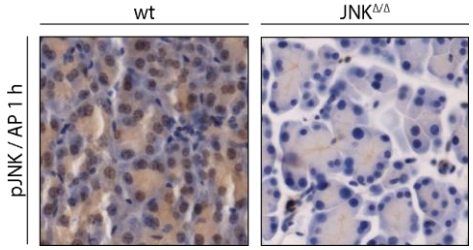

Figure 12 Confirmation of pJNK antibody specificity
In contrast to nuclei of JNK knockout mice, nuclei of wild type mice, show pJNK reactivity one hour after iAP. Mice prior to induction do not stain for pJNK (data not shown). Scale bar: 20 µm.

At eight weeks of age, the body weight of JNK$^{\Delta/\Delta}$ mice was not significantly changed in comparison to the respective littermate controls. On average, male JNK$^{\Delta/\Delta}$ mice weighed 22.6 g versus 24.3 g and female JNK$^{\Delta/\Delta}$ mice 18.8 g versus 18.9 g (males: p = 0,1636, females: p = 0,8571)(Figure 13).

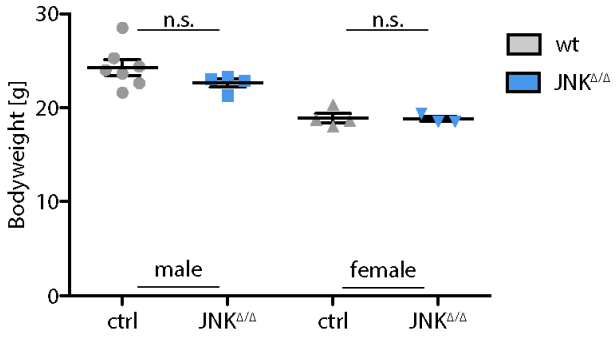

Figure 13 Body weight of eight week old male and female JNK$^{\Delta/\Delta}$ mice versus controls
Body weight was not significantly changed between male or female JNK knockout mice versus littermate controls.

Next, the effects of JNK knockout on the tissue architecture of adult mice was tested. Interestingly, HE staining of eight week old $JNK^{\Delta/\Delta}$ mice was nearly similar to controls (see 5.2.2). Furthermore, lineage specification in $JNK^{\Delta/\Delta}$ mice is not affected since no differences between $JNK^{\Delta/\Delta}$ and control mice were observed in the expression of markers for acinar cells (amylase), ductal compartment (CK19) and endocrine compartment (insulin) (Figure 14).

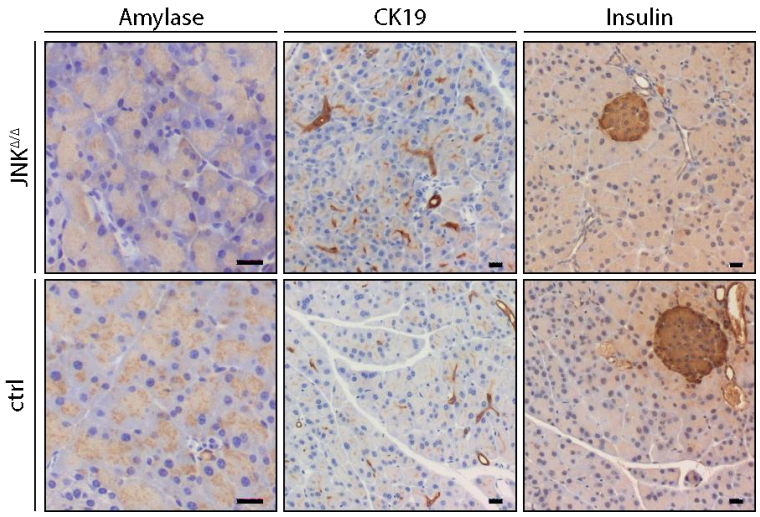

Figure 14 Amylase, CK19 and insulin staining reveals no defects in lineage specification
Protein expression of amylase, CK19 and insulin, markers for the exocrine, ductal and endocrine compartment respectively are unchanged between eight week old JNK knockout mice and controls. Scale bar: 20 µm.

This indicates that JNK signaling is dispensable for embryonal pancreatic development and pancreatic lineage specification.

5.2.2 JNK signaling is required for acinar maintenance

Small areas of lesions resembling ADM were already detected in eight week old pancreata from $JNK^{\Delta/\Delta}$ mice. Thus, maintenance of pancreatic architecture might be affected in aging $JNK^{\Delta/\Delta}$ mice. Pancreas slides of $JNK^{\Delta/\Delta}$ mice of eight, 26 and 52 weeks were HE stained and display progressive destruction of normal pancreatic architecture (Figure 15). Increasing amounts of tissue get dedifferentiated towards acinar ductal metaplasia (ADM) and are eventually replaced by fat tissue. Therefore, JNKs are required for maintenance of pancreatic architecture over time.

5.2.3 Acinar differentiation markers are unchanged in $JNK^{\Delta/\Delta}$ mice versus controls

The slow progression of tissue remodeling in $JNK^{\Delta/\Delta}$ mice indicated that small random stress events may initiate lesion development. To analyze impaired global terminal acinar differentiation as a cause, the levels of acknowledged genes regulating terminal acinar differentiation were measured in $JNK^{\Delta/\Delta}$ mice via qRT-PCR.

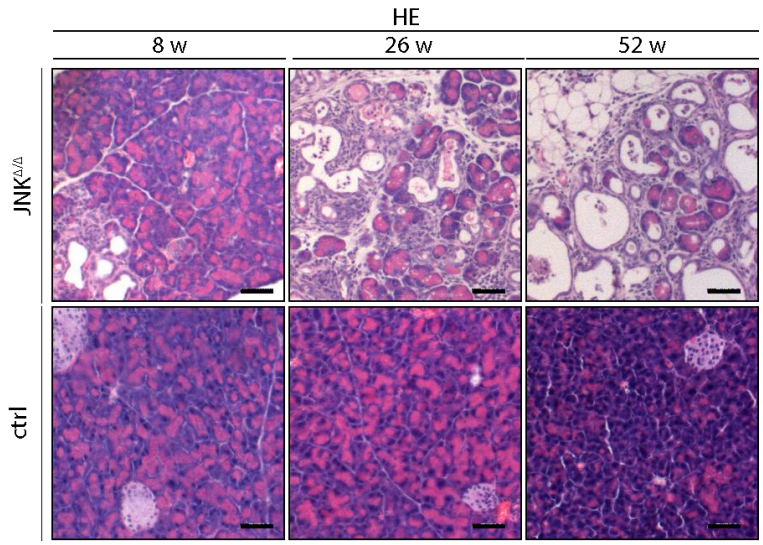

Figure 15 HE staining reveals progressive remodeling of pancreatic histology in JNK$^{\Delta/\Delta}$ mice
At eight weeks of age, JNK knockout mice display nearly unchanged histoarchitecture with some lobules occasionally containing lesions. These lesions progressed until weeks 26 and 52, when most of the physiologic parenchyma is replaced by ADM, slight fibrosis and fat tissue. Scale bar: 50 µm.

Figure 16 shows a statistically non-significant tendency towards lower global acinar terminal differentiation for the markers amylase, Nr5a2, Mist1 and Cpa1. Markers for progenitor-like cells such as Hnf1b, Ptf1a and Sox9 are not upregulated either. These results argue against a direct and global change in pancreatic lineage specification or terminal acinar differentiation and together with the HE staining suggest localized inflammatory stress events to be the trigger of this remodeling process.

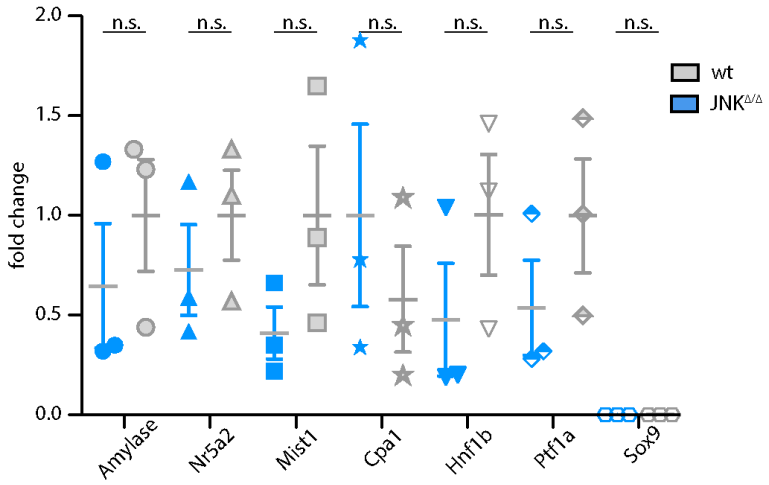

Figure 16 Markers for terminal acinar differentiation are unchanged in JNK knockout mice
Amylase, Nr5a2, Mist1 and Cpa1, markers for terminal acinar differentiation are not significantly changed between JNK knockout mice and controls. Upregulation of Hnf1b, Ptf1a and Sox9, markers for embryonal progenitor-like cells, is also not detectable at eight weeks of age.

5.2.4 Acinar differentiation is quickly lost upon explantation into 3D-culture

To further investigate a possible role of stress-dependent JNK signaling in the maintenance of terminal differentiation, acini from JNK$^{\Delta/\Delta}$ and control mice were explanted and subjected to culture stress in 3D collagen culture with or without EGF, a known trigger for dedifferentiation. Already one day after explantation and

irrespective of EGF treatment, roughly 85 % of acini from JNK$^{\Delta/\Delta}$ mice dedifferentiated into duct-like structures, while control cells remained acinar in more than 90 % (Figure 17A,B). To prove a transdifferentiation towards the ductal compartment, CK19 was stained. Indeed, CK19 staining was positive in JNK$^{\Delta/\Delta}$ mice three days after explantation (Figure 18). This demonstrates a stress-dependent role for JNKs in maintaining acinar differentiation. As terminal differentiation suppresses transformation, this implies a role of JNKs in suppression of PDAC development.

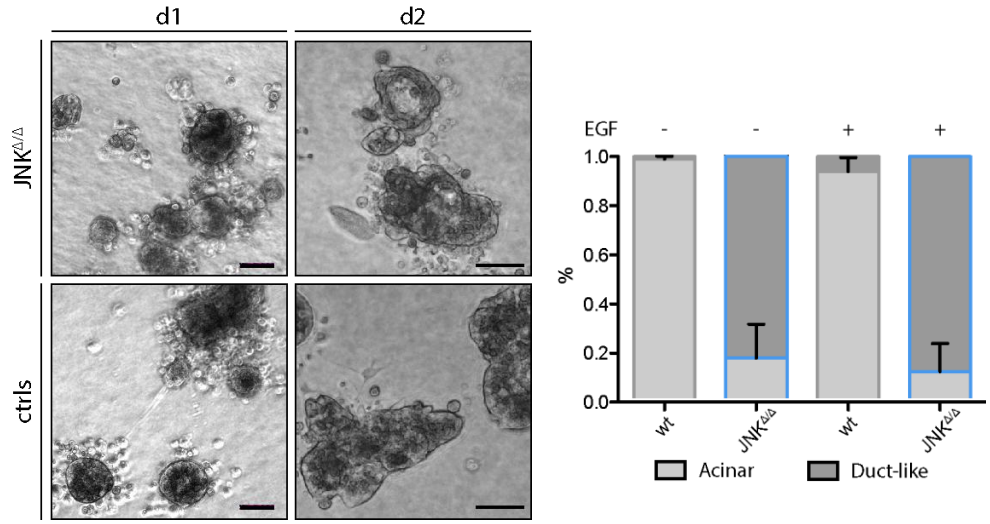

Figure 17 Microscopy and quantification of acinar berries on day 1 and day 2 after explantation
(A) No obvious differences of acinar berries explanted from mouse into 3D collagen matrix can be detected on the day of explantation (d1). Already one day later (d2), the majority of acinar aggregates from JNK knockout mice dedifferentiated into duct-like structures while JNK competent acinar aggregates remained acinar. Explantation performed by Katharina Alexandrow. Scale bar: 20 µm. (B) One day after explantation, 97 % of acinar berries from untreated wt mice remained acinar in morphology while 84 % of berries from JNK knockout mice dedifferentiated into duct-like structures. EGF was initially used to trigger this dedifferentiation process. Wild type acini treated with EGF usually dedifferentiate until day 4. Treatment with EGF, therefore, was probably not long enough to show an effect during the first 24 hours.

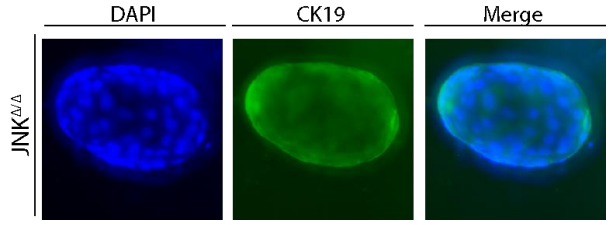

Figure 18 Transdifferentiation in JNK knockout explants
CK19 staining three days after explantation (day 4) in JNK knockout explants confirms transdifferentiation into duct-like structures.

5.2.5 Impaired acinar regeneration after iAP in JNK$^{\Delta/\Delta}$ mice

To better understand the stress-induced dedifferentiation of acinar cells in JNK$^{\Delta/\Delta}$ mice, the ability to restore acinar differentiation in JNK$^{\Delta/\Delta}$ mice was tested. To this end, acute pancreatitis was induced with cerulein (iAP) and the histology of JNK$^{\Delta/\Delta}$ mice and controls was assessed seven and 28 days after the last injection, when control mice have already restored physiologic histoarchitecture. Figure 19 shows the time course of induced acute pancreatitis. Eight injections of cerulein induce lesions in both JNK$^{\Delta/\Delta}$ mice and controls that can be detected one and three days after the last injection (Figure 20). In contrast to controls, JNK$^{\Delta/\Delta}$ mice were not able

to resolve their lesions. Even four weeks after iAP, lesions were still not resolved in JNK$^{\Delta/\Delta}$ mice demonstrating that regeneration is JNK-dependent.

Figure 19 Protocol of cerulein-induced acute pancreatitis

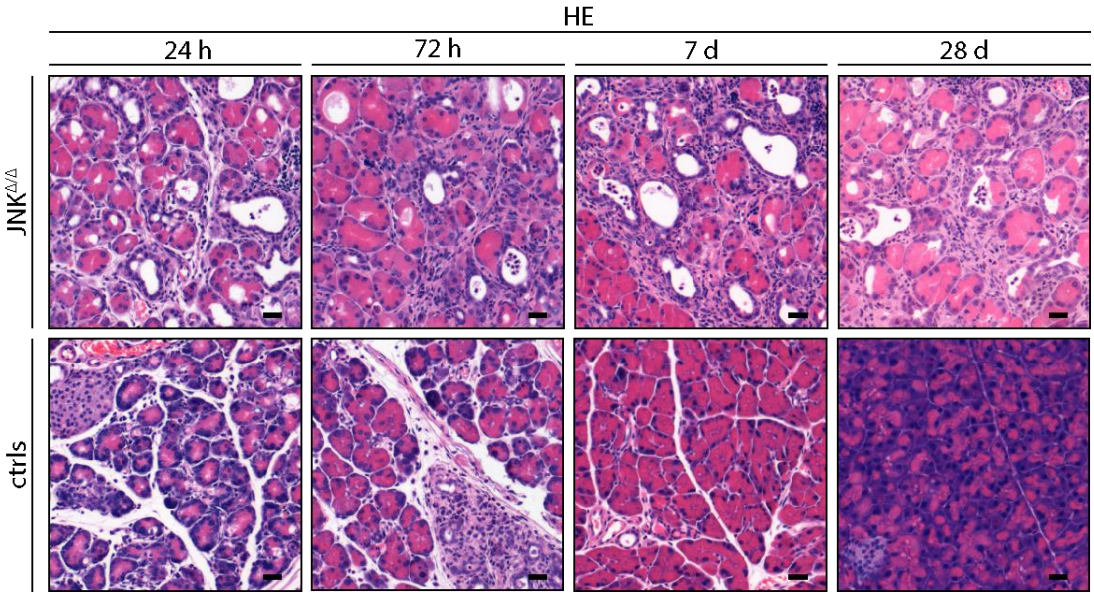

Figure 20 JNK knockout mice are incapable of resolving iAP-induced lesions after iAP
HE staining shows formation of lesions one day after iAP, which peaks three days after iAP. While controls are able to restore the inflicted damage until day 7 after iAP, JNK knockout mice are unable to resolve the lesions with accompanying inflammation even 28 days later. Scale bar: 20 µm.

5.3 JNKs and Kras^{G12D} cooperate to initiate and accelerate PDAC

5.3.1 Kras^{G12D};JNK$^{\Delta/\Delta}$ mice quickly succumb to pancreatic neoplasia

So far, lack of JNK signaling was shown to be responsible for stress-induced dedifferentiation of the acinar compartment, and the inability to regenerate stress-induced lesions. Impaired acinar maintenance and loss of terminal differentiation has been shown to facilitate progression towards PDAC development. Hyperactive Kras is the acknowledged driver of PDAC and mutated in over 90 % of PDACs. Thus, the endogenous LoxP-Stop-LoxP (LSL) Kras^{G12D} allele can be employed to drive PDAC with a pancreas-specific Cre driver line to generate tumors that closely resemble the human situation. In order to test the effect of JNK-deficiency on Kras^{G12D} driven pancreatic tumorigenesis, JNK-deficient mice were crossed to LSL-Kras^{G12D} mice to obtain Kras^{G12D};JNK$^{\Delta/\Delta}$ mice.

Kras^{G12D};JNK$^{\Delta/\Delta}$ mice were born according to Mendelian ratio. Already three weeks after birth, however, they displayed visible abdominal enlargement and died between four to five weeks after birth (median: 29 days, Figure 21, red). This is

highly significant compared to Kras^{G12D} mice ($p<0.0001$). In contrast, retention of one allele of JNK1 and homozygous knockout of JNK2 (Figure 21, petrol) or homozygous knockout of JNK1 under retention of one allele of JNK2 (Figure 21, green) resulted in a median survival of 310 and 245 days, respectively while Kras^{G12D} mice survived 325 days. Thus, based on Kaplan-Meier survival analysis, retention of one allele of either JNK1 or JNK2 rescued the phenotype and did not significantly alter overall survival compared to Kras^{G12D} mice (Figure 21, black).

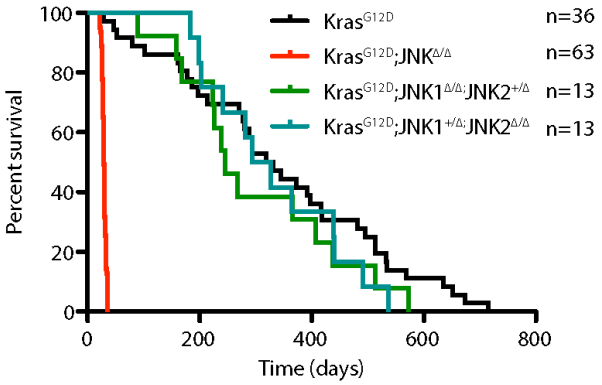

Figure 21 Kaplan-Meier survival of Kras^{G12D} mice with and without retention of JNK alleles
Kras^{G12D};JNK knockout mice show a dramatically shortened survival with a median of 29 days in contrast to K Kras^{G12D} mice with a median of 325 days ($p<0.0001$). The retention of one allele of JNK1 or JNK2 restores overall survival to that of Kras^{G12D} mice.

This quick progression to death is associated with decreased body weights. Total body weights of only two week old Kras^{G12D};JNK$^{\Delta/\Delta}$ mice are already slightly but significantly lower than Kras^{G12D}-positive controls (mean: 6.33 g versus 7.68 g, $p<0.01$) (Figure 22A). Notably, the increase in pancreas to body weight ratio at two weeks after birth is even more pronounced. It has more than tripled in Kras^{G12D};JNK$^{\Delta/\Delta}$ mice in comparison to Kras^{G12D}-positive littermate controls (mean: 2.11 versus 0.53 %, $p<0.001$) (Figure 22B).

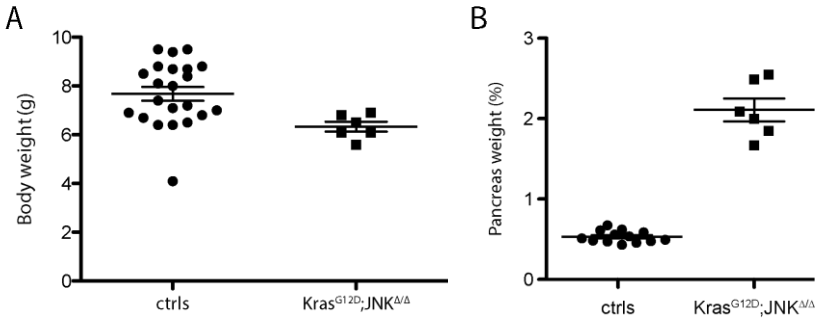

Figure 22 Body weight and pancreas to body weight ratio of Kras^{G12D};JNK$^{\Delta/\Delta}$ mice and controls
(A) Two weeks after birth, Kras^{G12D};JNK$^{\Delta/\Delta}$ mice weighed significantly less than Kras^{G12D}-positive littermate controls ($p<0.01$, mean: 6.33 g versus 7.68 g). (B) The pancreas to body weight ratio more than tripled and is significantly higher in Kras^{G12D};JNK$^{\Delta/\Delta}$ mice ($p<0.001$, mean 0.53 % versus 2.11 %).

Macroscopic analysis revealed a quick progression of fibrosis between one and four weeks of age (Figure 23). One week after birth, histoarchitecture of Kras^{G12D};JNK$^{\Delta/\Delta}$ mice was comparable to that of Kras^{G12D}-positive littermate controls. At two weeks of age, however, Kras^{G12D};JNK$^{\Delta/\Delta}$ mice, show extended areas of acinar-ductal metaplasia (ADM) in contrast to Kras^{G12D}-positive littermate controls (Figure 24).

Over the next two to three weeks, $Kras^{G12D}$;$JNK^{\Delta/\Delta}$ mice develop profound fibrosis, inflammatory infiltrates and pancreatic intraepithelial neoplasias (PanINs) in addition to ADM. Especially the strong fibrotic reaction in three and four week old pancreata is already visible in macroscopic pictures. Due to the huge amount of pancreatic precursor lesions and the fast progression a closer look at the specific distribution of precursor lesions and possible areas of commencing PDAC was taken.

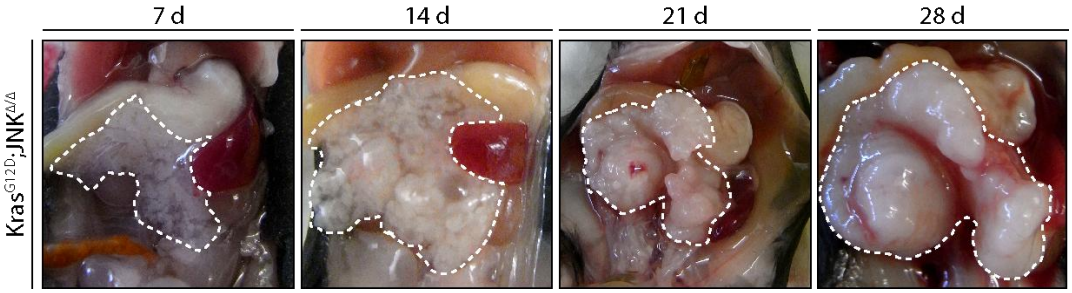

Figure 23 Pancreas macroscopy of $Kras^{G12D}$;$JNK^{\Delta/\Delta}$ mice
Macroscopic progression of the pancreas of $Kras^{G12D}$;$JNK^{\Delta/\Delta}$ mice from one week after birth until death at four to five weeks. While macroscopy looks healthy at 7 days, the pancreas starts to increase in volume between day 14 and day 28. Already at day 21 the pancreas is stiff and progresses to a hard and very defined structure at day 28, when mice are preterminal.

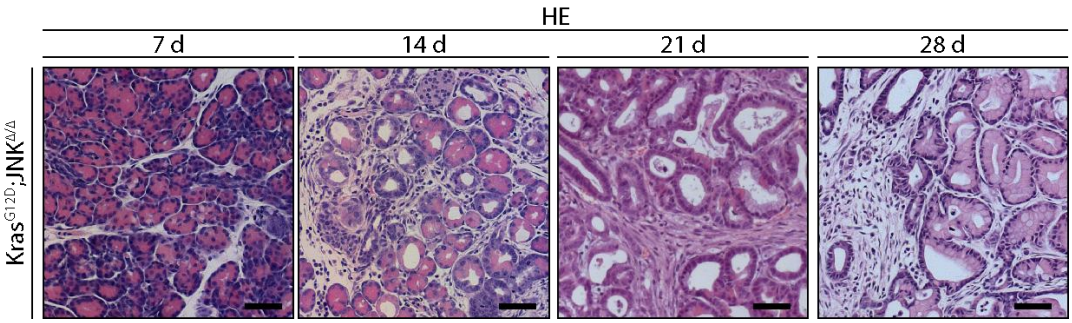

Figure 24 Pancreas histology of $Kras^{G12D}$;$JNK^{\Delta/\Delta}$ mice
Histology reflects the macroscopic appearance of the fibrotic reaction that develops between day 7 and day 28. Furthermore, ADM starts to form at 14 days of age. At 21 days of age, more and more PanINs are detectable which are predominant at day 28, when the fibrotic reaction is also most prominent. Scale bar: 50 µm.

Markers for the acinar, ductal and endocrine compartment were assessed during the tissue remodelling process in $Kras^{G12D}$;$JNK^{\Delta/\Delta}$ mice versus $Kras^{G12D}$-positive controls. The obvious destruction of the acinar compartment as seen in HE cannot be verified through staining for amylase (Figure 25), likely due to antibody trapping in mucinous areas of PanIN lesions, which are present in four week old $Kras^{G12D}$;$JNK^{\Delta/\Delta}$ mice. In contrast, the ductal marker CK19 is progressively upregulated during the assessed time period, while CK19 is restricted to very small areas of ducts and ductules in $Kras^{G12D}$-positive control mice (Figure 26).

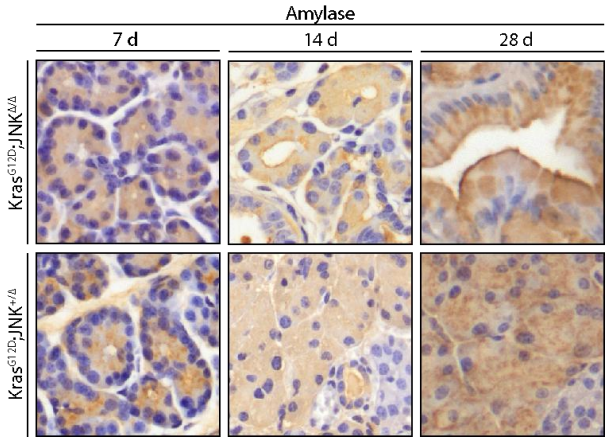

Figure 25 Amylase staining of Kras^{G12D};JNK$^{\Delta/\Delta}$ mice
Amylase expression detected through immunohistochemistry is inconclusive as the mucinous cytoplasm traps amylase antibodies, as can be seen in PanINs at 28 days of age.

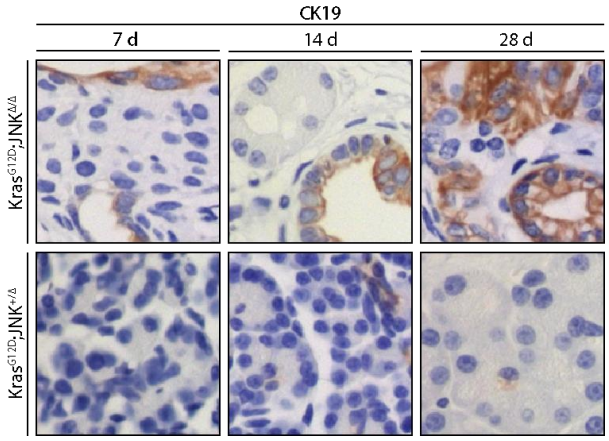

Figure 26 CK19 staining of Kras^{G12D};JNK$^{\Delta/\Delta}$ mice
In Kras^{G12D};JNK$^{+/\Delta}$ mice, CK19 immunostaining is detectable only in ducts and ductules. In contrast, CK19 staining is prominent in ADM and PanIN lesions in Kras^{G12D};JNK$^{\Delta/\Delta}$ mice that begin to form around day 14 and continue to increase.

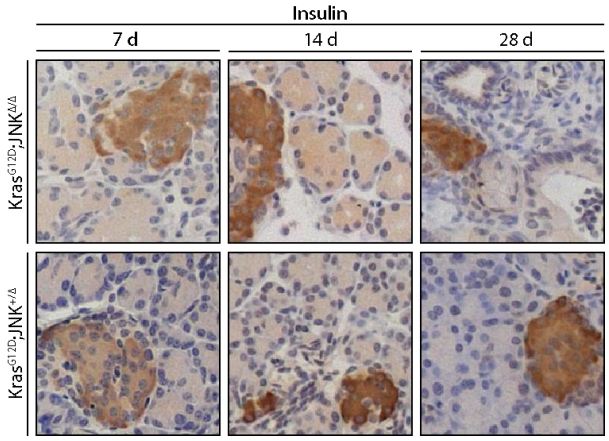

Figure 27 Insulin staining of Kras^{G12D};JNK$^{\Delta/\Delta}$ mice
Staining for insulin does not display obvious changes in islet number or insulin positive area in Kras^{G12D};JNK$^{\Delta/\Delta}$ mice versus controls.

Insulin a marker for the endocrine compartment, on the other hand, seems unchanged. No obvious differences can be detected either in number of islets or the total area of islets in Kras^{G12D};JNK$^{\Delta/\Delta}$ mice versus controls (see also 5.3.5).

5.3.2 Kras^{G12D};JNK$^{\Delta/\Delta}$ mice show marked desmoplasia

Interestingly, Sirius Red staining revealed an extensive fibrotic reaction in Kras^{G12D};JNK$^{\Delta/\Delta}$ mice. During the progression to PDAC, the amount of collagen steadily increased and peaked in terminal Kras^{G12D};JNK$^{\Delta/\Delta}$ mice (Figure 28).

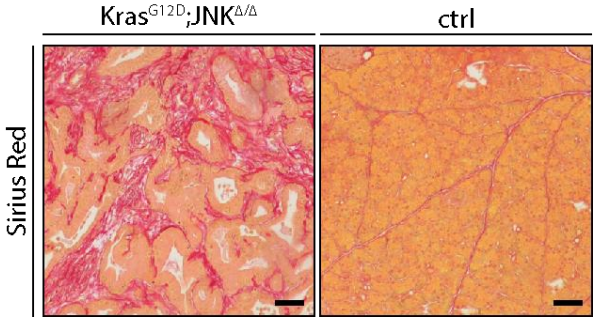

Figure 28 Desmoplastic reaction in terminal Kras^{G12D};JNK$^{\Delta/\Delta}$ mice
Terminal, four to five week old Kras^{G12D};JNK$^{\Delta/\Delta}$ mice show a marked desmoplastic reaction. Scale bar: 20 µm.

Likely sources of collagen deposits are αSMA positive stellate cells in the pancreas. Immunohistochemistry for αSMA revealed large amounts of activated stellate cells in four week old Kras^{G12D};JNK$^{\Delta/\Delta}$ mice. In addition, extensive staining for infiltrating F4/80-positive macrophages was visible (Figure 29).

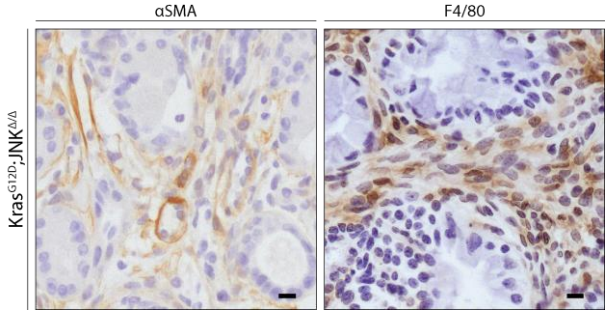

Figure 29 Stellate cells and macrophages are abundant in terminal Kras^{G12D};JNK$^{\Delta/\Delta}$ mice
The desmoplastic reaction is very pronounced in four week old Kras^{G12D};JNK knockout mice. Likely sources are αSMA-positive stellate cells and F4/80-positive macrophages. Scale bar: 20 µm.

5.3.3 JNK-deficiency in Kras^{G12D} mice drastically increases initiation of precursor lesions and progression to PDAC

The physiologic acinar compartment almost completely vanished in terminal Kras^{G12D};JNK$^{\Delta/\Delta}$ mice. Thus, it was interesting to assess the specific distribution of lesions per total (Figure 30A,B). Kras^{G12D};JNK$^{\Delta/\Delta}$ mice display extended areas of ADM, which increased to 17.5 % in comparison to 0.1 % in controls (Figure 30C). AFL absent from controls accounted for 0.01 %. Low-grade PanIN1 covered 28.7 % and high-grade PanINs 0.2 % of the total area in contrast to 0.1 % and 0.0 % in controls, respectively. PDAC accounted for 1.2 % of the total area in Kras^{G12D};JNK$^{\Delta/\Delta}$ mice but was completely absent from age matched controls. Notably, several

independent small entities of PDAC were identified. Therefore, Kras^{G12D};JNK$^{\Delta/\Delta}$ mice had multifocal PDAC at only four to five weeks of age.

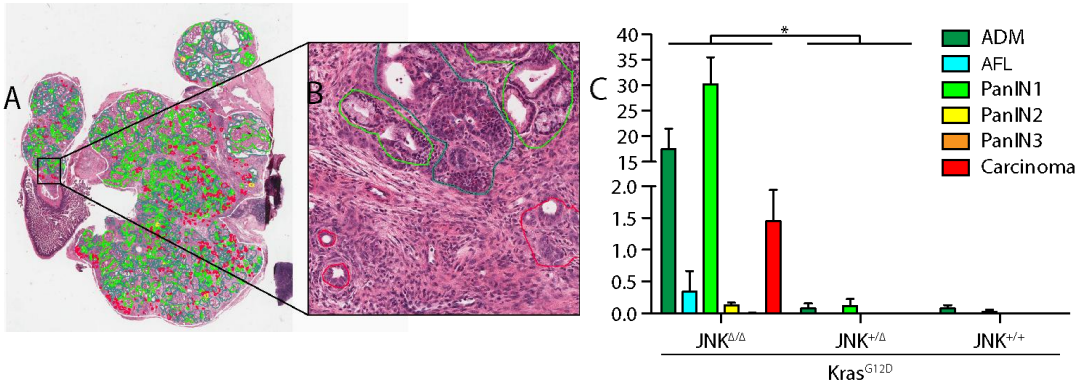

Figure 30 Overview and quantification of precursor lesion and PDAC area in Kras^{G12D};JNK$^{\Delta/\Delta}$ mice

(A) Representative picture of a whole pancreas slice as assessed by veterinary pathologist (light green = PanIN1, dark green = ADM and red = carcinoma) and magnification (B). (C) At four weeks of age, only occasional lesions were present in Kras^{G12D} mice and controls, while 17.5 % of the total area in Kras^{G12D};JNK knockout mice are ADM and 28.7 % PanIN1 (right). AFL covered 0.01 %, PanIN2 0.2 % and PanIN3 0.02 % although PanIN3 were only detected in 3 of 5 Kras^{G12D};JNK$^{\Delta/\Delta}$ mice. Multifocal carcinoma added up to a total area of 1.2 % separated into several small entities.

5.3.4 PDAC in Kras^{G12D};JNK$^{\Delta/\Delta}$ mice is occasionally invasive but not metastatic

To test if these tumors invade the surrounding tissue and metastasize to other organs, HE stained sections of pancreatic tumors of Kras^{G12D};JNK$^{\Delta/\Delta}$ mice still connected to the duodenum were examined. Only in one mouse invasive PDAC was noted, invading into the duodenum (Figure 31). Interestingly, macroscopic metastases were neither detected in the liver nor the lung. In addition, serial sections of liver and lung taken every 30 µm were HE stained and did also not reveal any micrometastasis.

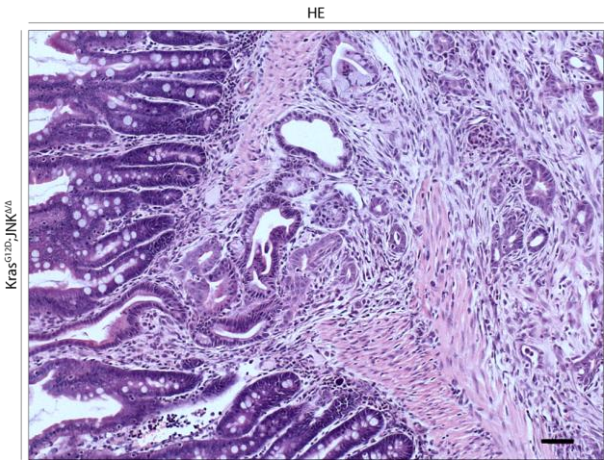

Figure 31 Invasion front of pancreatic tumor into the muscularis mucosae of the gut

Only in a single case, invasion of pancreatic tumor into other organs (here the duodenum) was detectable in Kras^{G12D};JNK$^{\Delta/\Delta}$ mice. Scale bar: 50 µm.

5.3.5 Cause of death cannot be attributed to endocrine or exocrine insufficiency

Our initial hypothesis on cause of death in Kras^{G12D};JNK$^{\Delta/\Delta}$ mice was exocrine pancreatic insufficiency, as most if not all of the acinar parenchyma is lost at late stages in these mice. Therefore, mice were fed with Pancrex®, a special diet

providing digestive enzymes from three weeks onwards. However, a survival benefit of Kras^{G12D};JNK$^{\Delta/\Delta}$ mice on Pancrex could not be detected. Another possible cause of death is endocrine pancreatic insufficiency with blood glucose levels being too low to maintain body functions. With approximately 113 mg/dl, blood glucose levels of Kras^{G12D};JNK$^{\Delta/\Delta}$ mice were, however, at the expected level (Figure 32).

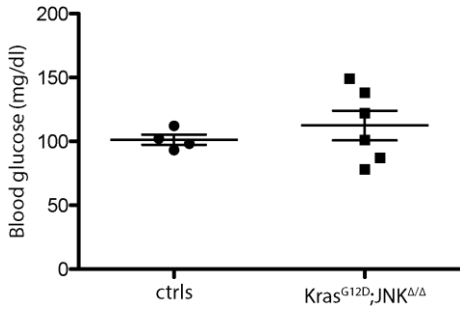

Figure 32 Blood glucose in terminal Kras^{G12D};JNK$^{\Delta/\Delta}$ mice does not differ from age-matched healthy controls
Blood glucose in terminal Kras^{G12D};JNK$^{\Delta/\Delta}$ mice is not significantly changed from levels in age-matched healthy controls (p = 0.76, mean 113 versus 101 mg/dl).

To confirm this finding, measurement of ketones in the urine of terminal Kras^{G12D};JNK$^{\Delta/\Delta}$ mice was performed and no increase (data not shown) was detected. The actual cause of death of Kras^{G12D};JNK$^{\Delta/\Delta}$ mice could therefore not be determined. It is nonetheless still possible that the huge tumor bulk present in the mouse might have limited uptake and digestion of food.

5.3.6 Global proliferation indices are unchanged in Kras^{G12D};JNK$^{\Delta/\Delta}$

As pancreas weight is strongly increasing in Kras^{G12D};JNK$^{\Delta/\Delta}$ mice, it was analyzed whether this is due to an increase in proliferation or a decrease in apoptosis. Ki67 staining was performed for proliferation and did not reveal a significant difference between Kras^{G12D};JNK$^{\Delta/\Delta}$ mice and age matched controls (Figure 33A,B).

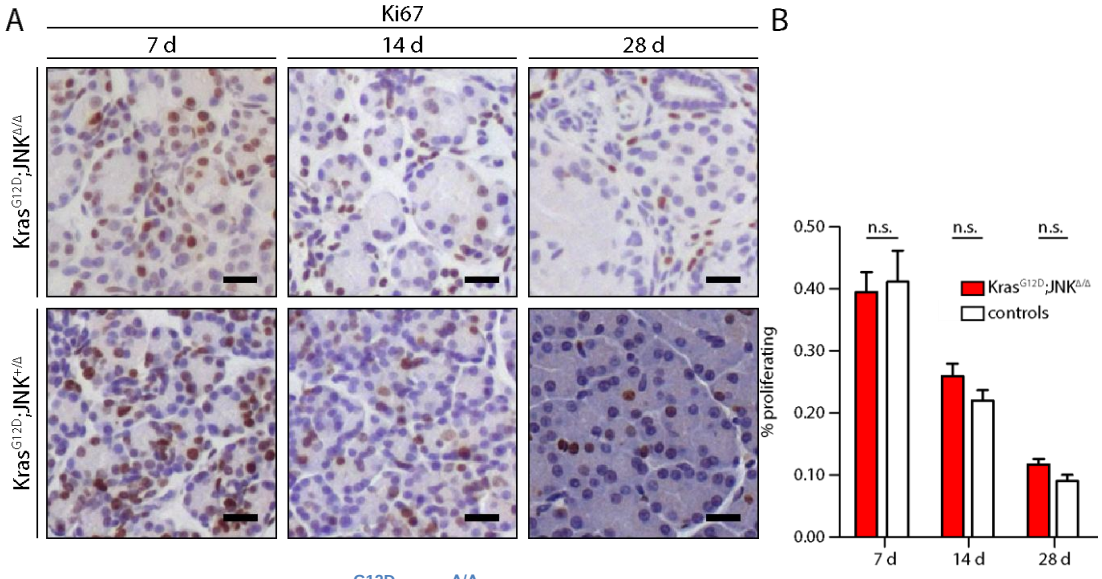

Figure 33 Ki67 staining in Kras^{G12D};JNK$^{\Delta/\Delta}$ mice versus controls
(A) Global proliferation index in Kras^{G12D};JNK$^{\Delta/\Delta}$ mice versus controls as assessed by Ki67 staining. (B) Quantification reveals no significant change in proliferation at seven, 14 or 28 days of age. Scale bar: 20 µm.

5.3.7 Apoptosis is slightly increased in terminal $Kras^{G12D};JNK^{\Delta/\Delta}$

As proliferation was not changed on a global level, cleaved Caspase 3 was assessed as a marker for apoptosis. No significant differences were found between $Kras^{G12D};JNK^{\Delta/\Delta}$ mice and controls except for a slight increase in apoptotic cells in 4 week old $Kras^{G12D};JNK^{\Delta/\Delta}$ mice, which however remained at very low levels (Figure 34).

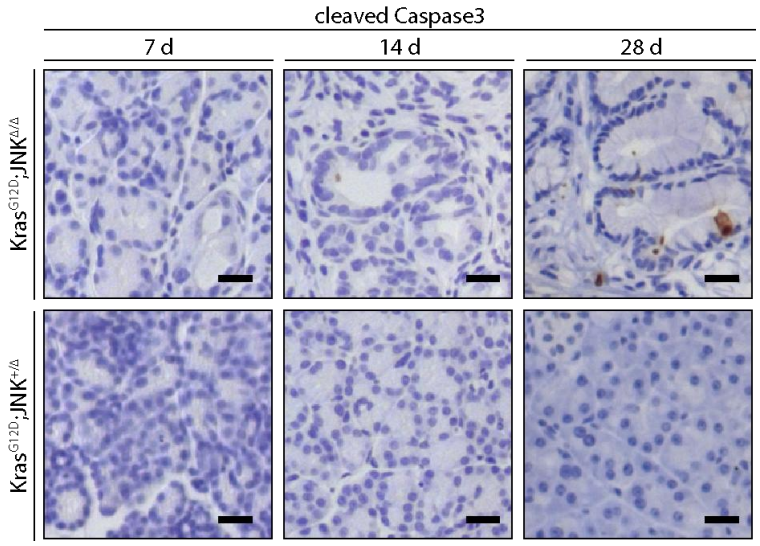

Figure 34 Cleaved Caspase3 staining in $Kras^{G12D};JNK^{\Delta/\Delta}$ mice versus controls
Global apoptotic index in $Kras^{G12D};JNK^{\Delta/\Delta}$ mice versus controls as assessed by cleaved Caspase 3 staining. Only rare apoptotic events could be detected in both cohorts. Scale bar: 20 µm.

5.3.8 Elastase-CreER;$Kras^{G12D};JNK^{\Delta/\Delta}$ mice confirm transformation of acinar cells as cause of PDAC formation

To determine if acinar rather than centroacinar or ductal cells are the transformed cells and source of PDAC, $Kras^{G12D};JNK^{\Delta/\Delta}$ mice, which express Cre recombinase under the acinar-specific elastase promoter (ElaCreER;$Kras^{G12D};JNK^{\Delta/\Delta}$ mice) were generated. Cre recombinase activity in these mice can be controlled in a temporal manner by injection of tamoxifen. Tamoxifen changes the conformation of the fused estrogen receptor unmasking a hidden nuclear localization signal, which imports the recombinase into the nucleus. Upon nuclear translocation, it recombines the LoxP sequences, activating $Kras^{G12D}$ and deleting JNK1 and JNK2. ElaCreER;$Kras^{G12D};JNK^{\Delta/\Delta}$ mice were injected with tamoxifen at four weeks of age. These mice developed tumors with a mean onset of 31 weeks after injection while controls (ElaCreER;$Kras^{G12D};JNK^{+/\Delta}$) did not even display any precursor lesions. This result confirms that JNK knockout in acinar cells can give rise to PDAC.

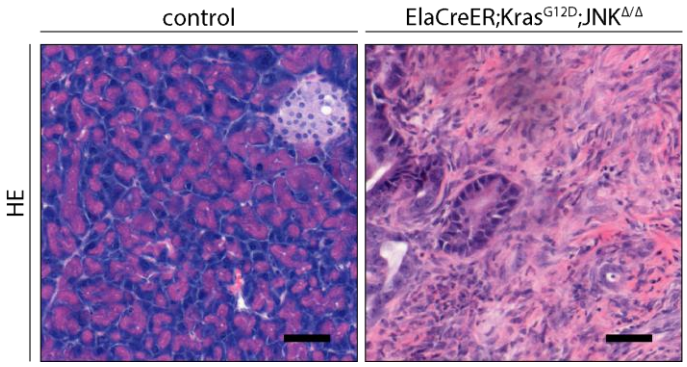

Figure 35 PDAC in ElaCreER-driven Kras^{G12D};JNK$^{\Delta/\Delta}$ mice
PDAC in elastase promoter driven CreER expressing Kras^{G12D};JNK knockout mice. Tamoxifen-induction at four weeks of age results in acinar specific activation of Kras^{G12D} and deletion of JNK1 and JNK2. After a mean of 31 weeks, ElaCreER;Kras^{G12D};JNK$^{\Delta/\Delta}$ mice develop fatal PDAC from acinar cells while ElaCreER;Kras^{G12D};JNK$^{+/\Delta}$ mice do not even display precursor lesions. Scale bar: 50 µm.

5.4 Molecular analysis of Kras^{G12D};JNK$^{\Delta/\Delta}$ mice

5.4.1 AKT signaling is unchanged in Kras^{G12D};JNK$^{\Delta/\Delta}$ mice

Before checking particular pathways and their contribution to the strong phenotype of Kras^{G12D};JNK$^{\Delta/\Delta}$ mice, the two core signaling pathways downstream of Kras^{G12D}, PI3K/AKT and MAPK/ERK, were examined. Western Blot did not show any difference in Thr308-phosphorylated AKT between Kras^{G12D};JNK$^{\Delta/\Delta}$ and control mice. Thus, AKT seems not to contribute to the phenotype of Kras^{G12D};JNK$^{\Delta/\Delta}$ mice.

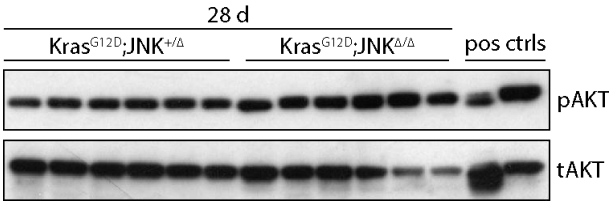

Figure 36 AKT signaling in JNK knockout mice versus controls
WB does not reveal changes in AKT signaling between Kras^{G12D};JNK knockout mice and controls. pAkt = phospho-AKT, tAKT = total AKT.

5.4.2 ERK signaling is active in most Kras^{G12D};JNK$^{\Delta/\Delta}$ mice

Interestingly, Western Blot for Thr202/Tyr204-phosphorylated ERK shows increased levels of activated ERK in 4 out of 6 Kras^{G12D};JNK$^{\Delta/\Delta}$ mice, while ERK signaling was activated in only 1 out of 6 controls. This difference in ERK activity most likely stems from disinhibited Kras^{G12D} signaling in pancreatic precursors, which are absent in age matched control mice.

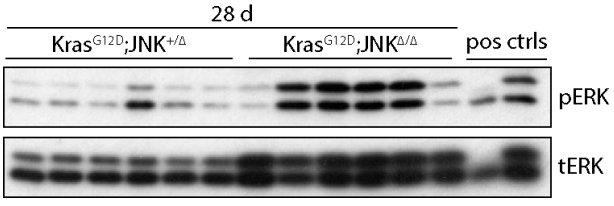

Figure 37 ERK signaling in JNK knockout mice versus controls
Upregulation of ERK signaling is detectable in Kras^{G12D};JNK knockout mice. pERK = phospho-ERK, tERK = total ERK.

5.4.3 The DNA damage response is not active in Kras^{G12D};JNK$^{\Delta/\Delta}$ mice

MKK7, one of two JNK upstream kinases, has been shown to be involved in the DNA damage response (DDR) pathway. To test if the DDR pathway is active in Kras^{G12D};JNK$^{\Delta/\Delta}$ mice, tissue lysate from four week old Kras^{G12D};JNK$^{\Delta/\Delta}$ and controls were blotted. Interestingly, they did not display an upregulation of γH2AX, a histone variant central to the DDR pathway (Figure 38). Only very few nuclei in IHC of four week old mice stained positive for γH2AX. Earlier time points (one and two weeks) showed a moderate expression of γH2AX, which however is unchanged between Kras^{G12D};JNK$^{\Delta/\Delta}$ and control mice.

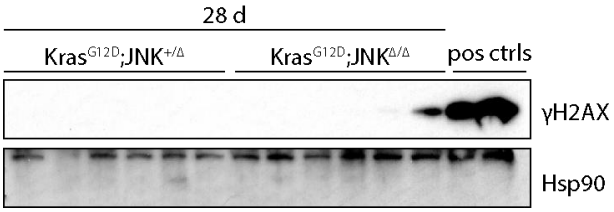

Figure 38 γH2AX is not detectable in JNK knockout mice
γH2AX, a marker for active DNA damage response is not detectable in terminal Kras^{G12D};JNK knockout mice or controls.

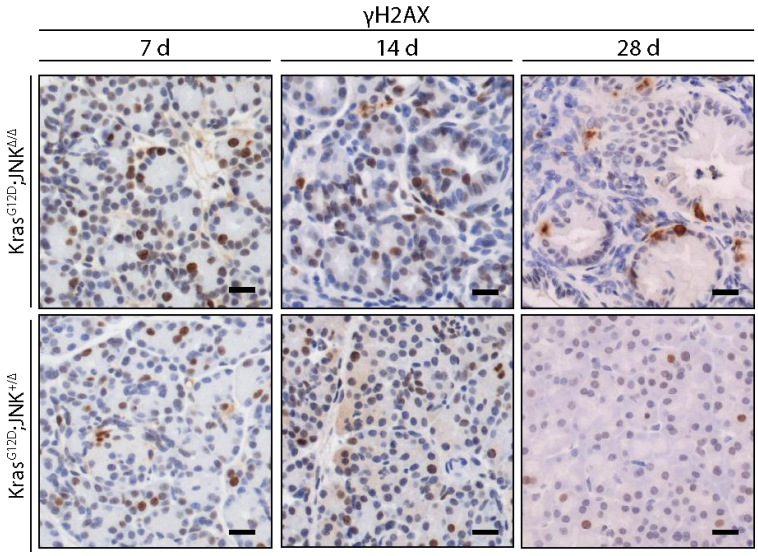

Figure 39 γH2AX staining in Kras^{G12D};JNK knockout mice versus controls
Global macroscopic assessment of γH2AX positive nuclei does not reveal changes in the amount of S139-phosphorylated H2AX nuclei. Scale bar: 20 µm.

5.4.4 p53 misregulation might be involved in the rapid phenotype of Kras^{G12D};JNK$^{\Delta/\Delta}$ mice

p53 is a major tumor suppressor and a known direct target of JNK [180]. Therefore, inhibition of p53 activation might be one possible cause for the rapid phenotype of Kras^{G12D};JNK$^{\Delta/\Delta}$ mice. At seven days of age, overall p53 protein levels were similarly low in Kras^{G12D};JNK$^{\Delta/\Delta}$ mice and Kras^{G12D};JNK$^{+/\Delta}$ mice (Figure 40). In 28 day old Kras^{G12D};JNK$^{\Delta/\Delta}$ mice, however, slight upregulation is detectable (Figure 41), which is in agreement with immunohistochemical staining of p53 (Figure 42). Although nuclear localization of p53 is detectable in 14 day old Kras^{G12D};JNK$^{\Delta/\Delta}$ mice minor shifts in band size in the Western Blot of 28 day old Kras^{G12D};JNK$^{\Delta/\Delta}$ mice hint at a

possible differential posttranslational modification of p53 that might inhibit its transactivation potential. Thus, further in-depth analysis is needed to clarify a possible engagement of p53 in PDAC development of Kras^{G12D};JNK$^{\Delta/\Delta}$ mice.

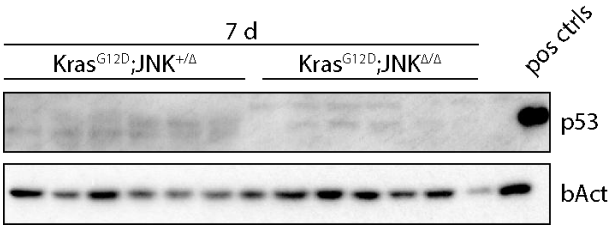

Figure 40 p53 in seven day old Kras^{G12D};JNK$^{\Delta/\Delta}$ mice versus controls
Immunoblot of p53 in seven day old Kras^{G12D};JNK$^{\Delta/\Delta}$ mice versus controls does not show activation of p53.

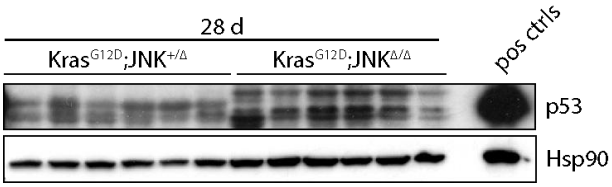

Figure 41 p53 in 28 day old Kras^{G12D};JNK$^{\Delta/\Delta}$ mice versus controls
Slight upregulation of p53 is detectable in Kras^{G12D};JNK$^{\Delta/\Delta}$ mice compared to controls. Interestingly, minor shifts in band size hint at a possible difference in posttranslational modification of p53 in JNK$^{\Delta/\Delta}$ mice.

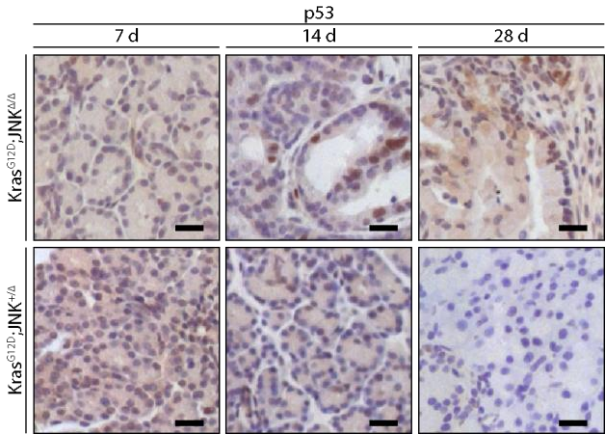

Figure 42 p53 in seven, 14 and 28 day old Kras^{G12D};JNK$^{\Delta/\Delta}$ mice and controls
Upregulation of p53 is most prominent in ADM of 14 day old Kras^{G12D};JNK$^{\Delta/\Delta}$ mice and seems lost in most of the PanINs seen at 28 days of age. Scale bar: 20 µm.

5.4.5 SOX9 is drastically upregulated from two weeks onward in Kras^{G12D};JNK$^{\Delta/\Delta}$ mice versus controls

Acinar maintenance poses a significant barrier for transformatory events [239], while upregulation of progenitor-like markers seems to been an important prerequisite in the formation of ADM and transformation [178]. As acinar maintenance in JNK$^{\Delta/\Delta}$ mice was impaired, expression of Sox9, a marker for MPC of the pancreas was tested. Indeed, strong upregulation of SOX9 in precursor lesions of Kras^{G12D};JNK$^{\Delta/\Delta}$ mice (day 14 and day 28) was detected, while expression of SOX9 in seven day old Kras^{G12D};JNK$^{\Delta/\Delta}$ was comparable to controls.

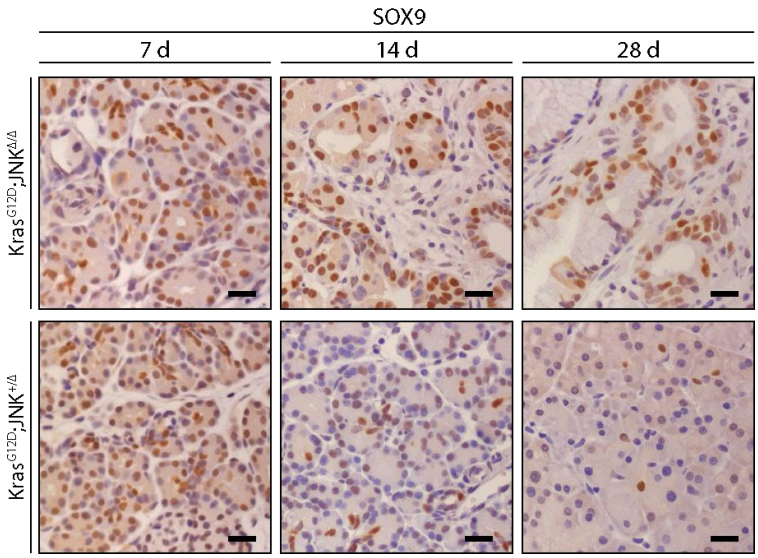

Figure 43 Expression of SOX9 in Kras^{G12D};JNK$^{\Delta/\Delta}$ tissue
Staining for SOX9 is strong in Kras^{G12D};JNK$^{\Delta/\Delta}$ mice and controls seven days after birth, indicating ongoing embryonal signaling pathways. While expression of SOX9 in controls is restricted to centroacinar cells at 14 and 28 days of age, expression remains high in Kras^{G12D}; JNK$^{\Delta/\Delta}$ mice. Scale bar: 20 µm.

5.4.6 Array profiling of seven day old Kras^{G12D};JNK$^{\Delta/\Delta}$ mice reveals a plethora of enriched oncogenic and inflammatory gene sets

The quick progression of Kras^{G12D};JNK$^{\Delta/\Delta}$ mice towards PDAC, which is even faster than in Kras^{G12D};p53$^{\Delta/\Delta}$ mice (data not shown) most likely involves several different misregulated pathways. To elucidate the earliest affected pathways in an unbiased way, expression arrays of morphologically still largely unchanged pancreata of seven day old Kras^{G12D};JNK$^{\Delta/\Delta}$ and Kras^{G12D};JNK$^{+/\Delta}$ mice were performed at the KFB in Regensburg. Additionally, seven day old JNK$^{\Delta/\Delta}$ and JNK$^{+/\Delta}$ mice were included. Microarray results were analyzed by gene set enrichment analysis (GSEA). GSEA revealed a plethora of signaling pathways to be regulated already in one week old Kras^{G12D};JNK$^{\Delta/\Delta}$ versus control mice. Gene sets were considered significantly enriched with $p<0.05$ and FDR<25 %. Accordingly, 30.7 % of the analyzed MSig Database Gene Sets in the collection Canonical Pathways (CP) were enriched (Figure 44). Chemical and Genetic Perturbations (CGP) showed a global enrichment of 51.8 % and Transcription Factor Targets (TFT) of 11.8 %. Interestingly, none of the microRNA signatures was significantly enriched in Kras^{G12D};JNK$^{\Delta/\Delta}$ mice, while more than half of the oncogenic and immunologic signatures were enriched (62.0 % and 54.2 %, respectively). Figure 45 shows the fifteen most regulated mRNAs detected in the array. Although, IL6, an agonist of the STAT3 pathway, is not among the highest scoring, it is, similar to SOCS3, a negative regulator of the STAT3 signaling axis, significantly enriched. Furthermore, the IL6 pathway was significantly enriched in the CP collection besides many other inflammatory pathways in the immunologic collection.

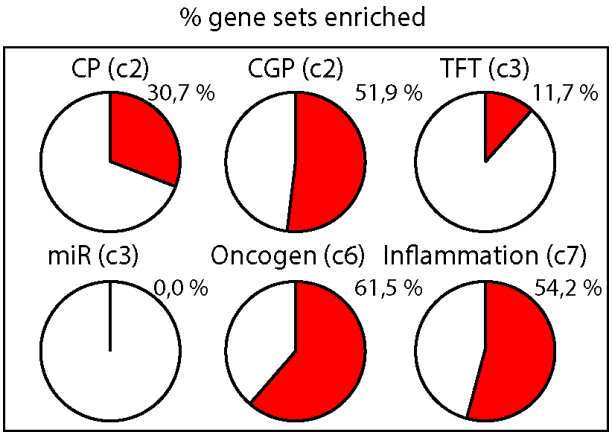

Figure 44 Percentage of significantly enriched gene sets

Percentage of significantly (p<0.05, FDR<25 %) enriched gene sets in the respective collections of the MSigDB, Broad Institute, CA, USA. CP = Canonical Pathways 30.7 %, CGP = Chemical and Genetic Perturbations 51.9 %, TFT = Transcription Factor Targets 11.7 %, miR = microRNA Targets 0.0 %, Oncogenic signatures 61.5 %, Immunologic signatures 54.2 %.

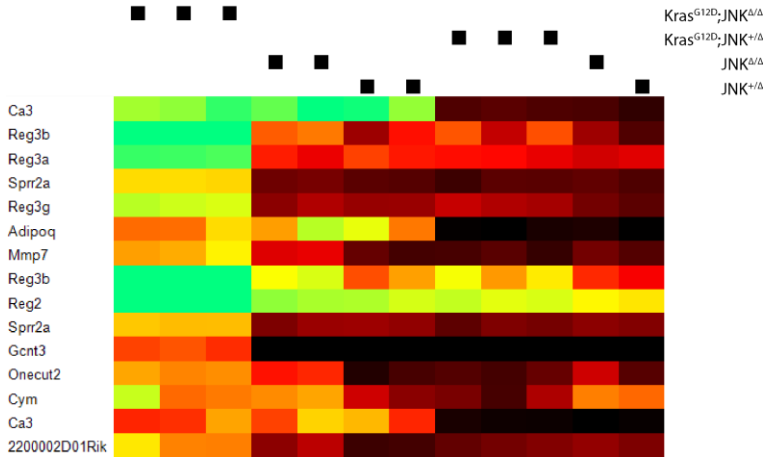

Figure 45 Most upregulated genes in Kras^{G12D};JNK$^{\Delta/\Delta}$ mice versus controls

Fifteen most upregulated gene expression levels in Kras^{G12D};JNK$^{\Delta/\Delta}$ mice versus controls at seven days of age. Interestingly, no difference for most gene expression levels can be detected between Kras^{G12D};JNK$^{+/\Delta}$, JNK$^{\Delta/\Delta}$ and JNK$^{+/\Delta}$ mice at seven days of age. Picture generated by Tar Viturawong, MPIB, Martinsried.

5.4.7 NF-κB signaling is slightly downregulated in Kras^{G12D};JNK$^{\Delta/\Delta}$ mice

Inflammation is a main driver of PDAC [33]. Thus, possible involvement of the two most investigated inflammatory pathways in tumorigenesis, NF-κB and STAT3, was tested in Kras^{G12D};JNK$^{\Delta/\Delta}$ mice. To test activation of the NF-κB pathway, an electromobility shift assay (EMSA) was performed in collaboration with Dr. Björn Lamprecht at the Charité, Berlin. Although the results of the EMSA imply an induction of NF-κB target genes (Figure 46A), the levels of phosphorylated and activated pp65 were not increased (Figure 46B). Whole tissue lysates of one week and four week old Kras^{G12D};JNK$^{\Delta/\Delta}$ mice even showed slight downregulation of phosphorylated p65. It is therefore unlikely that the NF-κB pathway contributes to the strong phenotype of Kras^{G12D};JNK$^{\Delta/\Delta}$ mice.

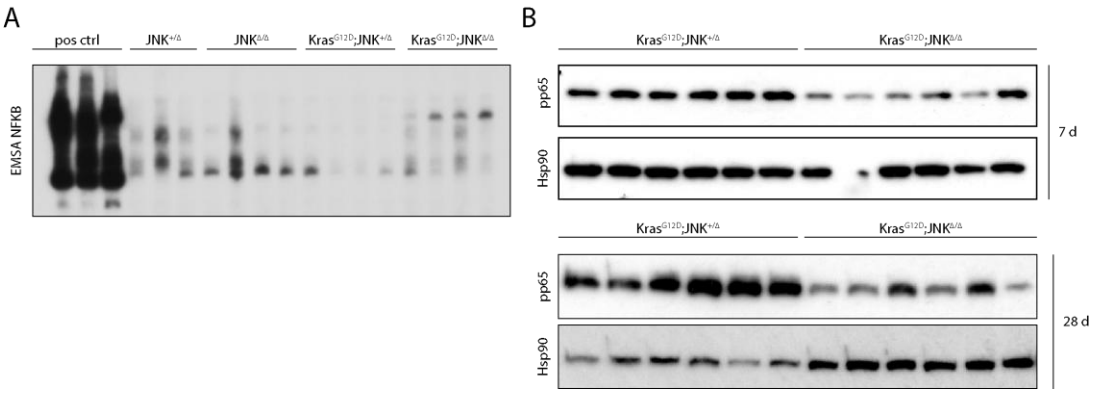

Figure 46 NF-κB signaling in Kras^{G12D};JNK$^{Δ/Δ}$ mice
(A) EMSA of Kras^{G12D}; JNK$^{Δ/Δ}$ mice reveals slight upregulation of NF-κB promoter binding in contrast to controls. (B) To confirm the activation of the NF-κB pathway on protein level, phospho-p65 was assessed in seven day and 28 day old Kras^{G12D}; JNK$^{Δ/Δ}$ mice. NF-κB activity was slightly decreased in comparison to controls.

5.4.8 AP-1 signaling is active in Kras^{G12D};JNK$^{Δ/Δ}$ mice

As previously reported, c-Jun is not only a direct target of JNKs but also of Kras. To test whether the c-Jun signaling axis is activated in Kras^{G12D};JNK$^{Δ/Δ}$ mice and whether c-Jun is still able to form the transcription factor AP-1 together with Fos proteins, EMSA was performed. AP-1 responsive target promoters are occupied in seven day old Kras^{G12D};JNK$^{Δ/Δ}$ mice (Figure 47A). A supershift assay confirmed that several components required for AP-1 activity, such as Jun and Fos proteins, are present (Figure 47B). These data are further supported by the profound increase in Fra1 expression in terminal Kras^{G12D};JNK$^{Δ/Δ}$ mice (Figure 48), which is an AP-1 responsive target gene. Immunohistochemistry, however, indicated that c-Jun signaling is activated in stromal rather than epithelial cells.

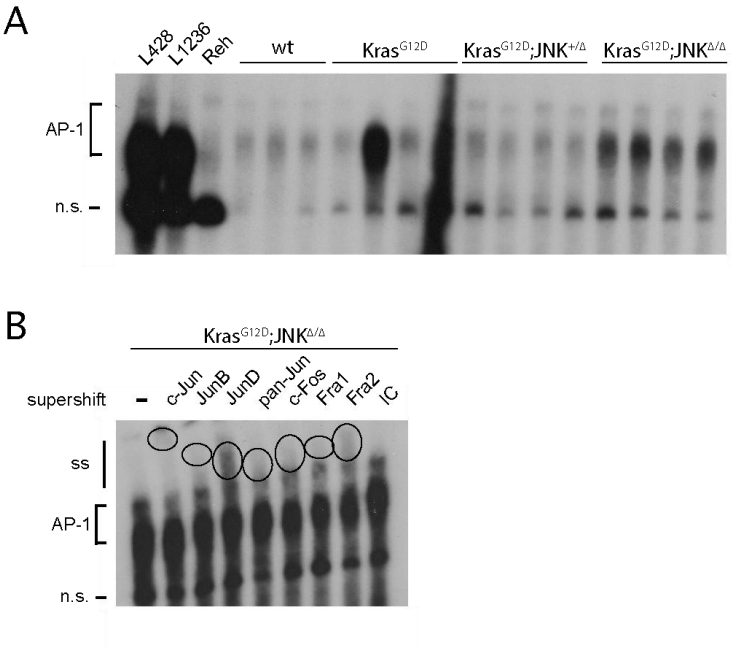

Figure 47 AP-1 constituting transcription factors are present in seven day old Kras^{G12D};JNK$^{Δ/Δ}$ mice
(A) AP-1 signaling components are upregulated in Kras^{G12D};JNK$^{Δ/Δ}$ mice. (B) Supershifts (ss) confirm several Jun and Fra proteins to be upregulated already seven days after birth in a Kras^{G12D};JNK$^{Δ/Δ}$ mouse. Performed by Dr. Björn Lamprecht, Charité, Berlin. N.s. = non-specific.

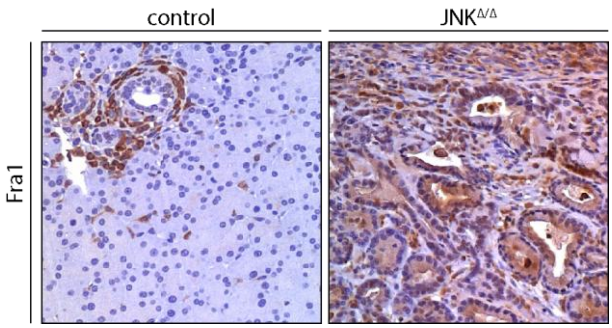

Figure 48 AP-1 responsive Fra1 is active in the stromal compartment
Immunohistochemistry reveals strong Fra1 expression in terminal Kras^{G12D};JNK$^{\Delta/\Delta}$ mice although in the stromal rather than the epithelial compartment. Performed by Dr. Sandra Diersch, MRI, München.

5.5 STAT3 signaling is active in Kras^{G12D};JNK$^{\Delta/\Delta}$ mice

5.5.1 STAT3 signaling is upregulated in Kras^{G12D};JNK$^{\Delta/\Delta}$ mice

Previous studies demonstrated a profound contribution of STAT3 signaling to PDAC development [158, 159]. IL6, an upstream activator of STAT3 signaling and SOCS3, an inhibitor of STAT3 signaling were among the significantly upregulated genes in the microarrays of one week old Kras^{G12D};JNK$^{\Delta/\Delta}$ versus control mice. Confirmation of active STAT3 signaling on protein level could be demonstrated by Western Blot (Figure 49). Although there is some variation, expression of active (pY705) STAT3 in one and four week old whole tissue lysates is on average higher in Kras^{G12D};JNK$^{\Delta/\Delta}$ mice compared to controls. To investigate active STAT3 signaling on a cellular level, immunohistochemistry was performed (Figure 50). This experiment demonstrates that STAT3 signaling is activated in both, stromal and epithelial cells.

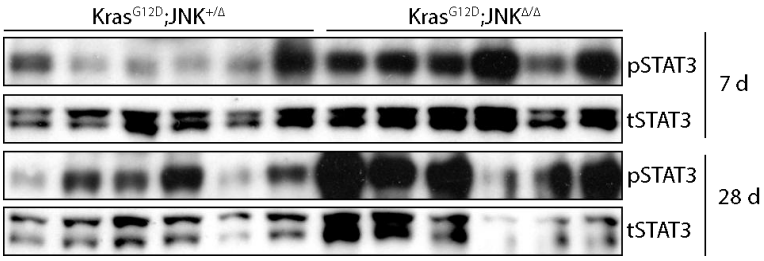

Figure 49 STAT3 signaling in Kras^{G12D};JNK$^{\Delta/\Delta}$ mice
Active STAT3 signaling (pSTAT3) was markedly upregulated in seven day and 28 day old Kras^{G12D};JNK$^{\Delta/\Delta}$ mice.

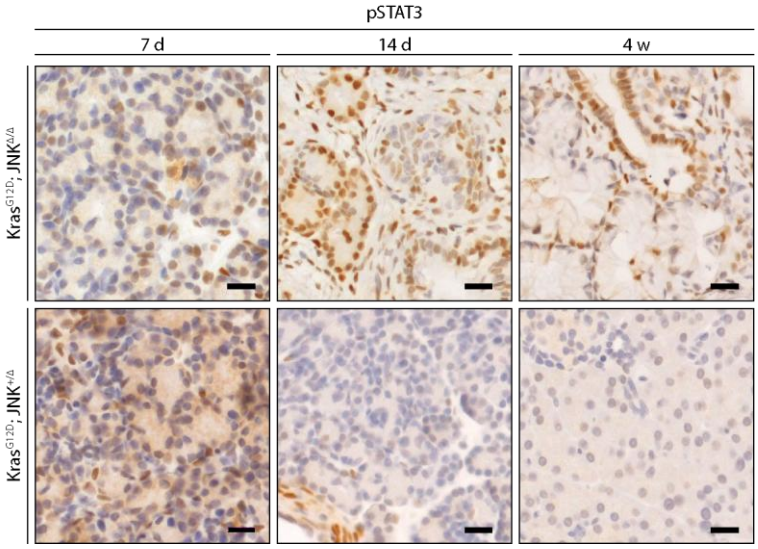

Figure 50 Pancreatic epithelial and stromal cells stain positive for active STAT3 in $Kras^{G12D}$;$JNK^{\Delta/\Delta}$ mice
Immunostaining confirmed Western Blot results with clear pSTAT3 positive nuclei of epithelial cells in ADM and PanIN of $Kras^{G12D}$;$JNK^{\Delta/\Delta}$ mice, which were not observed in age-matched controls. Scale bar: 20 µm.

5.5.2 Activity of STAT3 signaling after JNK inhibition depends on the context of the particular pancreatic cancer cell line

In 1999, Lim *et al*. reported an inhibitory effect of JNK signaling on STAT3 signaling [240]. To test a potential activation of STAT3 signaling after inhibition of JNKs in pancreatic cancer, JNKs were inhibited with the JNK-specific inhibitor JNK-IN-8 in murine PDAC-derived $Kras^{G12D}$ positive cell lines. Afterwards, STAT3 signaling was stimulated with IL6 and activation detected via Western Blot in different pancreatic cancer cell lines (Figure 51A). However, a clear correlation of IL6-triggered STAT3 activation and JNK inhibition could not be detected in the tested cell lines (Figure 51B). This indicates that JNK signaling might not directly be linked to STAT3 signaling in murine PDAC-derived cell lines.

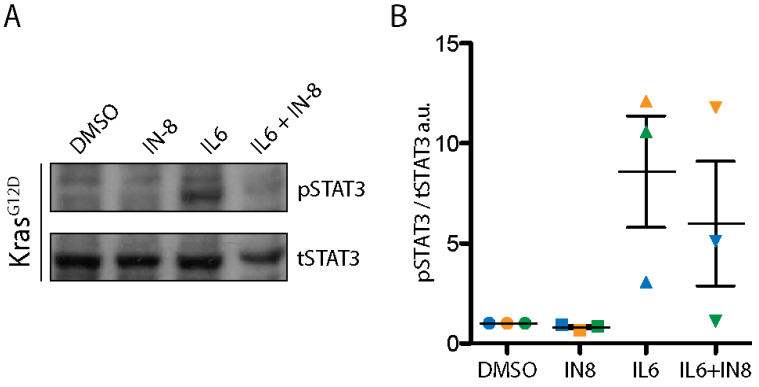

Figure 51 IL6-triggered STAT3 activation is not enhanced by JNK inhibition
(A) Western Blot of active (pSTAT3) and total (tSTAT3) STAT3 in one murine $Kras^{G12D}$ positive pancreatic cancer cell line treated with a JNK signaling inhibitor (IN-8) and a trigger for STAT3 signaling (IL6) or the combination of both. (B) Densitometry of different $Kras^{G12D}$ positive pancreatic cancer cell lines does not show a consistent alteration of IL6-triggered STAT3 activation after JNK inhibition.

5.6 Knockout of STAT3 does not change survival or histology of $Kras^{G12D}$;$JNK^{\Delta/\Delta}$ mice

5.6.1 Knockout of STAT3 in $Kras^{G12D}$;$JNK^{\Delta/\Delta}$ mice does not affect survival

Despite the lack of STAT3 activation in JNK-inhibited cells *in vitro,* a putative cooperative effect of STAT3 and JNK signaling in the development of PDAC *in vivo* could not be excluded. Thus, to analyze the interference of STAT3 and JNK signaling *in vivo*, $STAT3^{LoxP/LoxP}$ mice were intercrossed with $Kras^{LSL\text{-}G12D/+}$;$JNK^{LoxP/LoxP}$ mice (Figure 52).

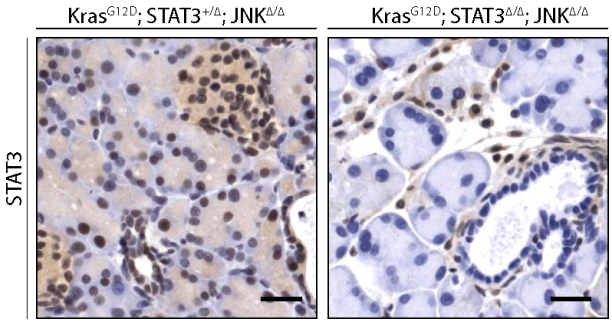

Figure 52 Confirmation of STAT3 knockout in $Kras^{G12D}$; $STAT3^{\Delta/\Delta}$; $JNK^{\Delta/\Delta}$ mice
STAT3 protein is not detectable in epithelial cells of STAT3 knockout mice in contrast to controls and the stromal compartment in both mice. Scale bar: 20 µm.

Using this approach the hypothesis that the knockout of STAT3 prolongs the survival of $Kras^{G12D}$; $STAT3^{\Delta/\Delta}$;$JNK^{\Delta/\Delta}$ mice in contrast to $Kras^{G12D}$; $STAT3^{+/\Delta}$; $JNK^{\Delta/\Delta}$ controls through delayed precursor generation and at least partial inhibition of the profound fibrotic reaction was tested. Mice were born at the expected Mendelian ratio and Kaplan-Meier survival analysis somewhat surprisingly showed no significant increase in overall survival of $Kras^{G12D}$; $STAT3^{\Delta/\Delta}$; $JNK^{\Delta/\Delta}$ mice versus controls ($Kras^{G12D}$; $STAT3^{+/\Delta}$; $JNK^{\Delta/\Delta}$) (p = 0.7098, median 24.5 versus 25.0 days) (Figure 53).

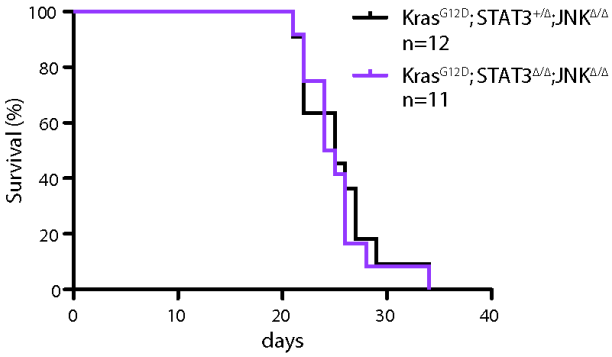

Figure 53 Kaplan-Meier survival of $Kras^{G12D}$;$JNK^{\Delta/\Delta}$ mice with and without deletion of STAT3
Overall survival is not significantly changed between $Kras^{G12D}$;$STAT3^{\Delta/\Delta}$;$JNK^{\Delta/\Delta}$ mice and controls.

5.6.2 Histology in $Kras^{G12D}$;$STAT3^{\Delta/\Delta}$;$JNK^{\Delta/\Delta}$ mice is unchanged to STAT3 heterozygous controls

As survival was unchanged in $Kras^{G12D}$; $STAT3^{\Delta/\Delta}$; $JNK^{\Delta/\Delta}$ mice versus controls, macroscopic and histologic appearance of the pancreas were examined.

Unexpectedly, macroscopy of the pancreas of $Kras^{G12D}$; $STAT3^{\Delta/\Delta}$; $JNK^{\Delta/\Delta}$ mice was not different from controls and HE staining did not reveal any obvious changes in histology of $Kras^{G12D}$;$STAT3^{\Delta/\Delta}$;$JNK^{\Delta/\Delta}$ mice versus STAT3 heterozygous controls (Figure 54).

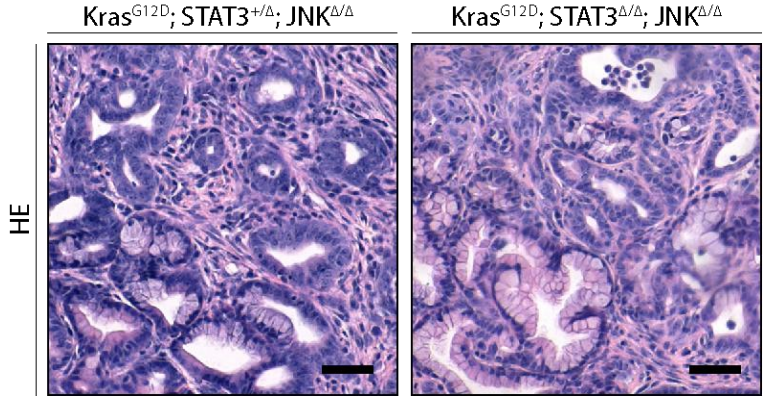

Figure 54 Histology of $Kras^{G12D}$;$JNK^{\Delta/\Delta}$ mice with and without STAT3
HE staining does not show obvious changes in the histology of $Kras^{G12D}$;$STAT3^{\Delta/\Delta}$;$JNK^{\Delta/\Delta}$ compared to $Kras^{G12D}$;$STAT3^{+/\Delta}$;$JNK^{\Delta/\Delta}$ control mice. Scale bar: 50 µm.

These results indicate that STAT3 signaling is dispensable for the phenotype of JNK-deficient mice and does not affect the life expectancies or the histology of these mice.

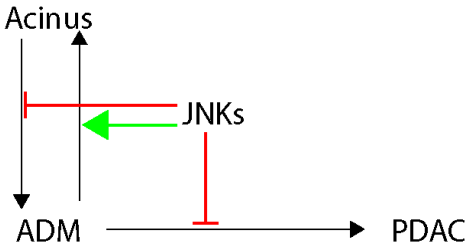

Figure 55 Model of JNK signaling on pancreatic tumorigenesis

In summary, the results of this thesis show that JNK is dispensable for pancreatic development but essential for maintenance of acinar differentiation after cell stress. Furthermore, these results place JNK1/2 as a strong tumor suppressor of PDAC (Figure 55). Microarray data and GSEA revealed that many oncogenic and inflammatory pathways are dysregulated in $Kras^{G12D}$;$JNK^{\Delta/\Delta}$ mice. Although STAT3 signaling was upregulated in $Kras^{G12D}$;$JNK^{\Delta/\Delta}$ mice, additional knockout of STAT3 neither prolonged overall survival nor changed histology compared to STAT3 heterozygous controls. Further investigation will be needed to clarify the detailed mechanism of JNK signaling in suppressing PDAC.

6 Discussion

Kras, the acknowledged driver of PDAC, is a central player in the growth/survival MAPK module. Furthermore, inflammation, an important source of cellular stress, is a known trigger for tumorigenesis as exemplified by the frequent transition of chronic pancreatitis to PDAC. Therefore, it was tempting to speculate that JNKs, which are at the center of the MAPK signaling module and responsible for the detection of cellular stress may be involved in the development of PDAC. Thus, the overall aim of this thesis was to identify the role of JNK signaling in PDAC.

To better understand the role of JNK signaling in organogenesis of the pancreas and PDAC development, JNK knockout mice were investigated. These models are far superior to oversimplified *in vitro* systems where clones of pancreatic cancer cell lines are treated with JNK inhibitors in an artificial monolayer without any stromal cells and their respective production of cytokines, mitogens or other soluble and insoluble factors. Notably, the lack of improper vasculature, a common feature of PDAC and a functional immune system are further limiting the benefits of these cell culture systems.

Since JNK1 and JNK2 are the only JNKs expressed in the pancreas, conditional pancreas-specific knockout of JNK1 and JNK2 was employed alone or in combination with $Kras^{G12D}$.

6.1 JNK signaling is dispensable for pancreatic embryonal development but important for acinar maintenance and terminal differentiation

It has been reported that compound JNK1, JNK2 null allele mice die during embryonal development from epithelial sheet closure defects, such as defective neural tube closure, and impaired epithelial proliferation [192]. Notably, JNK knockout has been shown to be associated with a reduction in EGF expression in the intestine. As EGF is an important player in intestinal development JNK knockout might disturb intestinal organogenesis [241]. Ardito *et al*. however observed normal pancreatic development upon EGFR knockout [173]. In order to determine possible roles of JNK signaling in pancreatic embryonal development, JNK genes were pancreas-specifically deleted with the help of a $Ptf1a^{Cre/+}$ mouse line. Mice were born at normal Mendelian ratio and no differences in body weight of adult male or female $JNK^{\Delta/\Delta}$ mice were observed. Global assessment of histoarchitecture did not reveal morphological changes either. Furthermore, staining for the exocrine marker amylase, the ductal marker CK19 and the endocrine marker insulin were normal. Thus, deletion of JNK genes, a bottleneck in the JNK signaling pathway, did not affect pancreatic embryonal development or pancreatic lineage specification.

Although organ development was not affected by the absence of JNK1 and JNK2, physiological histoarchitecture of the pancreas could not be maintained over time. In some $JNK^{\Delta/\Delta}$ mice, small affected areas could already be detected as early as eight

weeks of age. In half a year and one year old JNK$^{\Delta/\Delta}$ mice, however, the amount of histological remodeling progressively increased with replacement of acinar parenchyma by ADM and fat tissue. Stromal deposits, however, did not emerge over time and the few remaining acinar cells in JNK$^{\Delta/\Delta}$ mice obviously allowed survival of more than two years. This slow progression suggested that spatially confined remodeling events accumulated over time. To exclude a global impairment of acinar terminal differentiation, the levels of several acinar terminal differentiation markers, such as amylase or Cpa1, were assessed and showed no significant differences. Therefore, minor stress event were the likely source for acinar dedifferentiation. To test if stress indeed triggers this dedifferentiation, acinar berries from JNK$^{\Delta/\Delta}$ mice were exposed to explantation-induced culture stress. Already one day after explantation, acinar cells from JNK$^{\Delta/\Delta}$ mice dedifferentiated into duct-like structures, whereas controls remained acinar with occasional duct-like structures. This strongly suggests that JNK signaling is important for maintenance of terminal differentiation and inhibits early transdifferentiation. These results are in agreement with reports demonstrating that JNK signaling is also involved in differentiation processes of other cell types, such as T cells or osteoclasts [197, 242]. JNK signaling, however, cannot completely prevent dedifferentiation, as JNK competent acini also transdifferentiated into duct-like structures roughly at day three to five after explantation. Notably, this balance between stable terminal differentiation and transdifferentiation reflects the need to suppress any tumorigenic potential versus the need to repair damaged tissue.

In order to repair damaged tissue, cells undergo transient dedifferentiation. This de- and redifferentiation is nicely recapitulated during acute pancreatitis. Therefore, iAP can be employed to test the de- and redifferentiation ability of pancreatic cells. Several reports have tried to shed light on the role of JNKs in the setting of acute pancreatitis. The results, however, are still controversial and while some suggested attenuation of iAP after JNK inhibition, others such as the one by Dahlhoff *et al.* showed more severe iAP after JNK inhibition [222, 223]. Notably, the use of unspecific JNK inhibitors, such as SP600125, may have caused artifacts in many studies. To clarify the role of JNKs in AP and to overcome previous limitations of JNK signaling inhibitors the ability of JNK knockout mice to exit the tissue repair process and regain acinar differentiation after iAP was tested. While pancreata from controls reconstituted normal physiologic histoarchitecture within one week after iAP, JNK knockout mice were unable to resolve their lesions even four weeks after iAP and inflammation and ADM persisted. These results are in agreement with the findings of Davies *et al.* showing impaired pancreatic regeneration after iAP in MKK4/MKK7 knockout mice [229]. JNKs are therefore either required for reacquisition of terminal acinar differentiation and/or for termination of the persistent inflammation, which might inhibit reacquisition of terminal differentiation. As terminal acinar differentiation in JNK$^{\Delta/\Delta}$ mice could initially be acquired after embryonal development, it seems more likely that JNK signaling is required for the termination of inflammation. This, however, is in contrast to several studies showing attenuated inflammation in the

setting of JNK inhibition or knockout, for example in DSS-induced colitis, rheumatoid arthritis, atherosclerosis or development of hepatocellular carcinoma [200, 201, 214, 243].

In summary, JNK signaling is required to inhibit quick dedifferentiation and is involved in modulating terminal redifferentiation and/or inflammation.

6.2 JNK signaling suppresses PDAC development

Dedifferentiation of acinar cells into ADM with at least partial reacquisition of embryonal markers is a key player in the development of PDAC [239]. As JNK knockout mice displayed impaired acinar maintenance, the effect of JNK deletion on PDAC development was studied. Pancreas-specific activation of $Kras^{G12D}$ results in PDAC in 50 % of cases after approximately one year. Therefore, $Kras^{G12D}$ alone is not sufficient to transform acinar cells and additional hits are needed. Surprisingly, already two weeks after birth $Kras^{G12D}$;$JNK^{\Delta/\Delta}$ mice displayed a significantly increased pancreas to body weight ratio, and died between four and five weeks post partum. This is in line with Davies *et al*. showing rapid death of pancreas-specific MKK4/MKK7 compound knockout in the $Pdx1Cre^{ER/+}$;$Kras^{G12D}$ model [229]. This clearly establishes a synergistic mechanism of JNK knockout and $Kras^{G12D}$ signaling in the development of PDAC and JNKs as tumor suppressors in PDAC.

An isotype-specific role of JNKs was shown for the development of several tumors including hepatocellular carcinoma [214] or skin tumor [212]. In case of PDAC, it could be shown that the majority of mutations in the JNK pathway occurs in MKK4 rather than MKK7, JNK1 or JNK2 [224, 244]. Thus it was interesting to determine a possible difference in tumor latency in $Kras^{G12D}$ mice under retention of either one allele of JNK1 or JNK2. Remarkably, one allele of either JNK1 or JNK2 was sufficient to rescue the phenotype of $Kras^{G12D}$;$JNK^{\Delta/\Delta}$ mice and resulted in overall survival comparable to $Kras^{G12D}$ mice. The quick progression to small, multifocal PDACs in $Kras^{G12D}$;$JNK^{\Delta/\Delta}$ mice and the observed rescue in the presence of a single JNK1 or JNK2 allele argues against an isotype-specific role of JNK signaling in initiation and progression of PDAC. Discovery of an isotype specific JNK inhibitor might therefore be a strategy in the treatment of respective tumor entities other than PDAC, without potentially triggering pancreatic cancer.

A linear PanIN progression model was suggested for PDAC [90]. Recently, however this linear model has been questioned [127]. Close histological examination of $Kras^{G12D}$;$JNK^{\Delta/\Delta}$ mice revealed extensive tissue remodeling with large areas of ADM and low-grade PanINs as well as small multifocal PDACs. These PDACs occupied a larger total area than high grade PanINs, which may argue against the linearity of the PanIN progression model. It can however not be excluded that high-grade PanINs are only short-lived, transient lesions or that proliferation of PDAC is highly increased. Notably, the multiple PDACs in $Kras^{G12D}$;$JNK^{\Delta/\Delta}$ mice were detected near stromal rich regions and ADM rather than PanIN convolutes. This might shed some light on the type of lesion preceding PDAC and is in line with Aichler *et al*. who suggest an alternative route to PDAC via ADM [88]. In contrast to the present study,

Davies *et al*. report widespread high-grade PanINs 2 and 3 in $Kras^{G12D}$;$MKK4^{\Delta/\Delta}$;$MKK7^{\Delta/\Delta}$ mice. while the model used in this study showed only occasional high-grade PanINs. This discrepancy may be explained by the time requirement of high-grade PanINs to evolve from low-grade PanINs. While the mice used in this study succumbed to death within five weeks after birth, mice in the study of Davies *et al*. lived twice as long.

The identity of the cell of origin in PDAC is currently still under debate. The $Kras^{G12D}$;$JNK^{\Delta/\Delta}$ model with its fast progression to PDAC primarily demonstrates a tumorigenic potential of JNK-deficient acinar cells. This finding is further supported by the observation that PDAC can be induced in $Kras^{G12D}$;$JNK^{\Delta/\Delta}$ mice expressing Cre recombinase under the elastase promoter, while JNK heterozygous controls do not even display precursor lesions at the same age. Thus, both models used in this study are in agreement with the concept that acinar cells are the cell of origin of PDAC. However, it remains unclear whether other pancreatic cells can also give rise to PDAC. Ray *et al*. for example showed tumorigenic potential in pancreatic duct cells and demonstrated that different epithelial tissues are not equally affected by $Kras^{G12D}$ expression [245]. As no consistent correlation was observed between environmental exposure of tissues and tumor formation, cell intrinsic differences were suggested to drive tumor formation. Terminal differentiation and a differing degree of “resilience” against dedifferentiation might be this cell intrinsic difference. An important role of terminal differentiation in the cellular susceptibility for transforming events is further supported by the fact, that acinar cells targeted by $Kras^{G12D}$ in older animals become refractory to transformation [32, 118]. Additionally, experiments of von Figura *et al*. demonstrated that acinar terminal differentiation is impaired in Nr5a2 knockout mice [27] and that deletion of Nr5a2, previously identified as a human PDAC susceptibility locus, facilitates ADM, inhibits regeneration after iAP and dramatically accelerates pancreatic neoplasia. The similarity of the phenotypes of $Kras^{G12D}$;$JNK^{\Delta/\Delta}$ and $Pdx1^{Crelate/+}$;$Nr5a2^{\Delta/\Delta}$ mice is striking enough to speculate about Nr5a2 being a target of JNK signaling in the setting of iAP. Interestingly, $Kras^{G12D}$;$JNK^{\Delta/\Delta}$ mice also continuously express the embryonal marker Sox9, which inhibits terminal differentiation and has been shown to be an important player in ADM, which enables PDAC development [178]. JNKs important role in terminal differentiation is further supported by a study showing increased numbers of immature prostate cells in $PTEN^{\Delta/\Delta}$;$JNK^{\Delta/\Delta}$ compound knockout mice in contrast to $PTEN^{\Delta/\Delta}$ mice, which resulted in increased numbers of prostaspheres and greatly accelerated development of prostate tumors [218]. As acinar cells, however, arguably seem to harbor the highest plasticity of pancreatic lineages they are likely to be the compartment that gives rise to PDAC at least in this model system. It will be interesting to determine the JNK downstream transcription factors involved in destabilizing acinar terminal differentiation to identify novel susceptibility loci for PDAC development.

The direct JNK downstream target ATF2 has recently been reported to be a crucial player in the development of liver cancer in an orthotopic mouse model [246]. Furthermore, NFATc1, a known direct target of JNK has been reported to play a role in PDAC [84]. Since the rapid progression of $Kras^{G12D}$;$JNK^{\Delta/\Delta}$ mice was reminiscent of the rapid progression of $Kras^{G12D}$;$p53^{\Delta/\Delta}$ mice and p53 is a another direct target of JNKs [247] p53 might be involved in generating the $Kras^{G12D}$;$JNK^{\Delta/\Delta}$ phenotype. Indeed, nuclear localization of p53 could be detected in $Kras^{G12D}$;$JNK^{\Delta/\Delta}$ mice at 14 days of age, implying transactivation of p53 target genes. Western Blot analysis of four week old mice, however, displayed minor p53 band shifts. As transactivation of p53 depends on its posttranslational modifications and JNKs are known to phosphorylate p53, the shift in band size might indicate impaired p53 target transactivation. Thus, it remains unclear whether nuclear p53 still possesses its full transactivation capability and contributes to the rapid phenotype of $Kras^{G12D}$;$JNK^{\Delta/\Delta}$ mice. Further research is needed to elucidate the particular role of JNK downstream targets in the initiation and progression of PDAC.

Unexpectedly, pancreatic cancer cell lines could neither be generated from $Kras^{G12D}$;$JNK^{\Delta/\Delta}$ mice despite the presence of small multifocal PDACs, nor from huge tumors of ElaCreER;$Kras^{G12D}$;$JNK^{\Delta/\Delta}$ mice. Furthermore, metastasis was not detectable in $Kras^{G12D}$;$JNK^{\Delta/\Delta}$ mice either. These findings are in agreement with several reports showing JNK signaling to be required for proliferation of cancer cells [248-250] and with the observation of an unchanged proliferation index in $Kras^{G12D}$;$JNK^{\Delta/\Delta}$ mice versus $Kras^{G12D}$ controls. Thus, while JNK deficiency accelerates the initial steps of malignant transformation, it may not be required or even inhibiting progression of tumors to a more aggressive phenotype, although the early death of mice and thus absent acquisition of additional genetic alterations may be a reasonable alternative hypothesis.

Overall, our data is in line with a recently published paper by Davies *et al*. knocking out the JNK upstream kinases MKK4/MKK7 in the pancreas of $Kras^{G12D}$ mice [229]. Their observed phenotype is slightly slower probably due to the mosaic expression of Cre by the Pdx1 promoter and incomplete tamoxifen-induced Cre translocation [19, 126]. In contrast to their findings, the data of this thesis establishes JNK signaling as a requirement for pancreatic acinar cell homeostasis. The difference observed might be due to the slow time course of defective acinar maintenance. Spatially confined stochastic stress events leading to lesions are probably repaired and inflammatory signaling is terminated by JNK competent neighboring cells in the Davies *et al.* model, before obvious morphological changes are detectable.

6.3 STAT3 signaling is dispensable for the rapid progression of $Kras^{G12D}$;$JNK^{\Delta/\Delta}$ mice

Inflammation is an important trigger of cellular stress and the initiation of PDAC [251]. Major inflammation pathways are the NF-κB and STAT3 pathways. While the role of NF-κB in PDAC is still under debate [32, 252], pancreas-specific STAT3 knockout has

been shown to delay the progression of murine PanIN lesions, which correlated with reduced cytokine expression and immune cell infiltration [159]. Furthermore, a synergistic activation of the IL6/STAT3 pathway by $Kras^{G12D}$ in combination with JNK knockout has been suggested to be causal for the rapid phenotype of $Kras^{G12D}$;$JNK^{\Delta/\Delta}$ mice [229]. While EMSA analysis of $Kras^{G12D}$;$JNK^{\Delta/\Delta}$ mice indicated active NF-κB signaling, pp65, a component of active NF-κB signaling showed slight downregulation in seven and 28 day old $Kras^{G12D}$;$JNK^{\Delta/\Delta}$ mice. It is therefore unlikely that NF-κB signaling contributes to the strong phenotype of this model. In contrast, gene set enrichment analysis (GSEA) following microarrays of seven day old morphologically nearly unchanged $Kras^{G12D}$;$JNK^{\Delta/\Delta}$ mice indicated enrichment of many inflammatory signaling pathways, especially STAT3. Indeed, pSTAT3 levels were markedly increased in seven and 28 day old $Kras^{G12D}$;$JNK^{\Delta/\Delta}$ mice. These results further support a role of STAT3 signaling in the phenotype of $Kras^{G12D}$;$JNK^{\Delta/\Delta}$ mice.

In agreement with a direct interaction of JNK and STAT3 signaling Liu *et al*. showed JNK-mediated phosphorylation of STAT3 in bronchial epithelial cells, which led to AKT activation [253]. Additionally, Lim *et al*. demonstrated a disinhibition of STAT3 signaling upon inhibition of JNKs [240]. To test whether this holds true in $Kras^{G12D}$ positive pancreatic cancer cell lines, JNK signaling was blocked with JNK-IN-8 while STAT3 signaling was stimulated with IL6. IL6/IN-8 treatment, however, did not result in a clear correlation between JNK inhibition and STAT3 activation in different pancreatic cancer cell lines. One possible explanation is a varying degree of IL6 susceptibility of different pancreatic tumor cell lines that might reflect the heterogeneity of tumor cells present in a tumor.

As cell culture systems are prone to artifacts this hypothesis was further tested *in vivo* by crossing LoxP flanked STAT3 alleles into the $Kras^{G12D}$;$JNK^{\Delta/\Delta}$ background. Fukuda *et al*. and Lesina *et al.* showed that STAT3 activation through IL6 promotes proliferation and survival of transformed cells and sustains metaplasia-associated inflammation [159, 254]. Therefore, it was unexpected that loss of STAT3 did not have a significant effect on overall survival of $Kras^{G12D}$;$JNK^{\Delta/\Delta}$ mice. Furthermore, knockout of STAT3 did not obviously alter the histology of arising tumors, including the amount of stromal deposits. Therefore, STAT3 was not able to repress initiation of or progression to PDAC. It can be speculated that STAT3 signaling plays a marginal role in fast developing PDAC, especially as Lesina *et al.* reported STAT3 signaling to be important for precursor lesion progression but not initiation. Therefore STAT3 signaling may preferentially affect the evolution of long-latency tumors.

Overall, it could be shown that JNK1 and JNK2 are dispensable for embryonic development of the pancreas and lineage specification. After physiologic, acute and oncogenic stress, however, JNK-deficient terminally differentiated acinar cells quickly transdifferentiate into ADM and fail to re-establish terminal differentiation in an appropriate time span. This leads to rapidly emerging tumor precursor lesions and PDAC, establishing JNKs as bona fide tumor suppressors. Further investigation

of the underlying mechanisms of JNK signaling may therefore provide more insights into the development of PDAC, the role and regulation of inflammatory signaling cascades and thus reveal possibilities for detection and targeting approaches.

7 Acknowledgements

Herzlich danke ich meinem Thesis Advisory Comittee, bestehend aus
Frau Prof. Angelika Schnieke, Dekan, Wissenschaftszentrum Weihenstephan, TUM
Herr Prof. Roland M Schmid, Direktor, II. Medizinische Klinik Rechts der Isar, TUM
Frau PD Dr. Sandra Hake, Arbeitsgruppenleiterin, Adolf-Butenandt-Institut, LMU
Herr Dr. Kyle Legate, Editor Nature Publishing Group, davor Juniorgruppenleiter Max-Planck-Institut für Biochemie und
Frau Dr. Marija Trajkovic-Arsic, Mentorin,
welches mich in meiner Doktorarbeit mit hilfreichem Input unterstützt hat und mir mit Material und Rat zur Seite stand.

Bei apl. Prof. Dr. Jens Siveke möchte ich mich für die Möglichkeit bedanken, diese Doktorarbeit in seinem Labor anzufertigen. Danke für das entgegengebrachte Vertrauen und die Unterstützung.

Herzlichen Dank schulde ich außerdem Dr. Ana Hidalgo-Sastre und Dr. Marija Trajkovic-Arsic die in verschiedenen Phasen meiner Doktorarbeit meine erste Anlaufstelle für wissenschaftliche Diskussionen waren.

Weiterhin Danke ich Jun.-Prof. Dr. Daniel Sauter und Judith Wagner, für die Motivation weiterzumachen wenn eines der zahlreichen Experimente nicht funktioniert hatte.

Herzlichen Dank auch an alle die weitere Daten und Auswertungen zu dieser Doktorarbeit beigesteuert haben, wie beispielsweise Dr. Björn Lamprecht, Charité Berlin, Katja Steiger, MRI, Tar Viturawong, Max-Planck Institut für Biochemie beziehungsweise deren Chefs für die effektive Kollaboration.

Nicht zu vergessen, gilt mein Dank auch meiner Arbeitsgruppe, die immer für einen Kuchen, Eis oder einfach einen Spaß zu haben waren. Besonderer Dank geht an Ana. Herzlichen Dank auch an Christina, Marija, Katharina, Clara, Vicky, Barbara, Flo, Roxanne, Pawel, Maya, Zahra, Annett, Mathilde, Silke, Aayush, Thomsa und Axel.

Liebe AG Quante, vielen Dank für die familiäre Atmosphäre und euren Humor. Ihr wart mehr Freunde als Kollegen. Besonderer Dank geht an Andreas Nuber.

Bedanken möchte ich mich auch bei Magdalena Kurkowski für die vielen Stunden, die wir gemeinsam in ihrer Küche verbracht haben um unsere Doktorarbeiten zu Papier zu bringen.

Herzlichen Dank auch allen Unterstützern am Rechts der Isar, wie der Apotheke, der Personalverwaltung, dem Sekretariat der 2. Medizinischen Klinik, den Tierpflegern, vor allem Cindy, Elisabeth und Marion und allen anderen.

Bedanken möchte ich mich zuletzt noch einmal bei meinen Eltern für ihre Unterstützung, dass sie immer zu mir gehalten haben, an mich geglaubt haben und für mich da waren.

8 List of figures

9 List of tables

10 Abbreviations

5-FU	5-Fluoruracil, chemotherapeutic drug
ADM	Acinar-ductal metaplasia
AFL	Atypical flat lesion
ATP	Adenosinetriphosphate
bHLH	Basic helix-loop-helix, class of transcription factors
CGP	Chemical and genetic perturbations, collection of gene sets in the MSigDB (see CP)
CK	Cre;$Kras^{G12D}$, mouse expressing $Kras^{G12D}$ in the pancreas
CP	Canonical pathways, collection of gene sets in the molecular signatures database
DDR	DNA damage response, a signaling pathway
DEN	Diethylnitrosamine
DMEM	Dulbeccos Modified Eagle Medium
DNA	Desoxyribonucleic acid
ELISA	Enzyme linked immunosorbent assay
EMSA	Electromobility shift assay
EMT	Epithelial mesenchymal transition
ER	Estrogen receptor
FFPE	Formalin fixed paraffin embedded
FOLFIRINOX	Combination of leucovorin and the chemotherapeutics 5-FU, irinotecan and oxaliplatin
GAP	GTPase activating protein
GEF	Guanine nucleotide exchange factor
GEM(M)	Genetically engineered mouse (model)
GRN	Gene regulatory networks
GSEA	Gene set enrichment analysis
GTP / GDP	Guanosinetriphosphate / Guanosinediphosphate
HCC	Hepatocellular carcinoma
HE	Hematoxylin & Eosin staining
i.p.	Intraperitoneal
iAP	Induced acute pancreatitis, with cerulein
IC_{50}	Inhibitory concentration 50 %
IHC	Immunohistochemistry
IPMN	Intraductal papillary mucinous neoplasm
JNK	C-Jun N-terminal kinase, exists in 3 isoform
MAP2K	MAPK kinase
MAP3K	MAPK kinase kinase
MAPK	Mitogen activated protein kinase
MCN	Mucinous cystic neoplasm
MEF	Mouse embryonic fibroblast
MEN	Multiple endocrine neoplasia
miR	microRNA
MKP	MAPK phosphatases
MPC	Multipotent progenitor cells
NDLB	Non-denaturing lysis buffer
NEAA	Non-essential amino acids
NFκB	Nuclear factor κ B
OIS	Oncogene induced senescence
PAGE	Polyacrylamide gel electrophoresis
PanIN	Pancreatic intraepithelial neoplasia
PBS(T) / TBS(T)	Phosphate buffered saline (with Tween) / Tris buffered saline (with Tween)
PCR	Polymerase chain reaction
PDAC	Pancreatic ductal adenocarcinoma
PTF-J	Transcription factor complex containing Ptf1a, Rbpj and any one bHLH TF
PTM	Posttranslational modification
RNA	Ribonucleic acid
siRNA	small interfering RNA
TF	Transcription factor
vHL	von Hippel Lindau, a genetic disease
WHO	World Health Organisation
wt	wild type

11 Literature

1. Habibi, H., D. Devuni, and L. Rossi, *Ectopic pancreas: a rare cause of abdominal pain.* Conn Med, 2014. **78**(8): p. 479-80.
2. Shih, H.P., A. Wang, and M. Sander, *Pancreas organogenesis: from lineage determination to morphogenesis.* Annu Rev Cell Dev Biol, 2013. **29**: p. 81-105.
3. Mastracci, T.L. and L. Sussel, *The endocrine pancreas: insights into development, differentiation, and diabetes.* Wiley Interdiscip Rev Dev Biol, 2012. **1**(5): p. 609-28.
4. Whitcomb, D.C. and M.E. Lowe, *Human pancreatic digestive enzymes.* Dig Dis Sci, 2007. **52**(1): p. 1-17.
5. Bardeesy, N. and R.A. DePinho, *Pancreatic cancer biology and genetics.* Nat Rev Cancer, 2002. **2**(12): p. 897-909.
6. Jorgensen, M.C., et al., *An illustrated review of early pancreas development in the mouse.* Endocr Rev, 2007. **28**(6): p. 685-705.
7. Arda, H.E., C.M. Benitez, and S.K. Kim, *Gene regulatory networks governing pancreas development.* Dev Cell, 2013. **25**(1): p. 5-13.
8. Spence, J.R., et al., *Sox17 regulates organ lineage segregation of ventral foregut progenitor cells.* Dev Cell, 2009. **17**(1): p. 62-74.
9. Ahlgren, U., J. Jonsson, and H. Edlund, *The morphogenesis of the pancreatic mesenchyme is uncoupled from that of the pancreatic epithelium in IPF1/PDX1-deficient mice.* Development, 1996. **122**(5): p. 1409-16.
10. Sumazaki, R., et al., *Conversion of biliary system to pancreatic tissue in Hes1-deficient mice.* Nat Genet, 2004. **36**(1): p. 83-7.
11. Puri, S. and M. Hebrok, *Cellular plasticity within the pancreas--lessons learned from development.* Dev Cell, 2010. **18**(3): p. 342-56.
12. Zhou, Q., et al., *A multipotent progenitor domain guides pancreatic organogenesis.* Dev Cell, 2007. **13**(1): p. 103-14.
13. Seymour, P.A., et al., *SOX9 is required for maintenance of the pancreatic progenitor cell pool.* Proc Natl Acad Sci U S A, 2007. **104**(6): p. 1865-70.
14. Fujikura, J., et al., *Notch/Rbp-j signaling prevents premature endocrine and ductal cell differentiation in the pancreas.* Cell Metab, 2006. **3**(1): p. 59-65.
15. Masui, T., et al., *Early pancreatic development requires the vertebrate Suppressor of Hairless (RBPJ) in the PTF1 bHLH complex.* Genes Dev, 2007. **21**(20): p. 2629-43.
16. Masui, T., et al., *Replacement of Rbpj with Rbpjl in the PTF1 complex controls the final maturation of pancreatic acinar cells.* Gastroenterology, 2010. **139**(1): p. 270-80.
17. Schaffer, A.E., et al., *Nkx6 transcription factors and Ptf1a function as antagonistic lineage determinants in multipotent pancreatic progenitors.* Dev Cell, 2010. **18**(6): p. 1022-9.
18. Masui, T., et al., *Transcriptional autoregulation controls pancreatic Ptf1a expression during development and adulthood.* Mol Cell Biol, 2008. **28**(17): p. 5458-68.
19. Magnuson, M.A. and A.B. Osipovich, *Pancreas-specific Cre driver lines and considerations for their prudent use.* Cell Metab, 2013. **18**(1): p. 9-20.
20. Steinberg, W. and S. Tenner, *Acute pancreatitis.* N Engl J Med, 1994. **330**(17): p. 1198-210.
21. Willemer, S., H.P. Elsasser, and G. Adler, *Hormone-induced pancreatitis.* Eur Surg Res, 1992. **24 Suppl 1**: p. 29-39.
22. Ward, J.B., et al., *Progressive disruption of acinar cell calcium signaling is an early feature of cerulein-induced pancreatitis in mice.* Gastroenterology, 1996. **111**(2): p. 481-91.
23. Jensen, J.N., et al., *Recapitulation of elements of embryonic development in adult mouse pancreatic regeneration.* Gastroenterology, 2005. **128**(3): p. 728-41.

24. Molero, X., et al., *Pancreas transcription factor 1alpha expression is regulated in pancreatitis.* Eur J Clin Invest, 2007. **37**(10): p. 791-801.
25. Morris, J.P.t., et al., *Beta-catenin blocks Kras-dependent reprogramming of acini into pancreatic cancer precursor lesions in mice.* J Clin Invest, 2010. **120**(2): p. 508-20.
26. Siveke, J.T., et al., *Notch signaling is required for exocrine regeneration after acute pancreatitis.* Gastroenterology, 2008. **134**(2): p. 544-55.
27. von Figura, G., et al., *Nr5a2 maintains acinar cell differentiation and constrains oncogenic Kras-mediated pancreatic neoplastic initiation.* Gut, 2014. **63**(4): p. 656-64.
28. Greer, R.L., et al., *Numb regulates acinar cell dedifferentiation and survival during pancreatic damage and acinar-to-ductal metaplasia.* Gastroenterology, 2013. **145**(5): p. 1088-1097.e8.
29. Reichert, M., et al., *The Prrx1 homeodomain transcription factor plays a central role in pancreatic regeneration and carcinogenesis.* Genes Dev, 2013. **27**(3): p. 288-300.
30. Braganza, J.M., et al., *Chronic pancreatitis.* Lancet, 2011. **377**(9772): p. 1184-97.
31. Pinho, A.V., L. Chantrill, and I. Rooman, *Chronic pancreatitis: a path to pancreatic cancer.* Cancer Lett, 2014. **345**(2): p. 203-9.
32. Guerra, C., et al., *Chronic pancreatitis is essential for induction of pancreatic ductal adenocarcinoma by K-Ras oncogenes in adult mice.* Cancer Cell, 2007. **11**(3): p. 291-302.
33. Guerra, C., et al., *Pancreatitis-induced inflammation contributes to pancreatic cancer by inhibiting oncogene-induced senescence.* Cancer Cell, 2011. **19**(6): p. 728-39.
34. Malvezzi, M., et al., *European cancer mortality predictions for the year 2014.* Ann Oncol, 2014. **25**(8): p. 1650-6.
35. *Krebs in Deutschland 2009/2010*. 2013, Robert Koch-Institut (Hrsg) und die Gesellschaft der epidemiologischen Krebsregister in Deutschland e.V. (Hrsg): Berlin.
36. Rustgi, A.K., *Familial pancreatic cancer: genetic advances.* Genes Dev, 2014. **28**(1): p. 1-7.
37. Permuth-Wey, J. and K.M. Egan, *Family history is a significant risk factor for pancreatic cancer: results from a systematic review and meta-analysis.* Fam Cancer, 2009. **8**(2): p. 109-17.
38. Hassan, M.M., et al., *Risk factors for pancreatic cancer: case-control study.* Am J Gastroenterol, 2007. **102**(12): p. 2696-707.
39. Ryan, D.P., T.S. Hong, and N. Bardeesy, *Pancreatic adenocarcinoma.* N Engl J Med, 2014. **371**(11): p. 1039-49.
40. Rustagi, T. and J.J. Farrell, *Endoscopic diagnosis and treatment of pancreatic neuroendocrine tumors.* J Clin Gastroenterol, 2014. **48**(10): p. 837-44.
41. Stotz, M., et al., *Clinico-pathological characteristics and clinical outcome of different histological types of pancreatic cancer in a large Middle European series.* J Clin Pathol, 2013. **66**(9): p. 753-7.
42. Morin, E., et al., *Hormone profiling, WHO 2010 grading, and AJCC/UICC staging in pancreatic neuroendocrine tumor behavior.* Cancer Med, 2013. **2**(5): p. 701-11.
43. Kuo, J.H., J.A. Lee, and J.A. Chabot, *Nonfunctional pancreatic neuroendocrine tumors.* Surg Clin North Am, 2014. **94**(3): p. 689-708.
44. Batcher, E., P. Madaj, and A.G. Gianoukakis, *Pancreatic neuroendocrine tumors.* Endocr Res, 2011. **36**(1): p. 35-43.
45. Luttges, J., *[What's new? The 2010 WHO classification for tumours of the pancreas].* Pathologe, 2011. **32 Suppl 2**: p. 332-6.
46. Chaudhary, P., et al., *Acinar cell carcinoma: a rare pancreatic malignancy.* Clin Pract, 2013. **3**(2): p. e18.

47. Salman, B., et al., *The diagnosis and surgical treatment of pancreatoblastoma in adults: a case series and review of the literature.* J Gastrointest Surg, 2013. **17**(12): p. 2153-61.
48. Hammer, S.T. and S.R. Owens, *Pancreatoblastoma: a rare, adult pancreatic tumor with many faces.* Arch Pathol Lab Med, 2013. **137**(9): p. 1224-6.
49. Stathis, A. and M.J. Moore, *Advanced pancreatic carcinoma: current treatment and future challenges.* Nat Rev Clin Oncol, 2010. **7**(3): p. 163-72.
50. Howlader, N., et al., *SEER Cancer Statistics Review*. 2014, National Cancer Institute: Bethesda.
51. Carpelan-Holmstrom, M., et al., *Does anyone survive pancreatic ductal adenocarcinoma? A nationwide study re-evaluating the data of the Finnish Cancer Registry.* Gut, 2005. **54**(3): p. 385-7.
52. Hidalgo, M., *Pancreatic cancer.* N Engl J Med, 2010. **362**(17): p. 1605-17.
53. Konstantinidis, I.T., et al., *Pancreatic ductal adenocarcinoma: is there a survival difference for R1 resections versus locally advanced unresectable tumors? What is a "true" R0 resection?* Ann Surg, 2013. **257**(4): p. 731-6.
54. Heinemann, V. and S. Boeck, *Perioperative management of pancreatic cancer.* Ann Oncol, 2008. **19 Suppl 7**: p. vii273-8.
55. Deady, S. and H. Comber, *Cancer Trends - Cancer of the pancreas*. 2012, National Cancer Registry Ireland (www.ncri.ie).
56. Burris, H.A., 3rd, et al., *Improvements in survival and clinical benefit with gemcitabine as first-line therapy for patients with advanced pancreas cancer: a randomized trial.* J Clin Oncol, 1997. **15**(6): p. 2403-13.
57. Moore, M.J., et al., *Erlotinib plus gemcitabine compared with gemcitabine alone in patients with advanced pancreatic cancer: a phase III trial of the National Cancer Institute of Canada Clinical Trials Group.* J Clin Oncol, 2007. **25**(15): p. 1960-6.
58. Heinemann, V., M. Haas, and S. Boeck, *Systemic treatment of advanced pancreatic cancer.* Cancer Treat Rev, 2012. **38**(7): p. 843-53.
59. Conroy, T., et al., *FOLFIRINOX versus gemcitabine for metastatic pancreatic cancer.* N Engl J Med, 2011. **364**(19): p. 1817-25.
60. Thota, R., J.M. Pauff, and J.D. Berlin, *Treatment of metastatic pancreatic adenocarcinoma: a review.* Oncology (Williston Park), 2014. **28**(1): p. 70-4.
61. Kleger, A., L. Perkhofer, and T. Seufferlein, *Smarter drugs emerging in pancreatic cancer therapy.* Ann Oncol, 2014. **25**(7): p. 1260-70.
62. Jamieson, J.D., *Prospectives for cell and organ culture systems in the study of pancreatic carcinoma.* J Surg Oncol, 1975. **7**(2): p. 139-41.
63. Brembeck, F.H., et al., *The mutant K-ras oncogene causes pancreatic periductal lymphocytic infiltration and gastric mucous neck cell hyperplasia in transgenic mice.* Cancer Res, 2003. **63**(9): p. 2005-9.
64. Pour, P.M. and B. Schmied, *The link between exocrine pancreatic cancer and the endocrine pancreas.* Int J Pancreatol, 1999. **25**(2): p. 77-87.
65. Bockman, D.E., et al., *Origin and development of the precursor lesions in experimental pancreatic cancer in rats.* Lab Invest, 2003. **83**(6): p. 853-9.
66. Habbe, N., et al., *Spontaneous induction of murine pancreatic intraepithelial neoplasia (mPanIN) by acinar cell targeting of oncogenic Kras in adult mice.* Proc Natl Acad Sci U S A, 2008. **105**(48): p. 18913-8.
67. Hingorani, S.R., et al., *Preinvasive and invasive ductal pancreatic cancer and its early detection in the mouse.* Cancer Cell, 2003. **4**(6): p. 437-50.
68. Morris, J.P.t., S.C. Wang, and M. Hebrok, *KRAS, Hedgehog, Wnt and the twisted developmental biology of pancreatic ductal adenocarcinoma.* Nat Rev Cancer, 2010. **10**(10): p. 683-95.
69. Hruban, R.H., et al., *Pathology of genetically engineered mouse models of pancreatic exocrine cancer: consensus report and recommendations.* Cancer Res, 2006. **66**(1): p. 95-106.

70. Hruban, R.H., et al., *An illustrated consensus on the classification of pancreatic intraepithelial neoplasia and intraductal papillary mucinous neoplasms.* Am J Surg Pathol, 2004. **28**(8): p. 977-87.
71. Luttges, J., et al., *The K-ras mutation pattern in pancreatic ductal adenocarcinoma usually is identical to that in associated normal, hyperplastic, and metaplastic ductal epithelium.* Cancer, 1999. **85**(8): p. 1703-10.
72. Day, J.D., et al., *Immunohistochemical evaluation of HER-2/neu expression in pancreatic adenocarcinoma and pancreatic intraepithelial neoplasms.* Hum Pathol, 1996. **27**(2): p. 119-24.
73. Moskaluk, C.A., R.H. Hruban, and S.E. Kern, *p16 and K-ras gene mutations in the intraductal precursors of human pancreatic adenocarcinoma.* Cancer Res, 1997. **57**(11): p. 2140-3.
74. Lennon, A.M., et al., *The early detection of pancreatic cancer: what will it take to diagnose and treat curable pancreatic neoplasia?* Cancer Res, 2014. **74**(13): p. 3381-9.
75. Basturk, O., et al., *Preferential expression of MUC6 in oncocytic and pancreatobiliary types of intraductal papillary neoplasms highlights a pyloropancreatic pathway, distinct from the intestinal pathway, in pancreatic carcinogenesis.* Am J Surg Pathol, 2010. **34**(3): p. 364-70.
76. Wu, J., et al., *Whole-exome sequencing of neoplastic cysts of the pancreas reveals recurrent mutations in components of ubiquitin-dependent pathways.* Proc Natl Acad Sci U S A, 2011. **108**(52): p. 21188-93.
77. Wu, J., et al., *Recurrent GNAS mutations define an unexpected pathway for pancreatic cyst development.* Sci Transl Med, 2011. **3**(92): p. 92ra66.
78. Klimstra, D.S., *Cystic, mucin-producing neoplasms of the pancreas: the distinguishing features of mucinous cystic neoplasms and intraductal papillary mucinous neoplasms.* Semin Diagn Pathol, 2005. **22**(4): p. 318-29.
79. Valsangkar, N.P., et al., *851 resected cystic tumors of the pancreas: a 33-year experience at the Massachusetts General Hospital.* Surgery, 2012. **152**(3 Suppl 1): p. S4-12.
80. Zamboni, G., et al., *Mucinous cystic tumors of the pancreas: clinicopathological features, prognosis, and relationship to other mucinous cystic tumors.* Am J Surg Pathol, 1999. **23**(4): p. 410-22.
81. Lee, L.S., et al., *Differential expression of GNAS and KRAS mutations in pancreatic cysts.* Jop, 2014. **15**(6): p. 581-6.
82. Miyamoto, Y., et al., *Notch mediates TGF alpha-induced changes in epithelial differentiation during pancreatic tumorigenesis.* Cancer Cell, 2003. **3**(6): p. 565-76.
83. Sandgren, E.P., et al., *Overexpression of TGF alpha in transgenic mice: induction of epithelial hyperplasia, pancreatic metaplasia, and carcinoma of the breast.* Cell, 1990. **61**(6): p. 1121-35.
84. Chen, N.M., et al., *NFATc1 Links EGFR Signaling to Induction of Sox9 Transcription and Acinar-Ductal Transdifferentiation in the Pancreas.* Gastroenterology, 2015.
85. Martinelli, P., et al., *The acinar regulator Gata6 suppresses KrasG12V-driven pancreatic tumorigenesis in mice.* Gut, 2015.
86. Reichert, M. and A.K. Rustgi, *Pancreatic ductal cells in development, regeneration, and neoplasia.* J Clin Invest, 2011. **121**(12): p. 4572-8.
87. Esposito, I., et al., *[New insights into the origin of pancreatic cancer. Role of atypical flat lesions in pancreatic carcinogenesis].* Pathologe, 2012. **33 Suppl 2**: p. 189-93.
88. Aichler, M., et al., *Origin of pancreatic ductal adenocarcinoma from atypical flat lesions: a comparative study in transgenic mice and human tissues.* J Pathol, 2012. **226**(5): p. 723-34.
89. Vogelstein, B., et al., *Genetic alterations during colorectal-tumor development.* N Engl J Med, 1988. **319**(9): p. 525-32.

90. Hruban, R.H., et al., *Progression model for pancreatic cancer.* Clin Cancer Res, 2000. **6**(8): p. 2969-72.
91. Cubilla, A.L. and P.J. Fitzgerald, *Morphological lesions associated with human primary invasive nonendocrine pancreas cancer.* Cancer Res, 1976. **36**(7 pt 2): p. 2690-8.
92. Kozuka, S., et al., *Relation of pancreatic duct hyperplasia to carcinoma.* Cancer, 1979. **43**(4): p. 1418-28.
93. Brat, D.J., et al., *Progression of pancreatic intraductal neoplasias to infiltrating adenocarcinoma of the pancreas.* Am J Surg Pathol, 1998. **22**(2): p. 163-9.
94. Feldmann, G., et al., *Molecular genetics of pancreatic intraepithelial neoplasia.* J Hepatobiliary Pancreat Surg, 2007. **14**(3): p. 224-32.
95. de Wilde, R.F., et al., *Reporting precursors to invasive pancreatic cancer: pancreatic intraepithelial neoplasia, intraductal neoplasms and mucinous cystic neoplasm.* Diagnostic Histopathology. **18**(1): p. 17-30.
96. Rochefort, M.M., et al., *Impact of tumor grade on pancreatic cancer prognosis: validation of a novel TNMG staging system.* Ann Surg Oncol, 2013. **20**(13): p. 4322-9.
97. Olive, K.P., et al., *Inhibition of Hedgehog signaling enhances delivery of chemotherapy in a mouse model of pancreatic cancer.* Science, 2009. **324**(5933): p. 1457-61.
98. Jacobetz, M.A., et al., *Hyaluronan impairs vascular function and drug delivery in a mouse model of pancreatic cancer.* Gut, 2013. **62**(1): p. 112-20.
99. Ozdemir, B.C., et al., *Depletion of carcinoma-associated fibroblasts and fibrosis induces immunosuppression and accelerates pancreas cancer with reduced survival.* Cancer Cell, 2014. **25**(6): p. 719-34.
100. Rhim, A.D., et al., *Stromal elements act to restrain, rather than support, pancreatic ductal adenocarcinoma.* Cancer Cell, 2014. **25**(6): p. 735-47.
101. Almoguera, C., et al., *Most human carcinomas of the exocrine pancreas contain mutant c-K-ras genes.* Cell, 1988. **53**(4): p. 549-54.
102. Kanda, M., et al., *Presence of somatic mutations in most early-stage pancreatic intraepithelial neoplasia.* Gastroenterology, 2012. **142**(4): p. 730-733.e9.
103. Park, J.T., et al., *Differential in vivo tumorigenicity of diverse KRAS mutations in vertebrate pancreas: A comprehensive survey.* Oncogene, 2014.
104. Mazur, P.K. and J.T. Siveke, *Genetically engineered mouse models of pancreatic cancer: unravelling tumour biology and progressing translational oncology.* Gut, 2012. **61**(10): p. 1488-500.
105. Collisson, E.A., et al., *Subtypes of pancreatic ductal adenocarcinoma and their differing responses to therapy.* Nat Med, 2011. **17**(4): p. 500-3.
106. Chang, D.K., S.M. Grimmond, and A.V. Biankin, *Pancreatic cancer genomics.* Curr Opin Genet Dev, 2014. **24**: p. 74-81.
107. Ishikawa, O., et al., *Minute carcinoma of the pancreas measuring 1 cm or less in diameter--collective review of Japanese case reports.* Hepatogastroenterology, 1999. **46**(25): p. 8-15.
108. Yachida, S., et al., *Distant metastasis occurs late during the genetic evolution of pancreatic cancer.* Nature, 2010. **467**(7319): p. 1114-7.
109. Rhim, A.D., et al., *EMT and dissemination precede pancreatic tumor formation.* Cell, 2012. **148**(1-2): p. 349-61.
110. Niero, E.L., et al., *The multiple facets of drug resistance: one history, different approaches.* J Exp Clin Cancer Res, 2014. **33**: p. 37.
111. Marincola, F.M., et al., *The nude mouse as a model for the study of human pancreatic cancer.* J Surg Res, 1989. **47**(6): p. 520-9.
112. Morikane, K., et al., *Organ-specific pancreatic tumor growth properties and tumor immunity.* Cancer Immunol Immunother, 1999. **47**(5): p. 287-96.

113. Capella, G., et al., *Orthotopic models of human pancreatic cancer.* Ann N Y Acad Sci, 1999. **880**: p. 103-9.
114. Hotz, H.G., et al., *An orthotopic nude mouse model for evaluating pathophysiology and therapy of pancreatic cancer.* Pancreas, 2003. **26**(4): p. e89-98.
115. Pour, P., et al., *A potent pancreatic carcinogen in Syrian hamsters: N-nitrosobis(2-oxopropyl)amine.* J Natl Cancer Inst, 1977. **58**(5): p. 1449-53.
116. Grippo, P.J., et al., *Preinvasive pancreatic neoplasia of ductal phenotype induced by acinar cell targeting of mutant Kras in transgenic mice.* Cancer Res, 2003. **63**(9): p. 2016-9.
117. Sandgren, E.P., et al., *Pancreatic tumor pathogenesis reflects the causative genetic lesion.* Proc Natl Acad Sci U S A, 1991. **88**(1): p. 93-7.
118. Gidekel Friedlander, S.Y., et al., *Context-dependent transformation of adult pancreatic cells by oncogenic K-Ras.* Cancer Cell, 2009. **16**(5): p. 379-89.
119. Hameyer, D., et al., *Toxicity of ligand-dependent Cre recombinases and generation of a conditional Cre deleter mouse allowing mosaic recombination in peripheral tissues.* Physiol Genomics, 2007. **31**(1): p. 32-41.
120. Feil, R., et al., *Ligand-activated site-specific recombination in mice.* Proc Natl Acad Sci U S A, 1996. **93**(20): p. 10887-90.
121. Schonhuber, N., et al., *A next-generation dual-recombinase system for time- and host-specific targeting of pancreatic cancer.* Nat Med, 2014. **20**(11): p. 1340-7.
122. Anastassiadis, K., et al., *Dre recombinase, like Cre, is a highly efficient site-specific recombinase in E. coli, mammalian cells and mice.* Dis Model Mech, 2009. **2**(9-10): p. 508-15.
123. Guerra, C., et al., *Tumor induction by an endogenous K-ras oncogene is highly dependent on cellular context.* Cancer Cell, 2003. **4**(2): p. 111-20.
124. Nakhai, H., et al., *Ptf1a is essential for the differentiation of GABAergic and glycinergic amacrine cells and horizontal cells in the mouse retina.* Development, 2007. **134**(6): p. 1151-60.
125. Sellick, G.S., et al., *Mutations in PTF1A cause pancreatic and cerebellar agenesis.* Nat Genet, 2004. **36**(12): p. 1301-5.
126. Mazur, P.K., et al., *Identification of epidermal Pdx1 expression discloses different roles of Notch1 and Notch2 in murine Kras(G12D)-induced skin carcinogenesis in vivo.* PLoS One, 2010. **5**(10): p. e13578.
127. Guerra, C. and M. Barbacid, *Genetically engineered mouse models of pancreatic adenocarcinoma.* Mol Oncol, 2013. **7**(2): p. 232-47.
128. Pylayeva-Gupta, Y., E. Grabocka, and D. Bar-Sagi, *RAS oncogenes: weaving a tumorigenic web.* Nat Rev Cancer, 2011. **11**(11): p. 761-74.
129. Hanahan, D. and R.A. Weinberg, *Hallmarks of cancer: the next generation.* Cell, 2011. **144**(5): p. 646-74.
130. Collins, M.A., et al., *Oncogenic Kras is required for both the initiation and maintenance of pancreatic cancer in mice.* J Clin Invest, 2012. **122**(2): p. 639-53.
131. Collisson, E.A., et al., *A central role for RAF-->MEK-->ERK signaling in the genesis of pancreatic ductal adenocarcinoma.* Cancer Discov, 2012. **2**(8): p. 685-93.
132. Eser, S., et al., *Selective requirement of PI3K/PDK1 signaling for Kras oncogene-driven pancreatic cell plasticity and cancer.* Cancer Cell, 2013. **23**(3): p. 406-20.
133. Neel, N.F., et al., *The RalB small GTPase mediates formation of invadopodia through a GTPase-activating protein-independent function of the RalBP1/RLIP76 effector.* Mol Cell Biol, 2012. **32**(8): p. 1374-86.
134. Vigil, D., et al., *Aberrant overexpression of the Rgl2 Ral small GTPase-specific guanine nucleotide exchange factor promotes pancreatic cancer*

growth through Ral-dependent and Ral-independent mechanisms. J Biol Chem, 2010. **285**(45): p. 34729-40.
135. Heid, I., et al., *Early requirement of Rac1 in a mouse model of pancreatic cancer.* Gastroenterology, 2011. **141**(2): p. 719-30, 730.e1-7.
136. Kimmelman, A.C., et al., *Genomic alterations link Rho family of GTPases to the highly invasive phenotype of pancreas cancer.* Proc Natl Acad Sci U S A, 2008. **105**(49): p. 19372-7.
137. Timpson, P., et al., *Spatial regulation of RhoA activity during pancreatic cancer cell invasion driven by mutant p53.* Cancer Res, 2011. **71**(3): p. 747-57.
138. Kandoth, C., et al., *Mutational landscape and significance across 12 major cancer types.* Nature, 2013. **502**(7471): p. 333-9.
139. Yachida, S., et al., *Clinical significance of the genetic landscape of pancreatic cancer and implications for identification of potential long-term survivors.* Clin Cancer Res, 2012. **18**(22): p. 6339-47.
140. Morton, J.P., et al., *LKB1 haploinsufficiency cooperates with Kras to promote pancreatic cancer through suppression of p21-dependent growth arrest.* Gastroenterology, 2010. **139**(2): p. 586-97, 597.e1-6.
141. Biankin, A.V., et al., *Overexpression of p21(WAF1/CIP1) is an early event in the development of pancreatic intraepithelial neoplasia.* Cancer Res, 2001. **61**(24): p. 8830-7.
142. Caldwell, M.E., et al., *Cellular features of senescence during the evolution of human and murine ductal pancreatic cancer.* Oncogene, 2012. **31**(12): p. 1599-608.
143. Gu, B. and W.G. Zhu, *Surf the post-translational modification network of p53 regulation.* Int J Biol Sci, 2012. **8**(5): p. 672-84.
144. Fuchs, S.Y., et al., *JNK targets p53 ubiquitination and degradation in nonstressed cells.* Genes Dev, 1998. **12**(17): p. 2658-63.
145. Morton, J.P., et al., *Mutant p53 drives metastasis and overcomes growth arrest/senescence in pancreatic cancer.* Proc Natl Acad Sci U S A, 2010. **107**(1): p. 246-51.
146. Fuchs, S.Y., et al., *MEKK1/JNK signaling stabilizes and activates p53.* Proc Natl Acad Sci U S A, 1998. **95**(18): p. 10541-6.
147. Hingorani, S.R., et al., *Trp53R172H and KrasG12D cooperate to promote chromosomal instability and widely metastatic pancreatic ductal adenocarcinoma in mice.* Cancer Cell, 2005. **7**(5): p. 469-83.
148. Caldas, C., et al., *Frequent somatic mutations and homozygous deletions of the p16 (MTS1) gene in pancreatic adenocarcinoma.* Nat Genet, 1994. **8**(1): p. 27-32.
149. Schutte, M., et al., *Abrogation of the Rb/p16 tumor-suppressive pathway in virtually all pancreatic carcinomas.* Cancer Res, 1997. **57**(15): p. 3126-30.
150. Ueki, T., et al., *Hypermethylation of multiple genes in pancreatic adenocarcinoma.* Cancer Res, 2000. **60**(7): p. 1835-9.
151. Michaloglou, C., et al., *BRAFE600-associated senescence-like cell cycle arrest of human naevi.* Nature, 2005. **436**(7051): p. 720-4.
152. Bardeesy, N., et al., *Both p16(Ink4a) and the p19(Arf)-p53 pathway constrain progression of pancreatic adenocarcinoma in the mouse.* Proc Natl Acad Sci U S A, 2006. **103**(15): p. 5947-52.
153. Chang, Z., et al., *Cooperativity of oncogenic K-ras and downregulated p16/INK4A in human pancreatic tumorigenesis.* PLoS One, 2014. **9**(7): p. e101452.
154. Yu, Y., W. Ren, and B. Ren, *Expression of signal transducers and activator of transcription 3 (STAT3) determines differentiation of olfactory bulb cells.* Mol Cell Biochem, 2009. **320**(1-2): p. 101-8.
155. Yu, Z.B., et al., *Restoration of SOCS3 suppresses human lung adenocarcinoma cell growth by downregulating activation of Erk1/2, Akt apart from STAT3.* Cell Biol Int, 2009. **33**(9): p. 995-1001.

156. Scholz, A., et al., *Activated signal transducer and activator of transcription 3 (STAT3) supports the malignant phenotype of human pancreatic cancer.* Gastroenterology, 2003. **125**(3): p. 891-905.
157. Miyatsuka, T., et al., *Persistent expression of PDX-1 in the pancreas causes acinar-to-ductal metaplasia through Stat3 activation.* Genes Dev, 2006. **20**(11): p. 1435-40.
158. Corcoran, R.B., et al., *STAT3 plays a critical role in KRAS-induced pancreatic tumorigenesis.* Cancer Res, 2011. **71**(14): p. 5020-9.
159. Lesina, M., et al., *Stat3/Socs3 activation by IL-6 transsignaling promotes progression of pancreatic intraepithelial neoplasia and development of pancreatic cancer.* Cancer Cell, 2011. **19**(4): p. 456-69.
160. Yamamoto, S., et al., *Prognostic significance of activated Akt expression in pancreatic ductal adenocarcinoma.* Clin Cancer Res, 2004. **10**(8): p. 2846-50.
161. Fruman, D.A. and C. Rommel, *PI3K and cancer: lessons, challenges and opportunities.* Nat Rev Drug Discov, 2014. **13**(2): p. 140-56.
162. Kennedy, A.L., P.D. Adams, and J.P. Morton, *Ras, PI3K/Akt and senescence: Paradoxes provide clues for pancreatic cancer therapy.* Small GTPases, 2011. **2**(5): p. 264-267.
163. Ruggeri, B.A., et al., *Amplification and overexpression of the AKT2 oncogene in a subset of human pancreatic ductal adenocarcinomas.* Mol Carcinog, 1998. **21**(2): p. 81-6.
164. Semba, S., et al., *Phosphorylated Akt/PKB controls cell growth and apoptosis in intraductal papillary-mucinous tumor and invasive ductal adenocarcinoma of the pancreas.* Pancreas, 2003. **26**(3): p. 250-7.
165. Asano, T., et al., *The PI 3-kinase/Akt signaling pathway is activated due to aberrant Pten expression and targets transcription factors NF-kappaB and c-Myc in pancreatic cancer cells.* Oncogene, 2004. **23**(53): p. 8571-80.
166. Hill, R., et al., *PTEN loss accelerates KrasG12D-induced pancreatic cancer development.* Cancer Res, 2010. **70**(18): p. 7114-24.
167. Kennedy, A.L., et al., *Activation of the PIK3CA/AKT pathway suppresses senescence induced by an activated RAS oncogene to promote tumorigenesis.* Mol Cell, 2011. **42**(1): p. 36-49.
168. Hansel, D.E., S.E. Kern, and R.H. Hruban, *Molecular pathogenesis of pancreatic cancer.* Annu Rev Genomics Hum Genet, 2003. **4**: p. 237-56.
169. Bardeesy, N., et al., *Smad4 is dispensable for normal pancreas development yet critical in progression and tumor biology of pancreas cancer.* Genes Dev, 2006. **20**(22): p. 3130-46.
170. Izeradjene, K., et al., *Kras(G12D) and Smad4/Dpc4 haploinsufficiency cooperate to induce mucinous cystic neoplasms and invasive adenocarcinoma of the pancreas.* Cancer Cell, 2007. **11**(3): p. 229-43.
171. Chen, Y.W., et al., *SMAD4 loss triggers the phenotypic changes of pancreatic ductal adenocarcinoma cells.* BMC Cancer, 2014. **14**: p. 181.
172. Siveke, J.T., et al., *Concomitant pancreatic activation of Kras(G12D) and Tgfa results in cystic papillary neoplasms reminiscent of human IPMN.* Cancer Cell, 2007. **12**(3): p. 266-79.
173. Ardito, C.M., et al., *EGF receptor is required for KRAS-induced pancreatic tumorigenesis.* Cancer Cell, 2012. **22**(3): p. 304-17.
174. Shih, H.P., et al., *A Notch-dependent molecular circuitry initiates pancreatic endocrine and ductal cell differentiation.* Development, 2012. **139**(14): p. 2488-99.
175. De La, O.J., et al., *Notch and Kras reprogram pancreatic acinar cells to ductal intraepithelial neoplasia.* Proc Natl Acad Sci U S A, 2008. **105**(48): p. 18907-12.
176. Mazur, P.K., et al., *Notch2 is required for progression of pancreatic intraepithelial neoplasia and development of pancreatic ductal adenocarcinoma.* Proc Natl Acad Sci U S A, 2010. **107**(30): p. 13438-43.

177. Hanlon, L., et al., *Notch1 functions as a tumor suppressor in a model of K-ras-induced pancreatic ductal adenocarcinoma.* Cancer Res, 2010. **70**(11): p. 4280-6.
178. Prevot, P.P., et al., *Role of the ductal transcription factors HNF6 and Sox9 in pancreatic acinar-to-ductal metaplasia.* Gut, 2012. **61**(12): p. 1723-32.
179. Kopp, J.L., et al., *Identification of Sox9-dependent acinar-to-ductal reprogramming as the principal mechanism for initiation of pancreatic ductal adenocarcinoma.* Cancer Cell, 2012. **22**(6): p. 737-50.
180. Weston, C.R. and R.J. Davis, *The JNK signal transduction pathway.* Curr Opin Cell Biol, 2007. **19**(2): p. 142-9.
181. Davis, R.J., *Signal transduction by the JNK group of MAP kinases.* Cell, 2000. **103**(2): p. 239-52.
182. Chang, L. and M. Karin, *Mammalian MAP kinase signalling cascades.* Nature, 2001. **410**(6824): p. 37-40.
183. Gupta, S., et al., *Selective interaction of JNK protein kinase isoforms with transcription factors.* Embo j, 1996. **15**(11): p. 2760-70.
184. Engstrom, W., A. Ward, and K. Moorwood, *The role of scaffold proteins in JNK signalling.* Cell Prolif, 2010. **43**(1): p. 56-66.
185. Tournier, C., et al., *MKK7 is an essential component of the JNK signal transduction pathway activated by proinflammatory cytokines.* Genes Dev, 2001. **15**(11): p. 1419-26.
186. Pulverer, B.J., et al., *Phosphorylation of c-jun mediated by MAP kinases.* Nature, 1991. **353**(6345): p. 670-4.
187. Ndong, C., et al., *Mitogen-activated protein kinase (MAPK) phosphatase-3 (MKP-3) displays a p-JNK-MAPK substrate preference in astrocytes in vitro.* Neurosci Lett, 2014. **575**: p. 13-8.
188. Nomura, J., et al., *Febuxostat, an inhibitor of xanthine oxidase, suppresses lipopolysaccharide-induced MCP-1 production via MAPK phosphatase-1-mediated inactivation of JNK.* PLoS One, 2013. **8**(9): p. e75527.
189. Liu, J., et al., *Analysis of Drosophila segmentation network identifies a JNK pathway factor overexpressed in kidney cancer.* Science, 2009. **323**(5918): p. 1218-22.
190. Ventura, J.J., et al., *Chemical genetic analysis of the time course of signal transduction by JNK.* Mol Cell, 2006. **21**(5): p. 701-10.
191. Wei, Y., et al., *JNK1-mediated phosphorylation of Bcl-2 regulates starvation-induced autophagy.* Mol Cell, 2008. **30**(6): p. 678-88.
192. Weston, C.R., et al., *The c-Jun NH2-terminal kinase is essential for epidermal growth factor expression during epidermal morphogenesis.* Proceedings of the National Academy of Sciences of the United States of America, 2004. **101**(39): p. 14114-14119.
193. Bennett, B.L., et al., *SP600125, an anthrapyrazolone inhibitor of Jun N-terminal kinase.* Proc Natl Acad Sci U S A, 2001. **98**(24): p. 13681-6.
194. Bain, J., et al., *The selectivity of protein kinase inhibitors: a further update.* Biochem J, 2007. **408**(3): p. 297-315.
195. Oh, S.W., et al., *JNK regulates lifespan in Caenorhabditis elegans by modulating nuclear translocation of forkhead transcription factor/DAF-16.* Proc Natl Acad Sci U S A, 2005. **102**(12): p. 4494-9.
196. Wang, M.C., D. Bohmann, and H. Jasper, *JNK extends life span and limits growth by antagonizing cellular and organism-wide responses to insulin signaling.* Cell, 2005. **121**(1): p. 115-25.
197. Dong, C., et al., *Defective T cell differentiation in the absence of Jnk1.* Science, 1998. **282**(5396): p. 2092-5.
198. Jaeschke, A., et al., *Disruption of the Jnk2 (Mapk9) gene reduces destructive insulitis and diabetes in a mouse model of type I diabetes.* Proc Natl Acad Sci U S A, 2005. **102**(19): p. 6931-5.

199. Tran, E.H., et al., *Inactivation of JNK1 enhances innate IL-10 production and dampens autoimmune inflammation in the brain.* Proc Natl Acad Sci U S A, 2006. **103**(36): p. 13451-6.
200. Hammaker, D.R., et al., *Regulation of the JNK pathway by TGF-beta activated kinase 1 in rheumatoid arthritis synoviocytes.* Arthritis Res Ther, 2007. **9**(3): p. R57.
201. Ricci, R., et al., *Requirement of JNK2 for scavenger receptor A-mediated foam cell formation in atherogenesis.* Science, 2004. **306**(5701): p. 1558-61.
202. Tuncman, G., et al., *Functional in vivo interactions between JNK1 and JNK2 isoforms in obesity and insulin resistance.* Proc Natl Acad Sci U S A, 2006. **103**(28): p. 10741-6.
203. Kaser, A., et al., *XBP1 links ER stress to intestinal inflammation and confers genetic risk for human inflammatory bowel disease.* Cell, 2008. **134**(5): p. 743-56.
204. Haeusgen, W., T. Herdegen, and V. Waetzig, *The bottleneck of JNK signaling: molecular and functional characteristics of MKK4 and MKK7.* Eur J Cell Biol, 2011. **90**(6-7): p. 536-44.
205. Cui, J., et al., *JNK pathway: diseases and therapeutic potential.* Acta Pharmacol Sin, 2007. **28**(5): p. 601-8.
206. Schutte, J., J.D. Minna, and M.J. Birrer, *Deregulated expression of human c-jun transforms primary rat embryo cells in cooperation with an activated c-Ha-ras gene and transforms rat-1a cells as a single gene.* Proc Natl Acad Sci U S A, 1989. **86**(7): p. 2257-61.
207. Smeal, T., et al., *Oncogenic and transcriptional cooperation with Ha-Ras requires phosphorylation of c-Jun on serines 63 and 73.* Nature, 1991. **354**(6353): p. 494-6.
208. Havarstein, L.S., et al., *Mutations in the Jun delta region suggest an inverse correlation between transformation and transcriptional activation.* Proc Natl Acad Sci U S A, 1992. **89**(2): p. 618-22.
209. Behrens, A., et al., *Oncogenic transformation by ras and fos is mediated by c-Jun N-terminal phosphorylation.* Oncogene, 2000. **19**(22): p. 2657-63.
210. Chen, N., et al., *Suppression of skin tumorigenesis in c-Jun NH(2)-terminal kinase-2-deficient mice.* Cancer Res, 2001. **61**(10): p. 3908-12.
211. Finegan, K.G. and C. Tournier, *The mitogen-activated protein kinase kinase 4 has a pro-oncogenic role in skin cancer.* Cancer Res, 2010. **70**(14): p. 5797-806.
212. She, Q.B., et al., *Deficiency of c-Jun-NH(2)-terminal kinase-1 in mice enhances skin tumor development by 12-O-tetradecanoylphorbol-13-acetate.* Cancer Res, 2002. **62**(5): p. 1343-8.
213. Shibata, W., et al., *c-Jun NH2-terminal kinase 1 is a critical regulator for the development of gastric cancer in mice.* Cancer Res, 2008. **68**(13): p. 5031-9.
214. Das, M., et al., *The role of JNK in the development of hepatocellular carcinoma.* Genes Dev, 2011. **25**(6): p. 634-45.
215. Hui, L., et al., *Proliferation of human HCC cells and chemically induced mouse liver cancers requires JNK1-dependent p21 downregulation.* J Clin Invest, 2008. **118**(12): p. 3943-53.
216. Ahn, Y.H., et al., *Map2k4 functions as a tumor suppressor in lung adenocarcinoma and inhibits tumor cell invasion by decreasing peroxisome proliferator-activated receptor gamma2 expression.* Mol Cell Biol, 2011. **31**(21): p. 4270-85.
217. Cellurale, C., et al., *Role of JNK in mammary gland development and breast cancer.* Cancer Res, 2012. **72**(2): p. 472-81.
218. Hubner, A., et al., *JNK and PTEN cooperatively control the development of invasive adenocarcinoma of the prostate.* Proc Natl Acad Sci U S A, 2012. **109**(30): p. 12046-51.
219. Hess, P., et al., *Survival signaling mediated by c-Jun NH(2)-terminal kinase in transformed B lymphoblasts.* Nat Genet, 2002. **32**(1): p. 201-5.

220. Kan, Z., et al., *Diverse somatic mutation patterns and pathway alterations in human cancers.* Nature, 2010. **466**(7308): p. 869-73.
221. Minutoli, L., et al., *Protective effects of SP600125 a new inhibitor of c-jun N-terminal kinase (JNK) and extracellular-regulated kinase (ERK1/2) in an experimental model of cerulein-induced pancreatitis.* Life Sci, 2004. **75**(24): p. 2853-66.
222. Yun, S.W., et al., *Melittin inhibits cerulein-induced acute pancreatitis via inhibition of the JNK pathway.* Int Immunopharmacol, 2011. **11**(12): p. 2062-72.
223. Dahlhoff, M., et al., *Betacellulin protects from pancreatitis by activating stress-activated protein kinase.* Gastroenterology, 2010. **138**(4): p. 1585-94, 1594.e1-3.
224. Mann, K.M., et al., *Sleeping Beauty mutagenesis reveals cooperating mutations and pathways in pancreatic adenocarcinoma.* Proc Natl Acad Sci U S A, 2012. **109**(16): p. 5934-41.
225. Perez-Mancera, P.A., et al., *The deubiquitinase USP9X suppresses pancreatic ductal adenocarcinoma.* Nature, 2012. **486**(7402): p. 266-70.
226. Verma, G., H. Bhatia, and M. Datta, *Gene expression profiling and pathway analysis identify the integrin signaling pathway to be altered by IL-1beta in human pancreatic cancer cells: role of JNK.* Cancer Lett, 2012. **320**(1): p. 86-95.
227. Okada, M., et al., *Targeting the K-Ras--JNK axis eliminates cancer stem-like cells and prevents pancreatic tumor formation.* Oncotarget, 2014. **5**(13): p. 5100-12.
228. Takahashi, R., et al., *Therapeutic effect of c-Jun N-terminal kinase inhibition on pancreatic cancer.* Cancer Sci, 2013. **104**(3): p. 337-44.
229. Davies, C.C., et al., *Impaired JNK signaling cooperates with KrasG12D expression to accelerate pancreatic ductal adenocarcinoma.* Cancer Res, 2014. **74**(12): p. 3344-56.
230. Stanger, B.Z., et al., *Pten constrains centroacinar cell expansion and malignant transformation in the pancreas.* Cancer Cell, 2005. **8**(3): p. 185-95.
231. Jackson, E.L., et al., *Analysis of lung tumor initiation and progression using conditional expression of oncogenic K-ras.* Genes Dev, 2001. **15**(24): p. 3243-8.
232. Das, M., et al., *Suppression of p53-dependent senescence by the JNK signal transduction pathway.* Proc Natl Acad Sci U S A, 2007. **104**(40): p. 15759-64.
233. Han, M.S., et al., *JNK expression by macrophages promotes obesity-induced insulin resistance and inflammation.* Science, 2013. **339**(6116): p. 218-22.
234. Sano, S., et al., *Keratinocyte-specific ablation of Stat3 exhibits impaired skin remodeling, but does not affect skin morphogenesis.* Embo j, 1999. **18**(17): p. 4657-68.
235. Lamprecht, B., et al., *Derepression of an endogenous long terminal repeat activates the CSF1R proto-oncogene in human lymphoma.* Nat Med, 2010. **16**(5): p. 571-9, 1p following 579.
236. Irizarry, R.A., et al., *Exploration, normalization, and summaries of high density oligonucleotide array probe level data.* Biostatistics, 2003. **4**(2): p. 249-64.
237. Subramanian, A., et al., *Gene set enrichment analysis: A knowledge-based approach for interpreting genome-wide expression profiles.* Proceedings of the National Academy of Sciences, 2005. **102**(43): p. 15545-15550.
238. Mootha, V.K., et al., *PGC-1alpha-responsive genes involved in oxidative phosphorylation are coordinately downregulated in human diabetes.* Nat Genet, 2003. **34**(3): p. 267-73.
239. Shi, G., et al., *Maintenance of acinar cell organization is critical to preventing Kras-induced acinar-ductal metaplasia.* Oncogene, 2013. **32**(15): p. 1950-8.

240. Lim, C.P. and X. Cao, *Serine phosphorylation and negative regulation of Stat3 by JNK.* J Biol Chem, 1999. **274**(43): p. 31055-61.
241. Spence, J.R., R. Lauf, and N.F. Shroyer, *Vertebrate intestinal endoderm development.* Dev Dyn, 2011. **240**(3): p. 501-20.
242. David, J.P., et al., *JNK1 modulates osteoclastogenesis through both c-Jun phosphorylation-dependent and -independent mechanisms.* J Cell Sci, 2002. **115**(Pt 22): p. 4317-25.
243. Roy, P.K., et al., *Role of the JNK signal transduction pathway in inflammatory bowel disease.* World J Gastroenterol, 2008. **14**(2): p. 200-2.
244. Su, G.H., et al., *Alterations in pancreatic, biliary, and breast carcinomas support MKK4 as a genetically targeted tumor suppressor gene.* Cancer Res, 1998. **58**(11): p. 2339-42.
245. Ray, K.C., et al., *Epithelial tissues have varying degrees of susceptibility to Kras(G12D)-initiated tumorigenesis in a mouse model.* PLoS One, 2011. **6**(2): p. e16786.
246. Gozdecka, M., et al., *JNK suppresses tumor formation via a gene-expression program mediated by ATF2.* Cell Rep, 2014. **9**(4): p. 1361-74.
247. Ljungman, M., *Dial 9-1-1 for p53: mechanisms of p53 activation by cellular stress.* Neoplasia, 2000. **2**(3): p. 208-25.
248. He, G., et al., *miR-92a/DUSP10/JNK signalling axis promotes human pancreatic cancer cells proliferation.* Biomed Pharmacother, 2014. **68**(1): p. 25-30.
249. Leventaki, V., et al., *c-JUN N-terminal kinase (JNK) is activated and contributes to tumor cell proliferation in classical Hodgkin lymphoma.* Hum Pathol, 2014. **45**(3): p. 565-72.
250. Song, W., et al., *JNK signaling mediates EPHA2-dependent tumor cell proliferation, motility, and cancer stem cell-like properties in non-small cell lung cancer.* Cancer Res, 2014. **74**(9): p. 2444-54.
251. Wormann, S.M., et al., *The immune network in pancreatic cancer development and progression.* Oncogene, 2014. **33**(23): p. 2956-67.
252. Baumgart, S., V. Ellenrieder, and M.E. Fernandez-Zapico, *Oncogenic transcription factors: cornerstones of inflammation-linked pancreatic carcinogenesis.* Gut, 2013. **62**(2): p. 310-6.
253. Liu, J., et al., *JNK-dependent Stat3 phosphorylation contributes to Akt activation in response to arsenic exposure.* Toxicol Sci, 2012. **129**(2): p. 363-71.
254. Fukuda, A., et al., *Stat3 and MMP7 contribute to pancreatic ductal adenocarcinoma initiation and progression.* Cancer Cell, 2011. **19**(4): p. 441-55.

12 Zusammenfassung

Das duktale Adenokarzinom des Pancreas (PDAC), mit einem Lebenszeitrisiko von 1,6 % ist die viert häufigste krebsassoziierte Todesursache in der entwickelten Welt. Zellulärer Stress, wie beispielsweise chronische Entzündung, kann Krebs auslösen, auch PDAC. Es ist deshalb wichtig für Zellen Stress zu detektieren und darauf zu reagieren. Diese Funktion wird vom c-Jun N-terminal kinase (JNK) MAP kinase Modul bereitgestellt. Interessanterweise wurden für verschiedene Krebsarten sowohl protoonkogene als auch tumorsuppressive Rollen dieses Moduls belegt. Unser Interesse galt deshalb dem Knockout des JNK Signalwegs im protonkogenen $Kras^{G12D}$ Mausmodel und seinen Folgen.

Jungtiere mit Pankreas-spezifischem JNK Knockout wurden im Mendelschen Verhältnis geboren und zeigen keine offensichtlichen Defekte in den drei großen Zellkompartimenten des Pankreas. Mit fortschreitender Zeit jedoch konnten azinäre Zellen ihre Differenzierung nicht aufrechterhalten. Marker der terminalen Differenzierung waren 8 Wochen nach Geburt unverändert. Deswegen explantierten wir azinäre Zellen in 3D Kultur und es zeigte sich eine beschleunigte Dedifferenzierung zu duktal-ähnlichen Strukturen. Darüber hinaus waren JNK Knockoutmäuse auch 4 Wochen nach induzierter akuter Pankreatitis nicht in der Lage ihre Läsionen zu beseitigen und normales Parenchym wiederherzustellen. JNKs spielen also eine wichtige Rolle in der azinären Differenzierung.

Mäuse mit JNK knockout im protonkogenen $Kras^{G12D}$ Model überlebten maximal 5 Wochen. Die Entwicklung von ADM und PanINs ab Woche 2 war begleitet von einer starken fibrotischen Reaktion. Terminale Mäuse zeigten multifokale PDACs unter unveränderter Proliferation und Apoptose. Im ElastaseCre Model resultierte der JNK Knockout in PDACs nach ungefähr 31 Wochen. JNKs sind damit starke Tumorsuppressoren im PDAC.

Die Analyse der Signalwege der Zelle zeigte keine Auffälligkeiten bei Akt Signalweg, der ERK Signalweg hingegen war hochreguliert. γH2AX, ein Marker der DNA Schadenskontrolle war nicht reguliert. Obwohl p53 in einigen Zellkernen nachweisbar war, zeigten sich im Western Blot kleine Verschiebungen in der Bandengröße, was auf veränderte posttranslationale Modifikation von p53 hinweist und damit möglicherweise die Transaktivierung von p53 Zielgenen stört. Sox9, ein Marker für embryonale Vorläuferzellen jedoch ist in vielen Zellen überexprimiert. Arrays von sieben Tage alten $Kras^{G12D}$;JNK knockout Mäusen und Kontrollen offenbarte eine Anreicherung vieler inflammatorischer Signaturen in der GSEA.

NFκB, ein zentraler inflammatorischer Signalweg, war etwas herunterreguliert, während STAT3 zu verschiedenen Zeitpunkten hochreguliert war. Wir konnten keine systematische Disinhibition in IL6-getriggerten $Kras^{G12D}$ Zelllinien nach JNK-Inhibition feststellen, wie von Lim *et al*. berichtet. Überraschenderweise verlängerte ein zusätzlicher Knockout von STAT3 im Pankreasepithelium das Gesamtüberleben der $Kras^{G12D}$;JNK Knockoutmäuse nicht. Histologische

Veränderungen waren erstaunlicherweise ebenfalls nicht ersichtlich. Dies spricht für eine untergeordnete Rolle de STAT3 Signalwegs in der rapiden Tumorigenese der $Kras^{G12D}$;JNK knockout Mäuse.

Zusammenfassend konnte mit dieser Doktorarbeit gezeigt werden, dass JNKs nicht für die Embryonalentwicklung des Pankreas in der Maus benötigt werden, JNK jedoch eine wichtige Rolle bei der Aufrechterhaltung der terminalen Differenzierung der azinären Zellen nach Stress spielen. Im $Kras^{G12D}$ PDAC Model beschleunigt der JNK knockout die Tumorigenese extrem und etabliert JNK als neuen Tumorsuppressor des PDACs. Darüber hinaus konnten wir zeigen, dass der STAT3 Signalweg, obwohl hochaktiv, überraschenderweise eine höchstens geringe Rolle im schnellen Tumorverlauf der $Kras^{G12D}$;$JNK^{\Delta/\Delta}$ Mäuse spielt.